

## Abstract

### Canonical and Non-Canonical Plant Heterotrimeric G Proteins in Plant Immunity

Jimi Craig Miller

2018

Plants are confronted with the dilemma to either invest their limited resources directly in growth to out-compete neighboring plants or expend limited resources directly in defense to protect themselves from herbivores and pathogens, which shifts resources away from growth. Plants sense these competing demands from their surroundings through receptor proteins that are synthesized at high levels in the endoplasmic reticulum. These receptor signals are transduced by the heterotrimeric G proteins, consisting of a  $G\alpha$  (GPA1, XLG1-3), a  $G\beta$  (AGB1), and a  $G\gamma$  (AGG1-3) subunit, in which receptor activation induces dissociation of the heterotrimeric G protein complex into an active  $G\alpha$  subunit and  $G\beta\gamma$  heterodimer that activate downstream responses. However, the regulation between growth and defense tradeoffs remains unclear as well as the possibility of other  $G\beta$  subunits. Here, we show plants use the unfolded protein response to balance the synthesis of receptor proteins to favor defense over growth. This regulation by heterotrimeric G protein complexes whose signaling function in the endoplasmic reticulum is independent of their canonical functions at the plasma membrane. We also show that the loss of two WD40 repeat proteins, structurally similar  $G\beta$ -like 1 and 2 (SGL1 and SGL2), causes broad spectrum resistance against bacterial and fungal pathogen infections, suggesting these proteins negatively regulate immune signaling. Taken together, this work proposes novel functions of plant G proteins as well as two potentially novel  $G\beta$  proteins and their function in plant defense.

Canonical and Non-Canonical Plant Heterotrimeric G Proteins in Plant Immunity

A Dissertation

Presented to the Faculty of the Graduate School

Of

Yale University

In Candidacy for the Degree of

Doctor of Philosophy

By

Jimi Craig Miller

Dissertation Director: Nicole Kho Clay

December 2018

© 2018 by Jimi Craig Miller

All rights reserved.

## **Acknowledgements**

I would like to thank my family for their support and encouragement that has helped me persevere through graduate school so that they can see me graduate. Sadly, my father will not be able to see me graduate because of his passing during my last year of graduate school.

I also would like to thank the members of my lab for their help during my journey through graduate school. They helped me with experimental protocols, troubleshooting, and discussing experimental design. Members of my lab provided an enjoyable atmosphere with many discussions about anything.

I want to thank my advisor, Nicole, for always encouraging me to go further with my science and answering all the questions I had from experimental protocols to data analysis and interpretation.

Finally, I am grateful to Ann Feke, the love of my life, who has always been there to support me in every aspect of my life.

## Table of Contents

Abstract . . . . .	i
Acknowledgements . . . . .	v
List of Figures . . . . .	viii
List of Tables . . . . .	x
List of Abbreviations . . . . .	xi
<b>Chapter 1. Ternary WD40 repeat-containing protein complexes: evolution, composition and roles in plant immunity . . . . .</b>	<b>1</b>
Preface . . . . .	1
Abstract . . . . .	2
Introduction . . . . .	3
Structural Conservation of WDR-containing proteins G $\beta$ and RACK1 . . . . .	4
Heterotrimeric G Protein Complex . . . . .	8
Elusive Receptor-Effector Signaling Mechanism . . . . .	9
Evolutionary History of the Plant G $\alpha\beta\gamma$ Trimer . . . . .	11
Combinatorial Diversity of Plant G proteins . . . . .	12
G protein Complexes in Defense . . . . .	13
RACK1s in defense . . . . .	15
Search for G protein Effectors in Defense . . . . .	15
Search for G protein Complexes in Pathogenesis . . . . .	17
Conclusion . . . . .	17
<b>Chapter 2. Heterotrimeric G-proteins in unfolded protein response mediate plant growth-defense tradeoffs upstream of steroid and immune signaling . . . . .</b>	<b>19</b>
Preface . . . . .	19
Abstract . . . . .	20
Introduction . . . . .	21

Results .....	23
Increased BRI1 signaling likely contributes to enhanced growth of <i>agg1 agg2</i> .....	23
Increased FLS2 protein turnover contributes to enhanced growth of <i>agg1 agg2</i> under defense-inducing conditions .....	26
Growth and defense are uncoupled in <i>agg1 agg2</i> mutant .....	28
AGG1 and AGG2 are involved in UPR signaling in the absence of ER stress .....	31
AGB1-AGG1/2 interact with FLS2 and BRI1 at the ER membrane .....	33
Combination of <i>agg1 agg2</i> and <i>atg7/3</i> promotes robust growth and defense .....	35
UPR is hardwired to promote FLS2 protein degradation in the absence of ER stress ...	38
Discussion .....	40
Materials and Methods .....	41
Supplemental Data .....	47
Acknowledgments .....	61
<b>Chapter 3. Discovery of novel structurally similar <math>\beta</math>-propeller WD40-repeat proteins SGL1/2 and their roles in plant immunity .....</b>	<b>62</b>
Preface .....	62
Abstract .....	63
Introduction .....	64
Results .....	66
WD40 G $\beta$ -like proteins SGL1 and SGL2 are part of a novel protein family and shares similar protein structures to AGB1 .....	66
SGL1 and SGL2 interact with Arabidopsis G proteins and localize to the plasma membrane. ....	68
SGL1/2 negatively regulate plant immune defenses .....	73
Discussion .....	76
Conclusion .....	77

Materials and Methods .....	77
Supplemental Data .....	82
Acknowledgments .....	85
References .....	86

## List of Figures

Figure 1.1. G proteins are involved in diverse signal transduction pathways . . . . .	5
Figure 1.2. G proteins are found across all major eukaryotic groups. . . . .	7
Figure 1.3. WDR-containing proteins share similar protein structure . . . . .	8
Figure 1.4. Plant G $\beta$ WDR-containing proteins share common ancestor as metazoan G $\beta$ WDR-containing proteins . . . . .	11
Figure 2.1. Increased BRI1 signaling contributes to enhanced growth of <i>agg1 agg2</i> mutant . . . .	24
Figure 2.2. Increased FLS2 turnover contributes to enhanced growth of <i>agg1 agg2</i> mutant under defense-inducing conditions . . . . .	27
Figure 2.3. Growth and defense are uncoupled in <i>agg1 agg2</i> mutant . . . . .	30
Figure 2.4. AGG1 and AGG2 are involved in UPR signaling . . . . .	32
Figure 2.5. AGB1-AGG1/2 interact with FLS2 at the ER membrane . . . . .	34
Figure 2.6. Combination of <i>agg1 agg2</i> and <i>atg7/3</i> promotes robust growth and defense . . . . .	37
Figure 2.7. UPR is hardwired to promote FLS2 protein degradation in the absence of ER stress .	39
Figure S2.1. The <i>agg1 agg2</i> mutant exhibits increased vegetative growth and faster transition to inflorescence development . . . . .	47
Figure S2.2. BRI1 transcript and protein expression are elevated due loss of G $\gamma$ subunits . . . . .	48
Figure S2.3. Loss of AGG1/2 leads to reduced FLS2 protein on the plasma membrane . . . . .	49
Figure S2.4. MAPK activation is reduced in the absence of AGG1/2 . . . . .	50
Figure S2.5. Flg-induced callose deposition is reduced in the absence of AGG1/2 . . . . .	51
Figure S2.6. High BL levels cause growth inhibition in <i>agg1 agg2</i> . . . . .	52
Figure S2.7. UPR markers BIP and PDI are unaffected in <i>agg1 agg2</i> . . . . .	53
Figure S2.8. C-terminal tag does not affect AGG1 subcellular localization . . . . .	54
Figure S2.9. G $\beta\gamma$ heterodimer interact with BRI1 at the ER membrane . . . . .	55
Figure S2.10. Inhibiting autophagy and proteasome in <i>agg1 agg2</i> rescues flagellin response back to WT . . . . .	56

Figure S2.11. <i>agg1 agg2 atg3/7</i> triple mutants have restored MAPK activation upon flagellin elicitation . . . . .	57
Figure S2.12. <i>agg1 agg2 atg3/7</i> triple mutants exhibit WT bacterial resistance and adult growth	58
Figure S2.13. The <i>agg1 agg2</i> mutant exhibits increased growth . . . . .	59
Figure 3.1. SGL1 and SGL2 proteins share similar protein structures as canonical AGB1 . . . . .	67
Figure 3.2. SGL1/2 are phylogenetically distinct from that of AGB1 and RACK1 proteins . . . . .	69
Figure 3.3. SGL2 interacts with G $\gamma$ subunits AGG1/2 . . . . .	70
Figure 3.4. SGL2 interacts with G $\alpha$ subunits GPA1 and XLG1 . . . . .	71
Figure 3.5. SGL2 localizes to the plasma membrane . . . . .	72
Figure 3.6. Loss of SGL1 and SGL2 does not affect MAPK activation . . . . .	74
Figure 3.7. SGL1 and SGL2 negatively regulate plant immunity . . . . .	75
Figure S3.1. WD40 repeat proteins SGL1 and SGL2 are down-regulated upon flg22 elicitation .	82
Figure S3.2. <i>sgl1/2</i> single and double mutants resemble WT growth development . . . . .	83
Figure S3.3. <i>agb1 sgl1/2</i> double mutants are as susceptible as <i>agb1</i> against <i>P. syringae</i> . . . . .	84

**List of Tables**

Table S2.1 Q-PCR primer sequences and efficiencies ..... 70

### List of Abbreviations

LRR	Leucine-rich repeat
RLK	Receptor-like kinase
RLP	Receptor-like protein
BRI1	BRASSINOSTEROID INSENSITIVE 1
FLS2	FLAGELLING SENSING 2
BAK1	BRASSINOSTEROID INSENSITIVE 1-associated receptor kinase 1
NB-LRR	Nucleotide-binding site leucine-rich repeat
ER	Endoplasmic reticulum
UPR	Unfold protein response
Flg22	Flagellin fragment (QRLSTGSRINSAKDDAAGLQIA)
WDR	WD40-repeat
ABA	Absciscic acid
DNA	Deoxyribonucleic acid
DAMP	Damage-associated molecular patterns
MAMP	Microbe-associated molecular patterns
PAMP	Pathogen-associated molecular patterns
MAPK	Mitogen-activated protein kinase
RACK1	Receptor of activated protein C kinase 1
GPCR	G-protein-coupled receptor
YFP	Yellow fluorescing protein
GFP	Green fluorescing protein
RFP	Red fluorescing protein
T-DNA	Transfer-DNA
FPWD	Fungal-plant WDR-containing

## **Chapter 1. Ternary WD40 repeat-containing protein complexes: evolution, composition and roles in plant immunity**

### **Preface**

This chapter was published in *Frontiers in Plant Science* 06, January 2016 and can be found here: <https://doi.org/10.3389/fpls.2015.01108>. J.C.M. wrote the G $\beta$  section. W.C. wrote the TTG1 section. N.K.C. wrote introduction and edited manuscript. All three wrote the conclusion. Only the sections related to G $\beta$  WD40 repeat proteins are described here in this chapter.

**Authors:** Jimi C. Miller<sup>1</sup>, William R. Chezem<sup>2</sup>, Nicole K. Clay<sup>1,2</sup>

### **Affiliations:**

<sup>1</sup>Department of Molecular Biophysics and Biochemistry, Yale University, New Haven, CT 06511, USA.

<sup>2</sup>Department of Molecular, Cellular, and Developmental Biology, Yale University, New Haven, CT 06511, USA.

## **ABSTRACT**

Plants, like mammals, rely on their innate immune system to perceive and discriminate among the majority of their microbial pathogens. Unlike mammals, plants respond to this molecular dialog by unleashing a complex chemical arsenal of defense metabolites to resist or evade pathogen infection. In basal or non-host resistance, plants utilize signal transduction pathways to detect “non-self,” “damaged-self,” and “altered-self”- associated molecular patterns and translate these “danger” signals into largely inducible chemical defenses. The WD40 repeat (WDR)-containing protein G $\beta$  is a constituent of a ternary protein complex functioning in plant immune signaling. It is also encoded by a single-copy gene that is ubiquitous in higher plants, implying the limited diversity and functional conservation of its respective complexes. In this review, we summarize what is currently known about the evolutionary history of WDR-containing ternary complexes, their repertoire and combinatorial interactions, and their downstream effectors and pathways in plant defense.

## INTRODUCTION

WD40 repeat (WDR)-containing proteins are prevalent in eukaryotes, but rarely present in prokaryotes (Janda et al., 1996; Stirnimann et al., 2010). Plant genomes typically encode more than 200 putative WDR-containing proteins (Ouyang et al., 2012; van Nocker and Ludwig, 2003), which is slightly less than the human genome (349; Letunic et al., 2014). The basic function of WDR-containing proteins is to serve as rigid scaffolds for protein-protein and protein-DNA interactions. WDR-containing proteins are involved in fundamental mechanisms such as signal transduction, chromatin modification and transcriptional regulation. They are also involved in a wide variety of plant processes, including cell division, meristem organization, light signaling, floral development, secondary metabolism, and innate immunity (Smith et al., 1999; van Nocker and Ludwig, 2003; Perfus-Barbeoch et al., 2004).

Plants, unlike mammals, lack mobile defender cells and an adaptive immune system. Instead, they rely on the innate immunity of each cell, systemic peptide and chemical signals emanating from infection sites, and preformed and inducible chemical defenses at infection sites to ward off invading pathogens (Dixon 2001; Jones and Dangl, 2006; Zipfel 2014). Plants, like mammals, have a two-tiered pathogen-detection system. The first layer is evolutionarily more ancient and involves the cell-surface perception of conserved microbial or “non self” molecular signatures known as microbe-/pathogen-associated molecular patterns (or MAMPs/PAMPs) and pathogen-generated “damaged/altered-self” molecular signatures known as damage-associated molecular patterns (or DAMPs). These “danger” signals are recognized by pattern recognition receptors (or PRRs), which in plants are plasma membrane-localized receptor-like proteins (RLPs) or receptor-like kinases (RLKs). MAMPs, *inter alia*, are also thought to be the molecular determinants of induced systemic resistance (ISR) that is activated by beneficial plant-microbe interactions in the roots (Meziane 2005; Bakker et al., 2007; Van Wees et al., 1997). The second layer of immunity involves the cytosolic perception of pathogen-specific effector proteins by intracellular nucleotide

binding leucine-rich repeat (or NB-LRR)-containing resistance proteins to trigger programmed cell death at infection sites and, in many cases, systemic acquired resistance in the host plant (Jones and Dangl, 2006).

Plant immunity, in particular, boasts two distinct but structurally similar classes of WDR-containing proteins: G $\beta$  and G $\beta$ -like receptor for activated C kinase 1 (RACK1) (Figures 1.1 and 1.3). In addition, they are widely conserved across a diversity of eukaryotes (Bradford et al., 2013; Adams et al., 2011) (Figure 1.2). The G $\beta$  and RACK1 proteins are coupled to type-I membrane receptors, mitogen-activated protein kinase (MAPK) cascades, and transcription factors, respectively, in a plant innate immune signaling pathway that convert extracellular signals into a subset of intracellular chemical defense responses.

#### *Structural Conservation of WDR-containing proteins G $\beta$ and RACK1*

The common and defining structural feature of the two WDR-containing proteins in plant immunity is the seven-tandem WDR motif sequence, which adopts a seven-bladed  $\beta$ -propeller-like structure with three potential surfaces for molecular interactions – the top, bottom and circumference (Figure 1.3) (Lambright et al., 1996; Smith et al., 1999; Ullah et al., 2008; Adams et al., 2011; Ruiz et al., 2012). Each blade of the propeller-like structure consists of four antiparallel  $\beta$  strands; the first three strands of one blade and the fourth strand of the next are formed by a single WDR motif; the overlap between two adjacent propeller blades provides an interlocking architecture that holds the propeller-like structure in a closed, rigid ring structure (Smith et al., 1999; Adams et al., 2011).

Unlike RACK1, the G $\beta$  protein additionally contains an *N*-terminal  $\alpha$ -helix (Figure 1.3) that forms a coiled-coil structure with the G $\gamma$  protein, as indicated by the crystal structure of the human G $\beta$  HsGNB1 partially encircled by the G $\alpha$  HsGNAT1 (Sondek et al., 1996). However, HsGNB1 remains the sole G $\beta$  with a solved crystal structure, which serves as the foundation

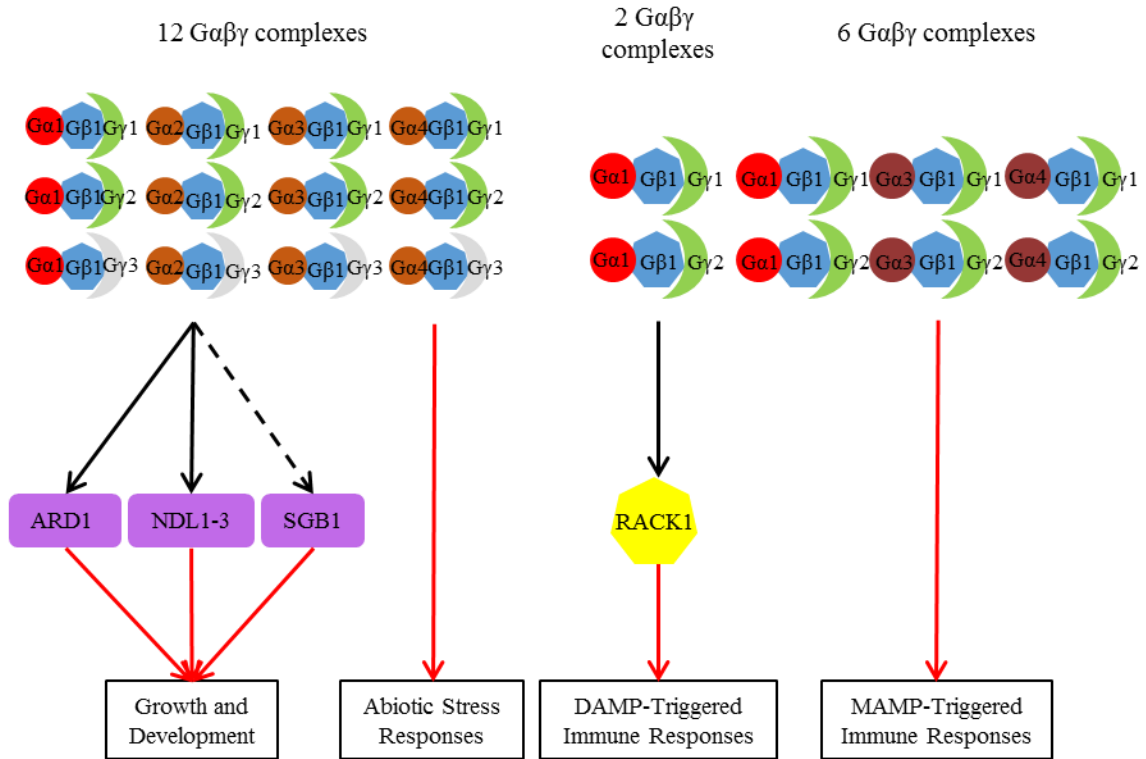


**Figure 1.1. G proteins are involved in diverse signal transduction pathways.** Regulatory network of known  $G\beta$ -dependent pathways in *Arabidopsis* illustrating the interactions between  $G\beta$  protein subunits and between  $G\beta$ 1 and its effectors for various regulated plant processes. Growth and development processes include stomatal density and opening, seed germination, hypocotyl elongation, and organ (i.e., leaf, silique, seed) morphology. Abiotic stress responses include salt stress, chemical-induced endoplasmic reticulum stress, and sugar stress. DAMP-triggered immune responses include MAP kinase activation and ROS generation. MAMP-triggered immune responses include aforementioned immune responses as well as modulation of the flavonoid anthocyanin pathway. Unbroken and broken black lines indicate indirect and direct interaction, respectively; red arrow indicates positive regulation. Shapes: heptagons, WDR-containing proteins  $G\beta$  and AtRACK1; circles,  $G\alpha$  proteins; moons,  $G\gamma$  proteins; rectangles, downstream  $G\beta\gamma$  effectors. For a given shape, different colors denote different classes of  $G$  protein subunit isoforms or WDR-containing proteins. *Arabidopsis* proteins:  $G\beta$ 1, AGB1;  $G\alpha$ 1, GPA1;  $G\alpha$ 2, XLG1;  $G\alpha$ 3, XLG2;  $G\alpha$ 4, XLG3;  $G\gamma$ 1, AGG1;  $G\gamma$ 2, AGG2; and  $G\gamma$ 3, AGG3. Note that the expanded diversity of the non-WDR-containing subunits in the complex likely provides functional specificity within plant innate immune signaling. Also note the paucity of identified effectors downstream of the  $G$  protein complexes for all known regulated processes.

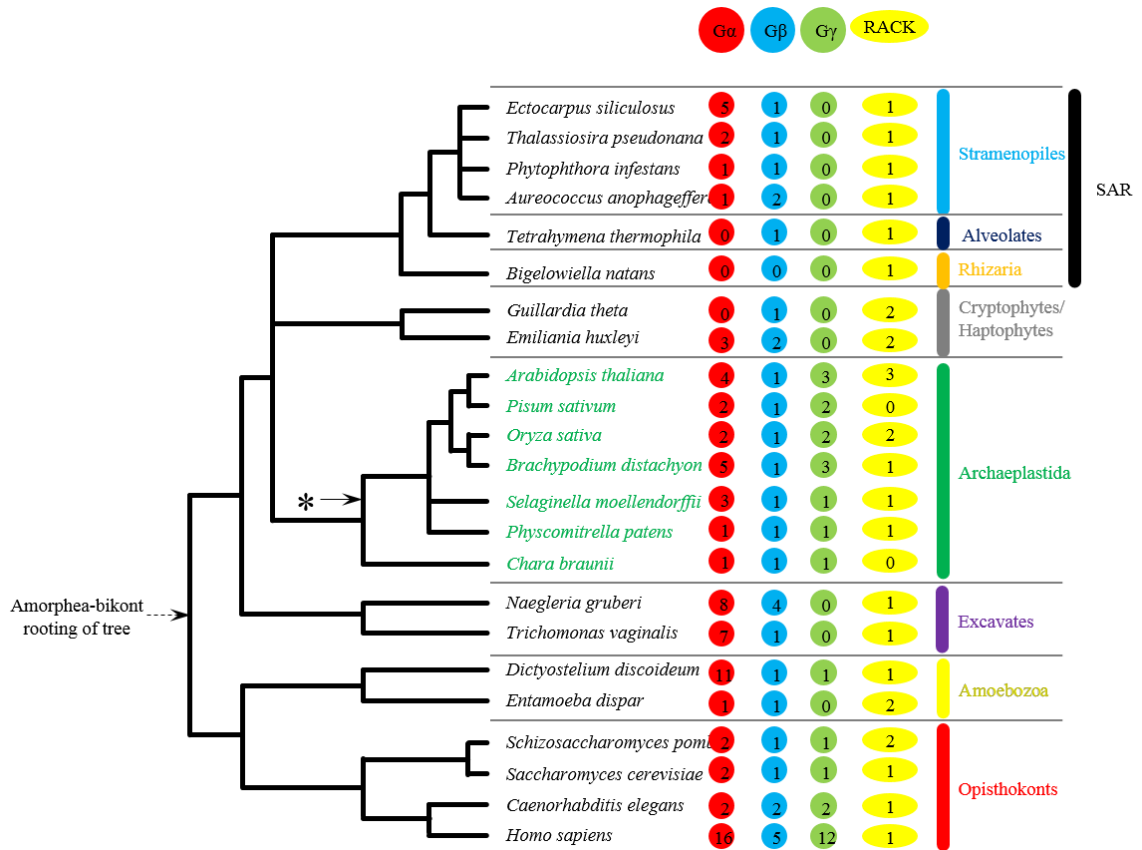


**Figure 1.2. G proteins are found across all major eukaryotic groups.** Tree of the five eukaryotic supergroups depicting the number of G $\beta$  and RACK1 sequences identified to date for a given representative species as well as two major plant evolutionary milestones: plant colonization of land (\*) Note that no G $\beta$ , RACK1 or TTG1 sequences were identified in the Rhizaria subgroup.

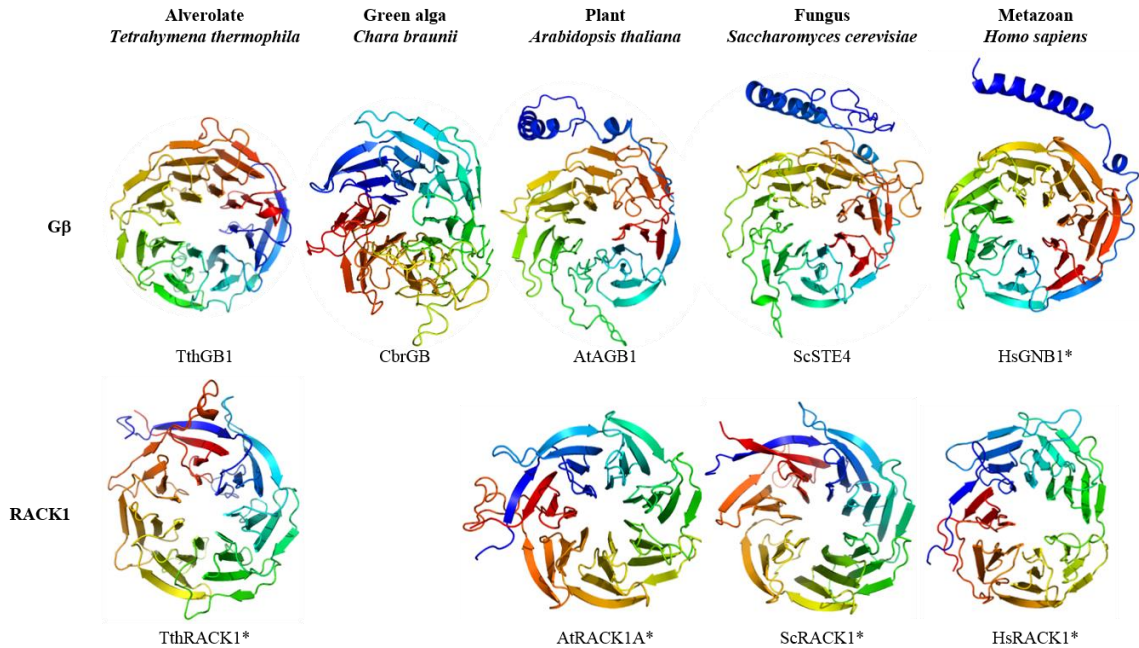


**Figure 1.3. WDR-containing proteins share similar protein structure.** Seven-bladed propeller-like structures of WDR-containing proteins G $\beta$  (top row), RACK1 (bottom row) proteins from an alveolate, green algal, plant, fungal, and metazoan species. Homology models were based on known structures of TthRACK1, AtRACK1A, ScRACK1, HsGNB1, and HsRACK1 (marked by asterisks) as well as predicted structures from multiple sequence templates using the PHYRE2 protein fold recognition server ([www.sbg.bio.ic.ac.uk/phyre2/](http://www.sbg.bio.ic.ac.uk/phyre2/); Kelley and Sternberg, 2009). Acronyms: Tth, *Tetrahymena thermophila*; Cbr, *Chara braunii*; At, *Arabidopsis thaliana*; Sc, *Saccharomyces cerevisiae*; Hs, *Homo sapiens*. Note the presence of an N-terminal alpha helix on the plant, fungal and metazoan G $\beta$  proteins but not on the alveolate and green algal G $\beta$  proteins.

(along with a handful of solved RACK1 structures) for the predicted G $\beta$  structures generated by structural bioinformatics. Within these confines, there is some evidence that the G $\beta$ -specific structure mediating the G $\beta\gamma$  interaction may not be conserved across eukaryotes. For example, G $\beta$  proteins from more primitive eukaryotes (e.g., alveolate *Tetrahymena thermophila* G $\beta$  and the green alga *Chara braunii* G $\beta$ ) are predicted to lack the *N*-terminal helix (Figure 1.3) but still retain the G $\beta\gamma$  interaction (Hackenberg et al., 2013), presumably through a novel G $\beta\gamma$  interaction domain(s) within the beta-propeller structure. Additional crystal structures of non-metazoan G $\beta$  sequences are needed to provide structural details on the G $\beta\gamma$  interaction across eukaryotes.

### **HETEROTRIMERIC G PROTEIN COMPLEX**

The most extensively studied WDR-containing protein to date is the G $\beta$  subunit of the heterotrimeric G protein complex, which is one of the most conserved and elaborate receptor-effector signaling mechanisms in eukaryotes. The G $\beta$  reversibly interacts with the GDP-bound G $\alpha$  subunit and forms an obligate heterodimer (G $\beta\gamma$ ) with the G $\gamma$  subunit. While the interaction between the G $\alpha$  and the G $\beta\gamma$  heterodimer serves as a molecular switch, the G $\beta$  serves as a scaffold for effector proteins (Figure 1.1). In animals and fungi, ligand perception by the heptahelical membrane receptors G protein-coupled receptors (GPCRs) leads to replacement of GDP with GTP in the G $\alpha$  subunit and activation of the heterotrimer (Li et al 2007; Oldham and Hamm, 2008). Upon activation, the GTP-bound G $\alpha$  and G $\beta\gamma$  heterodimer dissociate from each other and from the receptor complex, releasing their bound effectors to activate various signaling cascades. Signaling terminates when the intrinsic GTPase activity of the G $\alpha$  hydrolyzes GTP to GDP and the inactive heterotrimer reforms at the receptor. While all three constituents of the mammalian G protein complex interact with the GPCR (Taylor et al., 1994; Taylor et al., 1996), only the G $\gamma$  subunit of the plant heterotrimer has been shown to interact with the receptor complex (Aranda-Sicilla et al., 2015).

### Elusive Receptor-Effector Signaling Mechanism

Although signal transduction through a heterotrimeric G protein complex is common to animals and plants, there are some mechanistic differences between the evolutionary branches. For example, in plants and basal eukaryotes, the canonical G $\alpha$  subunit isoform is self-activating, and thus does not require GPCR-like proteins for its activation (Jones et al., 2011a; Jones et al., 2011b; Bradford et al., 2013). Plants also contain non-canonical G $\alpha$  subunit isoforms, which have a slower rate of GTP hydrolysis (Heo et al., 2012), but it is not yet known whether they are also self-activating. In addition, canonical GPCR-like sequences are absent or rare in plants (Urano et al., 2013; Taddese et al., 2014). Instead, plants have several families of non-canonical GPCR-like sequences, three of which (GCR1, GTG1 and GTG2) have been shown to interact *in planta* with the *Arabidopsis* canonical G $\alpha$  GPA1 and modulate an ABA-mediated drought response (Pandey and Assmann, 2004; Pandey et al., 2009). It remains controversial whether the GPCR-like proteins are *bona fide* GPCRs, although a recent structural bioinformatics study has found GCR1 to be a strong GPCR candidate based on its predicted heptahelical scaffold and GPCR fold (Taddese et al., 2014). Plants also contain hundreds of membrane RLP and RLK sequences (Shiu and Bleecker, 2001; Shiu and Bleecker, 2003; Fritz-Laylin et al., 2005), two of which (the maize RLP FEA2 and the *Arabidopsis* RLK RPK2) have been shown to interact *in planta* with the canonical G $\alpha$  CT2 and canonical G $\beta$  AGB1, respectively, to regulate stem cell proliferation (meristem organization) (Bommert et al., 2013; Ishida et al., 2014). Downstream, the plant G $\beta\gamma$  heterodimer has been shown to regulate the MAPK cascade by interacting directly with a MAPK protein (Bhardwaj et al., 2011; Xu et al., 2015) or by recruiting RACK1 proteins as MAPK cascade scaffolds (Cheng et al., 2015). By contrast, mammalian and fungal G $\beta\gamma$  heterodimers instead recruit the MAPK scaffolding proteins  $\beta$ -arrestin2 and Ste5, respectively (Witzel et al., 2012), while mammalian RACK1 proteins serve as Jun N-terminal kinase (JNK) MAPK cascade scaffolds for the protein kinase C (PKC) signaling pathway (Ron et al., 1994; López-Bergami

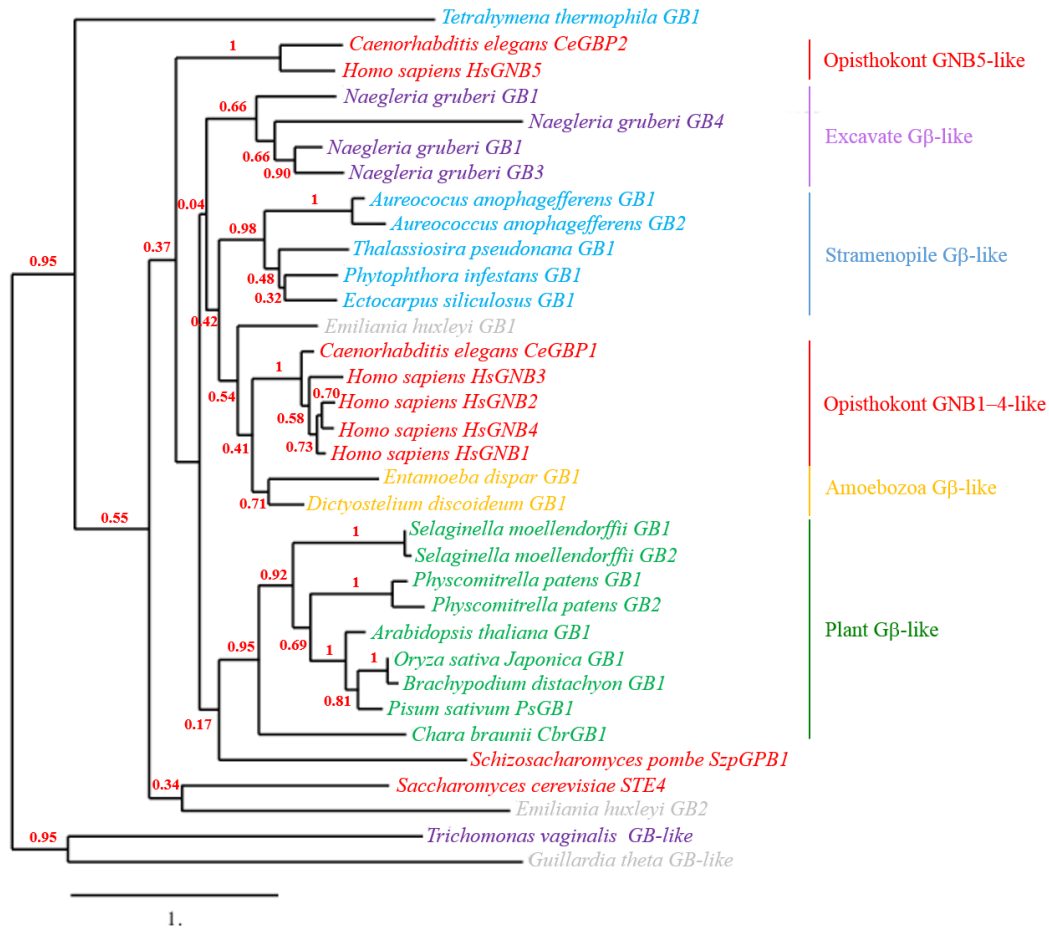


**Figure 1.4. Plant Gβ WDR-containing proteins share common ancestor as metazoan Gβ WDR-containing proteins.** Phylogenetic maximum likelihood tree of Gβ sequences from representative species in the five eukaryotic supergroups. Tree was generated using MUSCLE multiple sequence alignment, PhyML phylogeny, and TreeDyn tree viewer programs (<http://phylogeny.lirmm.fr>; Dereeper et al., 2008). Bootstrap value (n=100 replicate trees) is shown in red at the nodes. Note that the plant Gβ sequences cluster as a well-supported monophyletic group.

et al., 2005). Although RACK1 is highly conserved between plants and animals (Figure 1.4),  $\beta$ -arrestin2, Ste5 and second-messenger-regulated PKC proteins are absent in plants (Witzel et al., 2012; Stone and Walker, 1995). Despite the diversity of MAPK cascade scaffolds between plants and animals, the use of scaffolding proteins in signal transduction pathways appears universal.

### Evolutionary History of the Plant G $\beta$ $\gamma$ Trimer

G $\beta$  sequences (and those of the other two G protein subunits) are present in the genomes of all five eukaryotic supergroups, the Archaeplastida, Excavata, Opisthokonta, Amoebozoa, and Stramenopila/Alveolata/Rhizaria (or SAR), and are absent only in the Rhizaria subgroup of SAR (Figure 1.2). Although each supergroup consists of a diversity of eukaryotes, most of which are microbial (e.g., protists and algae) (Keeling et al., 2005; Burki 2014), the best-characterized G $\beta$  sequences are from animals/metazoans and fungi in the Opisthokonta supergroup. The oldest extant G $\beta$  sequence in the Archaeplastida supergroup (e.g., land plants and green/red algae) is a single-copy gene found in the green alga *Chara braunii* (Hackenberg et al., 2013) (Figure 1.2). This green algal G $\beta$  sequence is not distinct from the G $\beta$  sequences present in the genomes of basal plant lineages (e.g., bryophytes and lycophytes) and the diploid genomes of higher plant lineages (Figure 1.4) (Urano et al., 2013), indicating that they descended from a single ancestral plant G $\beta$  sequence. In contrast, phylogenetic analysis of metazoan G $\beta$  sequences identified three distinct G $\beta$  classes (GNB1–4-like, GNB5-like and Gbe-like); the first two are found in humans, and the third is specific for arthropods (De Mendoza et al., 2014; Krishnan et al., 2015). GNB1–4-like and GNB5-like sequences are likely present in the last common metazoan ancestor and are confined within metazoans (De Mendoza et al., 2014; Krishnan et al., 2015) (Figure 1.4).

Previous phylogenetic analysis for ancestral plant G $\beta$  sequences suggested that plant G $\beta$  sequences are more closely related to G $\beta$  sequences from the SAR (e.g., diatom) and Amoebozoa (e.g., entamoeba) supergroups than those of Excavata (Friedman et al., 2009). Although it is still

not clear how the eukaryotic supergroups relate to one another, the most popular hypothesis (Amorphea-bikont rooting) places the root of the eukaryotic tree between the last common ancestor of the amoebozoans and opisthokonts and the remaining eukaryotes (Keeling et al., 2005; Burki 2014). The Amorphea-bikont rooting positions the G $\beta$  sequences in the Excavata supergroup between the plant G $\beta$  sequences and those of the amoebozoans and opisthokonts (Figure 1.2). Phylogenetic analysis of a representative sampling of G $\beta$  sequences from all five supergroups supports this hypothesis by sandwiching the plant G $\beta$  sequences between the animal GNB5-like sequences and the G $\beta$  sequences in the Excavata supergroup (Figure 1.4).

### Combinatorial Diversity of Plant G proteins

Although the heterotrimeric G protein complex consists of three subunits, subunit isoforms can give rise to many heterotrimeric combinations, limited in part by amino acid sequence differences in the contact regions that lead to selective interactions. Given the large number of known G protein-mediated signaling pathways, a diversity of G protein isoforms is needed for signaling specificity (Wettschureck and Offermanns, 2005). For example, the human genome encodes 16 G $\alpha$ , 5 G $\beta$ , and 12 G $\gamma$  subunit isoforms, allowing for approximately 700 potential G $\alpha\beta\gamma$  combinations (Hillenbrand et al., 2015) (Figure 1.2). By contrast, *Arabidopsis thaliana*, like most diploid plants, contains 4 G $\alpha$  (GPA1, XLG1–3), one G $\beta$  (AGB1), and 3 G $\gamma$  (AGG1–3) subunit isoforms, allowing for 12 potential G $\alpha\beta\gamma$  combinations (Figure 1.2) (Ma et al., 1990; Weiss et al., 1994; Mason et al., 2000; Mason et al., 2001; Zhu et al., 2009; Thung et al., 2012; Chakravorty et al., 2015; Maruta et al., 2015). This number falls short of the specificity needed for the large number of known G protein-mediated signaling pathways regulating fundamental processes in plants, and remains a bottleneck issue in plant G protein signaling (Urano et al., 2013).

The sole G $\beta$  subunit isoform is a limiting factor for plant G protein combinatorial diversity. There are different complex models on how one G $\beta$  subunit isoform is able to transduce so many diverse signals (Urano and Jones, 2014). In addition, the ubiquitous presence of G $\beta$ -like

sequences across plant genomes has led to a hypothesis on the existence of additional non-canonical classes of plant G $\beta$  subunits that have yet to be discovered, a situation analogous to the recent discoveries of new classes of plant G $\alpha$  sequences (XLG1–3-like) and plant G $\gamma$  subunits (AGG3-like) (Lee and Assmann, 1999; Thung et al., 2012). The XLG1–3-like G $\alpha$  subunit differs from the canonical G $\alpha$  subunit in its possession of a long N-terminal extension of unknown function and its nuclear- and plasma membrane-localization (Ding et al., 2008; Chakravorty et al., 2015; Maruta et al., 2015). Similarly, the AGG3-like G $\gamma$  subunit differs from the canonical G $\gamma$  subunit in its possession of a C-terminal extension that is cysteine-rich and of unknown function (Chakravorty et al., 2011; Trusov et al., 2012).

Aside from genetic interaction data, there is physical interaction evidence from yeast three-hybrid studies supporting interaction specificity within the heterotrimer and its putative coupled receptor/adaptor. For example, the *Arabidopsis* G $\alpha$  subunit isoforms, XLG1 and XLG2 have been shown to strongly interact with the G $\beta\gamma$  heterodimers AGB1-AGG1/2, while the G $\alpha$  subunit isoforms GPA1 and XLG3 strongly interact with the G $\beta\gamma$  heterodimer AGB1-AGG3 (Chakravorty et al., 2015; Maruta et al., 2015), suggesting that all three G $\gamma$  isoforms are somewhat selective of their interaction partners, each preferring two of the four G $\alpha$  isoforms. In addition, yeast split-ubiquitin and Bimolecular Fluorescence Complementation (BIFC) studies indicate that the other two G $\gamma$  isoforms AGG1/2 mediate the interaction between the plant heterotrimer and the co-receptor proteins BAK1 and CERK1 (Aranda-Sicilla et al., 2015). These reports are consistent with similar reports of animal G $\gamma$  isoforms conferring specificity to the G protein complex-GPCR interaction (Im et al., 1988; Kisselev and Gautam, 1993).

### *G protein Complexes in Defense*

One of the best-characterized function of the *Arabidopsis* heterotrimeric G protein complex is in plant innate immunity, where it participates in multiple immune signaling pathways and defense responses (e.g., reactive oxygen species (ROS) production, mitogen-activated protein kinase

(MAPK) activation, defense gene activation, callose deposition, and programmed cell death) against a variety of fungal (Llorente et al., 2005; Trusov et al., 2006; Trusov et al., 2007; Trusov et al., 2009; Delgado-Cerezo et al., 2012; Torres et al., 2013) and bacterial pathogens (Zhang et al., 2008; Ishikawa et al., 2009; Zeng and He, 2010; Lee et al., 2013; Liu et al., 2013; Torres et al., 2013). Evidence of a physical interaction between a plant heterotrimer and a ligand-binding innate immune receptor (e.g., FLS2, EFR, LYK4/5) is still elusive, although a recent report showed a direct interaction between the canonical G $\alpha$  GPA1 and the G $\gamma$  isoforms AGG1/2 (but not the G $\beta$  AGB1) with the co-receptor proteins BAK1 and CERK1 by yeast split-ubiquitin assay and BiFC studies (Aranda-Sicilla et al., 2015). If validated, this is the first report of a novel plant-specific interaction between a heterotrimer and a receptor complex via co-receptor adaptors. If the plant heterotrimer is coupled directly to the receptor complex, then further research is needed to understand how the plant heterotrimer converts MAMP and/or DAMP signals from the receptors into intracellular defense responses, especially if the heterotrimer is self-activating. Nearly all of the *Arabidopsis* G protein subunit isoforms (save two – XLG1 and AGG3) participate in plant defense (Figure 1.1) (Maruta et al., 2015) and an even smaller subset of G protein subunit isoforms in a bacterial DAMP-triggered immune pathway involving RACK1 proteins as MAPK cascade scaffolds (Figure 1.1) (Cheng et al., 2015). The sole G $\beta$  AGB1 participates in all G protein-mediated processes, and positively contribute to all tested immune responses, including ROS production, callose deposition, MAPK activation, defense gene activation and programmed cell death (Llorente et al., 2006; Maeda et al., 2009; Liu et al., 2013; Torres et al., 2013). Among the G $\alpha$  subunit isoforms, XLG2 is the major contributor to resistance against the hemibiotrophic bacterium *Pseudomonas syringae*, necrotrophic fungi *Alternaria brassicicola* and *Plectosphaerella cucumerina*, and the hemibiotrophic fungus *Fusarium oxysporum*. The loss-of-function *xlg2* mutant most closely recapitulates the phenotypes of the loss-of-function *agb1* mutant in its pathogen susceptibility (Llorente et al., 2005; Trusov et al., 2006; Zhu et al., 2009; Torres et al., 2013; Maruta et al., 2015), and the XLG2 protein was shown to interact with the

AGB1 protein *in planta* by co-immunoprecipitation of overexpressed proteins (Zhu et al., 2009). In addition, the G $\alpha$  isoform GPA1 contributes to bacterial resistance by mediating stomatal closure, a MAMP-triggered immune response that retards pathogen entry through the stomata (natural openings in the plant surface) (Zhang et al., 2008), while the G $\alpha$  isoform XLG3 contributes partly to resistance against *Fusarium oxysporum* (Maruta et al., 2015) through an unknown mechanism. Among the G $\gamma$  subunit isoforms, AGG1 and AGG2 are mostly redundant in their contribution to plant immunity (Trusov et al., 2007; Thung et al., 2013). The loss-of-function *agg1 agg2* double mutant recapitulates the phenotypes of the *agb1* mutant in pathogen susceptibility (Trusov et al., 2007; Liu et al., 2013; Maruta et al., 2015; Torres et al., 2013).

#### RACK1s in defense

In addition to their involvement in *Arabidopsis* innate immunity (Cheng et al., 2015), RACK1 proteins also function in rice innate immunity by interacting with the GTP-bound form of the Rac1 GTPase protein to convert MAMP and pathogen-specific effector signals into immune responses, such as ROS generation, defense gene activation, programmed cell death, and defense metabolism, against the rice blast fungus *Magnaporthe grisea* and the bacterial blight pathogen *Xanthomonas oryzae* (Kawasaki et al., 1999; Ono et al., 2001; Suharsono et al., 2002; Nakashima et al., 2008). The RACK1-Rac1 interaction is also conserved in maize, functioning in immune responses against the northern corn leaf blight fungus *Setosphaeria turcica* (Wang et al., 2014). Interestingly, RACK1 proteins are also involved in mammalian adaptive immunity, but do not appear to operate downstream of G protein signaling as they do in plants (Mourtada-Maarabouni et al., 2005; Chen et al., 2008).

#### Search for G protein Effectors in Defense

Aside from the complexes surrounding the MAPK cascade, very few components in plant G protein-mediated signaling pathways have been identified (Figure 1.1). A binary protein

interaction approach to identify potential effectors of the G $\beta\gamma$  dimer AGB1-AGG2 by a yeast three-hybrid screen yielded a small family of N-Myc DOWNREGULATED-LIKE (NDL) proteins (NDL1-3) involved in auxin transport regulation (Mudgil et al., 2009). The AGB1-NDL1 interaction was verified by co-immunoprecipitation of overexpressed proteins in tobacco (Figure 1.1) (Mudgil et al., 2009). In addition, a genetic approach to identify potential effectors of G $\beta\gamma$  dimers AGB1-AGG1/2/3 by activation-tagging screen in the G $\beta$  mutant (*agb1*) background yielded two effectors involved in regulating hypocotyl elongation: the acireductone dioxygenase-like protein (ARD1) and the Golgi-localized hexose transporter SGB1 (Wang et al., 2007; Friedman et al., 2011). The AGB1-ARD1 interaction was verified by yeast three-hybrid and BiFC studies in tobacco (Figure 1.2) (Friedman et al., 2011). Finally, a binary protein interaction approach to identify potential effectors of the G $\alpha$  GPA1 and the G $\beta\gamma$  dimers AGB1-AGG1/2 by a classical yeast two-hybrid screen yielded NDL1 as well as a large number of potential candidate effectors, a significant number of which are identified by Gene Ontology terms to be involved in cell wall modification, a previously unknown G protein-mediated process (Klopffleisch et al., 2011). To date, no G protein effectors in plant immunity have been identified.

A more effective approach to uncover additional G protein effectors for the various immune signaling pathways may be a co-immunoprecipitation (Co-IP)-based screen for interacting proteins under native and pathogen-infection conditions followed by protein identification by liquid chromatography and tandem mass spectrometry (LC-MS/MS) because of its ability to query multi-protein complexes in a functional context. Major limitations to this approach are its preference for strong-interacting proteins and a strong negative correlation between the number of false-positives and antibody specificity (Bauer and Kuster, 2003). This approach was recently performed on the conserved cell death suppressor protein BAX INHIBITOR-1 (BI-1) during powdery mildew infection of *Arabidopsis*, yielding 95 BI-1-interacting proteins, three of which were successfully verified to genetically and/or physically interact with BI-1 (Weis et al., 2013).

One verified BI-1-interactor, CYP83A1, is involved in the synthesis of aliphatic glucosinolates (Hemm et al., 2003; Naur et al., 2003), a conserved class of defense metabolites in the Brassicales. Subsequent studies on CYP83A1 uncovered its role in the metabolic compatibility of *Arabidopsis* with its adapted powdery mildew pathogen *Erysiphe cruciferarum* (Weis et al., 2014).

#### Search for G protein Complexes in Pathogenesis

Although compatibility between plants and their pathogens leads to disease and symptom development, it is rarely found in nature due to the effectiveness of the plant innate immune system. One exceptional case is the small family of GPCR-like mildew resistance locus O (MLO) receptor proteins, which are found throughout flowering plants. A subset of MLO proteins has been shown to be a conserved requirement for the compatibility of monocots and dicots with their adapted powdery mildew pathogens (Devoto et al., 2003; Consonni et al., 2006; Humphry et al., 2006). While it remains controversial whether GPCR-like proteins are *bona fide* GPCRs, some *Arabidopsis* MLO proteins have predicted heptahelical scaffolds, GPCR folds, and G protein coupling (Taddese et al., 2014). However, the three MLO proteins involved in fungal pathogenesis (AtMLO2/6/12) do not contain these GPCR hallmarks and thus are unlikely to function as canonical GPCRs (Taddese et al., 2014). In addition, attempts to couple the two plant heterotrimers (GPA1-AGB1-AGG1/2) to the MLO receptor were not successful (Lorek et al., 2013). Still, further research is needed to discern whether other heterotrimeric combinations are involved in regulating the compatibility between plants and their pathogens.

#### **CONCLUSION**

Plants are the basis for human nutrition and a renewable source for fuel and chemical feedstocks. Diminishing food security from plant disease/pests, climate instability and population growth, concomitant with rising energy costs and dwindling petrochemical-based fossil fuel supplies, have placed high demands on the productivity of food crops and other crops of economic

importance (Krattiger, 1997; Lobell et al., 2011; Lobel and Gourджи, 2012; UN Population Division 2013). Because WDR-containing trimeric complexes are at the heart of immune signaling and transcriptional regulation of chemical defenses, continued basic and translational research on these complexes in plant immunity will certainly improve agriculture and food security as well as our understanding of fundamental processes of signal transduction and gene regulation.

Plant G $\beta$  sequences are ubiquitous across all five eukaryotic supergroups, with only a handful of species having more than two G $\beta$  sequences (Figure 1.2). Its signaling mechanism has evolved very slowly and yet pervasively so that it can't be easily extricated from multiple immune signaling pathways (Figure 1.1).

The plant G $\beta$  represents the apex of the hierarchy of network interactions in its pathway (Figure 1.1A), and is the sole constituents of its complexes to preside over all signaling and regulatory pathways in plant immunity that are mediated by WDR-containing ternary complexes. While there are still many open questions concerning the dynamics of these complexes and the specificity of their interactions with other protein partners and their downstream effectors, the large and still-growing body of research on these proteins and their complexes underscores the importance of these signaling and regulatory complexes.

## **Chapter 2. Heterotrimeric G-proteins in unfolded protein response mediate plant growth-defense tradeoffs upstream of steroid and immune signaling**

### **Preface**

S.A.L. generated *agb1/35S:YFP-AGB1* lines, and contributed to qPCR of *ire1a/b*, Endo H digestion and MAPK activation of *agg1 agg2 atg7/3*. J.C.M. generated all other constructs, and contributed to characterization of *agg1 agg2/XVE:FLS2* lines, Co-IPs and all other experiments. J.C.M. and N.K.C. interpreted the results and wrote the paper. N.K.C. generated *XVE:BRI1-RFP* construct and *agg1 agg2/XVE:FLS2* lines, and contributed to Co-IPs and pathogen assays. C.B. contributed to characterization of *agg1 agg2/XVE:FLS2* lines. T.C. contributed to Endo H digestion.

**Authors:** Jimi C. Miller<sup>1</sup>, Stacey A. Lawrence<sup>2</sup>, Caroline L. Beakes<sup>3</sup>, Teresa Ceserani<sup>2</sup>, Nicole K. Clay<sup>1,2</sup>

### **Affiliations:**

<sup>1</sup>Department of Molecular Biophysics and Biochemistry, Yale University, New Haven, CT 06511, USA.

<sup>2</sup>Department of Molecular, Cellular, and Developmental Biology, Yale University, New Haven, CT 06511, USA.

<sup>3</sup>Department of Ecology & Evolutionary Biology, Yale University, New Haven, CT 06511, USA.

## ABSTRACT

Plants prioritize growth over defense to gain a competitive advantage for limited resources, but change priorities to successfully fight infection and herbivory. Despite the importance of growth-defense tradeoffs in optimizing plant productivity in natural and agricultural populations, the molecular mechanisms that link growth and immunity remain unclear. Here, we demonstrate that growth-defense tradeoffs between pathways activated by BRI1, a steroid receptor, and FLS2, an innate immune receptor, are uncoupled in an *Arabidopsis* mutant (*agg1 agg2*) lacking two redundant heterotrimeric G-protein gamma subunits that form stable heterodimers with the G $\beta$  subunit AGB1 to control one arm of the unfolded protein response (UPR) independently of ER stress. Growth inhibition from induced immunity in wild-type plants is likely caused by AGB1-AGG1/2 dimers interacting with nascent BRI1 and FLS2 proteins on the endoplasmic reticulum (ER) membrane and repressing an UPR response that is hardwired to promote BRI1 protein biogenesis and FLS2 protein degradation via autophagy. The ability to unlock and fine-tune growth-defense tradeoffs through UPR signaling provides a novel strategy to increase the natural defenses of crops while maintaining optimal plant productivity.

## INTRODUCTION

Plants must maintain a precise balance between growth and defense in order to survive and reproduce, using a pool of limited resources (Huot et al. 2014). The tradeoff of shifting from growth to immunity upon detection of pathogens or herbivores has important ecological and agricultural consequences (Spoel and Dong, 2008; Dodds and Rathjen, 2010). The competing demands imposed on plants by their environments require mechanisms for sensing their surroundings and for effectively regulating the tradeoffs between growth and immunity. Over the past decade, a number of inhibitory crosstalks between individual pathways in growth and immunity have been characterized, including those involving the growth hormone brassinosteroids (BR)-perceiving transmembrane leucine-rich repeat-receptor kinase (LRR-RK) Brassinosteroid-Insensitive-1 (BRI1), bacterial flagellin-recognizing transmembrane LRR-RK Flagellin-Sensing-2 (FLS2), defense hormone salicylic acid (SA), and unfolded protein response (UPR) (Li and Chory, 1997; Gómez-Gómez and Boller, 2000; Rivas-San Vicente and Plasencia, 2011; Albrecht et al., 2012; Belkhadir et al., 2012; Nagashima et al., 2014; Jiménez-Góngora et al., 2015). The shared signaling components between BRI1- and FLS2-mediated signaling and between SA and UPR signaling have been characterized to mediate not only signal crosstalk between these pathways but also tradeoffs between growth and defense (Lozano-Durán et al., 2013; Fan et al., 2014; Meng et al., 2017).

The ER is the production and folding compartment for membrane proteins of the cell. Quality control mechanisms in the ER ensure that only properly folded proteins exit the ER via the secretory pathway, while improperly folded proteins exit the ER through ER-associated degradation (ERAD) or autophagy (Smith et al., 2011; Pu and Bassham, 2013). UPR is an evolutionarily conserved adaptive response triggered by the accumulation of unfolded proteins in the ER and aimed at restoring protein-folding homeostasis. However, the main function of UPR in vertebrates and plants is in growth and defense, where it acts as an anticipatory response that is

activated well before the disruption of protein homeostasis and aimed at handling high folding loads that are part of normal physiology (Janssens et al., 2014; Bao and Howell, 2017). The UPR signaling pathway in *Arabidopsis* has three overlapping but independent arms (Ruberti and Brandizzi, 2014). One arm is mediated by two homologs of the evolutionarily conserved transmembrane ER kinase/RNA splicing factor IRE1 (IRE1A and IRE1B), whose primary target is the transcription factor *bZIP60* mRNA (Koizumi et al., 2001; Deng et al., 2011). The second arm is mediated by ER membrane-associated transcription factors bZIP17 and bZIP28, which are functional homologs of ATF6 in metazoans (Liu et al., 2007). The last arm is mediated by the ER membrane-localized heterotrimeric G-protein  $\beta$  subunit AGB1 (Wang et al., 2007; Chen and Brandizzi, 2012) and possibly by other G-protein subunits, such as  $G\alpha$  subunits XLG1/2/3 and the  $G\gamma$  subunits AGG1/2/3 (Chakravorty et al., 2015). AGB1 is required for UPR signaling under ER stress conditions (Wang et al., 2007; Chen and Brandizzi, 2012), but its UPR function in growth and defense has not yet been reported.

Heterotrimeric G-proteins are the most commonly used signal transducers in eukaryotic cells. They transduce signals at the cytosolic surfaces of the plasma membrane (PM) and endoplasmic reticulum (ER) as  $G\alpha\beta\gamma$  heterotrimers,  $G\beta\gamma$  heterodimers or individual  $G\alpha$  subunits (Weiss et al., 1997; Kaydamov et al., 2000; Wang et al., 2007; Hewavitharana and Wedegaertner, 2012; Giannotta et al., 2012; Klayman and Wedegaertner, 2017).  $G\beta\gamma$  dimers and  $G\alpha\beta\gamma$  trimers are thought to assemble on the ER membrane (Dupre et al., 2007; Marrari et al., 2007), and are anchored to membranes by virtue of lipid modifications on the  $G\alpha$  and  $G\gamma$  subunits (Wedegaertner 1998; Adjobo-Hermans et al., 2006; Zeng et al., 2007). *Arabidopsis* has at least four  $G\alpha$  (GPA1, XLG1/2/3), a  $G\beta$  (AGB1), and three  $G\gamma$  (AGG1/2/3) subunits (Chakravorty et al., 2015; Maruta et al., 2015; Thung et al., 2012), and likely more non-canonical G-protein subunits yet to be discovered (Lee and Assmann, 1999; Chakravorty et al., 2011). All known G-protein subunits are involved in some aspect of growth and development (Lease et al., 2001;

Ullah et al., 2001; Ullah et al., 2003; Trusov et al., 2007; Ding et al., 2008; Chakravorty et al., 2011). In addition, a subset – G $\alpha$  GPA1, G $\beta$  AGB1 and G $\gamma$  AGG3 – are involved in BR signaling in sugar-responsive growth (Peng et al., 2018), and all save two – XLG1 and AGG3 – are involved in flagellin signaling (Ishikawa 2009; Zhang et al., 2008; Zhu et al., 2009; Liu et al., 2013; Torres et al., 2013; Maruta et al., 2015; Miller et al., 2016). Recently, AGB1 has been shown to be a shared component in BR and flagellin signaling via interactions with corresponding receptors BRI1 and FLS2, presumably at the PM, and with the BR transcription factor BES1 in the nucleus, downstream of receptor signaling (Liang et al., 2016; Peng et al., 2018; Zhang et al., 2018). The essential role of G-proteins in both BR and flagellin signaling pathways suggests that they may function as rate-limiting factors between both pathways to mediate tradeoffs between growth and immunity.

Here, we show that AGB1 and G $\gamma$  subunits AGG1 and AGG2 work together in UPR signaling to mediate growth-defense tradeoffs that are upstream of BR and flagellin signaling and independent of ER stress. Specifically, they interact with nascent FLS2 and BRI1 proteins at the ER membrane and repress an UPR response that is hardwired to promote BRI1 protein biogenesis and FLS2 protein degradation via autophagy.

## **RESULTS**

### *Increased BRI1 signaling likely contributes to enhanced growth of *agg1 agg2**

While the loss-of-function *agb1* mutant exhibited growth defects due to its involvement in multiple hormone signaling pathways, (Ullah et al., 2003; Chen et al., 2004; Pandey et al., 2006; Trusov et al., 2006), the loss-of-function *agg1 agg2* double mutant exhibited increased vegetative growth and faster transition to inflorescence development compared to WT and *agb1* (Fig. 2.1A; Fig. S2.1A). To identify the G $\gamma$  subunit(s) interacting with AGB1 in the crosstalk between BR and flagellin signaling, we performed a time course of seedling growth and BRI1

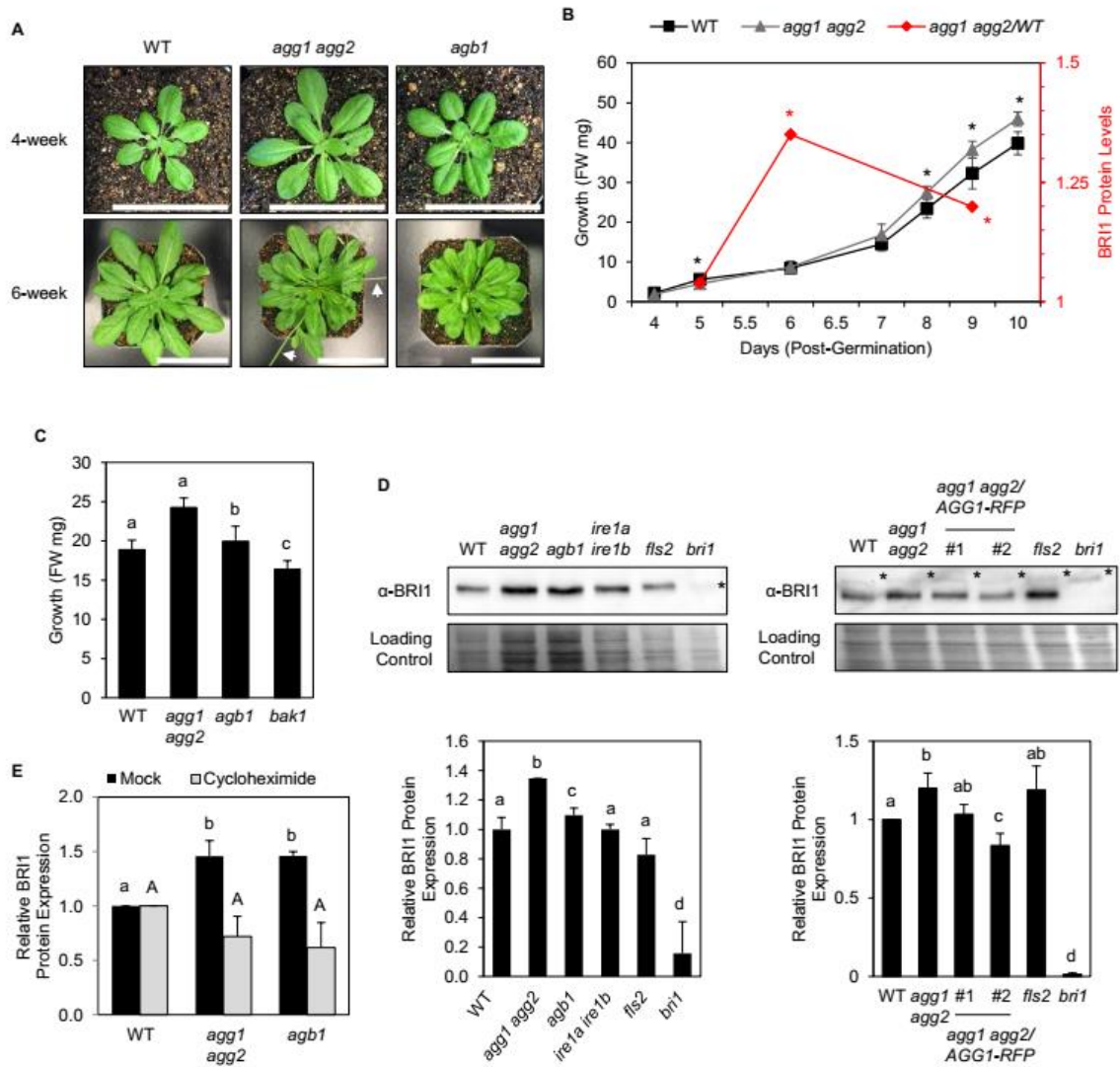


**Figure 2.1. Increased BRI1 signaling contributes to enhanced growth of *aggl aggl2* mutant.** (A) Growth pictures of 4-week-old and 6-week-old plants. White arrows indicate flowering stems. White bars represent 10 cm. (B) Time course of growth and BRI1 protein expression. Asterisks indicate significant differences from WT ( $P$ -value  $< 0.05$ , two-tailed  $t$  test) Data represent mean  $\pm$  SD of three replicates of five seedlings. FW, fresh weight. (C) Growth analysis of 9-day-old plants. (D) Immunoblot analysis of BRI1 protein in untreated 6-day-old plants (left) and 9-day-old plants pretreated with 20  $\mu$ M  $\beta$ -estradiol for 60 hr (right). Asterisks indicate non-specific protein bands. (E) BRI1 protein expression in 5.5-day-old plants in response to DMSO (mock) or 50  $\mu$ M cycloheximide for 6 hr. Data in (C–E) represent mean  $\pm$  SD of three replicates of twelve seedlings. Different letters in (C–E) indicate significant differences ( $P$ -value  $< 0.05$ , two-tailed  $t$  test).

protein expression under normal growth conditions. The loss-of-function *agg1 agg2* mutant exhibited increased BRI1 protein expression relative to WT after day 6 post-germination, correlating with its increased growth after day 8 (Fig. 2.1B–D; Fig. S2.2A). Although the loss-of-function *agb1* mutant exhibited normal seedling growth (Fig. 2.1C), it displayed slightly increased BRI1 protein expression after day 6 (Fig. 2.1C–D). To confirm our genetic results, we used the estrogen receptor-based *XVE* system to drive *AGG1-RFP* expression in *agg1 agg2 (agg1 agg2/XVE:AGG1-RFP)*. Induced expression of *AGG1-RFP* reduced BRI1 protein expression to WT level or below in 9-day-old seedlings (Fig. 2.1D).

To investigate whether increased BRI1 protein expression in *agg1 agg2* and *agb1* is due to increased transcription and/or translation, we measured *BRI1* gene expression during a 24-hr time period in 4-hr increments and measured BRI1 protein expression in 5.5-day-old seedlings pretreated with the protein translation inhibitor cycloheximide (CHX). *agg1 agg2* and *agb1* plants exhibited increased *BRI1* expression relative to WT throughout the time period (Fig. S2.2B), consistent with the observed BRI1 protein expression pattern (Fig. 2.1D) and indicative of G-protein-dependent transcription. In addition, CHX treatment inhibited developmental upregulation of BRI1 protein expression in *agg1 agg2* and *agb1* (Fig. 2.1E). These results indicate that increased transcription and translation are likely responsible for the increased BRI1 protein expression in G-protein mutants. *BRI1*-overexpression has been demonstrated to confer enhanced BR signaling in plants (Belkhadir et al., 2012), whereas mutants impaired in BRI1 signal transduction, such as *bak1*, exhibited reduced growth (Fig. 2.1C; Clouse et al., 1996; Li et al., 2002). Our findings suggest that BR signal transduction is increased in the *agg1 agg2* mutant, contributing to its increased growth under normal growth conditions.

Increased FLS2 protein turnover contributes to enhanced growth of *agg1 agg2* under defense-inducing conditions

*BRI1*-overexpression also confers reduced FLS2-mediated immune responses (Belkhadir et al., 2012). To investigate whether transient growth-defense tradeoffs are affected in the *agg1 agg2* mutant upon flagellin perception, we measured seedling growth inhibition (SGI) in response to the active epitope of bacterial flagellin, flg22. Consistent with *BRI1*-overexpression plants (Belkhadir et al., 2012), *agg1 agg2* exhibited a reduced flg22-induced growth inhibition response relative to WT after day 5 (Fig. 2.2A; Fig. S2.3A–B), whereas induced expression of *AGGI-RFP* restored flg22-induced growth inhibition in *agg1 agg2* to WT level (Fig. 2.2A). Although *agb1* exhibited a normal growth inhibition response (Fig. 2.2A), we used the 35S system to drive *YFP-AGBI* expression in *agb1* (*agb1/35S:YFP-AGBI*). Constitutive expression of *YFP-AGBI* increased flg22-induced growth inhibition in *agb1* relative to WT (Fig. 2.2A). As a control, we measured FLS2 protein expression in *agg1 agg2* and *agb1* and found that they exhibited reduced FLS2 protein expression (Fig. 2.2B), whereas induced expression of *AGGI-RFP* restored FLS2 protein expression to or above that of WT (Fig. 2.2B). To confirm these results, we measured FLS2 protein expression during a 24-hr time period in 4-hr increments. *agg1 agg2* exhibited decreased FLS2 protein expression relative to WT throughout most of the day with peak reductions occurring at night (Fig. S2.2C). To investigate whether reduced FLS2 protein expression in *agg1 agg2* is due to transcription, translation and/or protein degradation, we measured *FLS2* gene expression during a 20-hr period in non-treated plants and measured FLS2 protein expression during a 16-hr period in plants pretreated with CHX. *agg1 agg2* and *agb1* exhibited increased *FLS2* expression relative to WT 4 hr after dawn and reduced *FLS2* expression 4 hr after dusk, which does not correlate with the observed FLS2 protein expression pattern (Fig. S2.3C–D) and is indicative of G-protein-dependent transcription. In addition, CHX treatment revealed that FLS2 protein expression was more reduced in *agg1 agg2* relative to WT at an

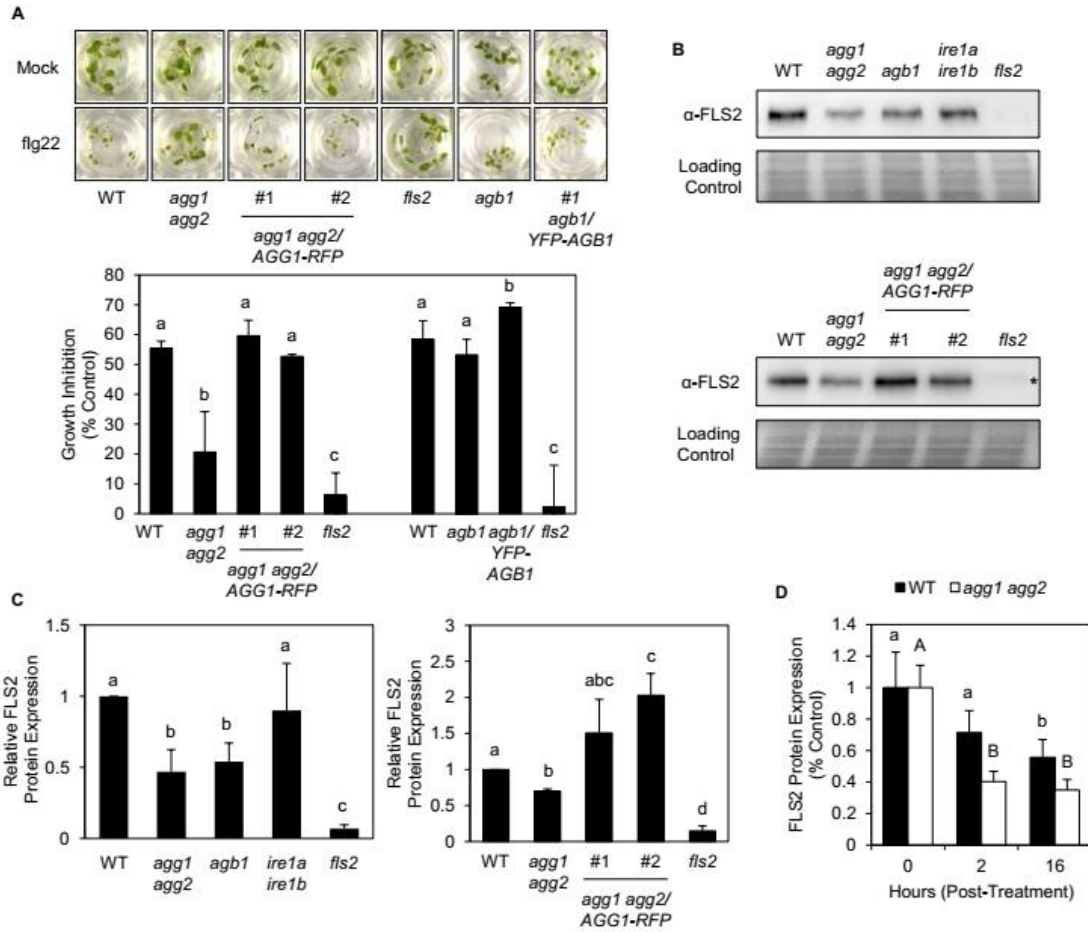


**Figure 2.2. Increased FLS2 turnover contributes to enhanced growth of *agg1 agg2* mutant under defense-inducing conditions.** (A) Growth inhibition analysis of 9-day-old plants pretreated with 20  $\mu$ M  $\beta$ -estradiol and water (control) or 100 nM flg22 for 6 days. Data represent mean  $\pm$  SD of four (*fls2*) or five (all others) replicates of five seedlings. (B–C) Immunoblot analysis of FLS2 protein in untreated (B, top) and  $\beta$ -estradiol-pretreated (B, bottom) 9-day-old plants. Asterisks indicate non-specific protein bands. Data in (C) represent mean  $\pm$  SD of six (left) and three (right) replicates of twelve seedlings. (D) Time course of FLS2 protein expression in 9-day-old plants in response to 50  $\mu$ M cycloheximide. Data represent mean  $\pm$  SD of three replicates of twelve seedlings. Different letters in (A and C–D) indicate significant differences ( $P$ -value  $< 0.05$ , two-tailed  $t$  test).

earlier time point (Fig. 2.2D), indicative of increased protein degradation. These findings suggest that increased FLS2 protein turnover contributes to the enhanced growth observed in *agg1 agg2* under defense conditions.

To determine whether the increased turnover in *agg1 agg2* affects newly synthesized FLS2 proteins on the ER membrane or mature FLS2 proteins on the PM, we performed aqueous two-phase partitioning of total membrane proteins and measured FLS2 abundance among microsomal membrane (MM) and PM proteins. *agg1 agg2* exhibited a decrease in FLS2 protein expression at both membrane populations (Fig. S2.3E). Since membrane proteins on the PM must exit the ER, this result suggests that nascent FLS2 proteins at the ER membrane are targeted for turnover in the *agg1 agg2* mutant.

To confirm that increased BRI1 signaling and/or increased FLS2 turnover in *agg1 agg2* contributes to reduced FLS2-mediated immune responses, we measured activation of mitogen-associated kinases (MAPKs) and callose deposition at the cell wall in response to flg22. *agg1 agg2* exhibited reduced flg22-induced MAPK activation and callose deposition responses relative to WT (Figs. S2.4 and S2.5), whereas induced expression of *AGG1-RFP* restored MAPK activation in *agg1 agg2* to WT level (Fig. S2.4C) and increased callose deposition 2-fold (Fig. S2.5). On the other hand, *agb1* exhibited a normal flg22-induced MAPK activation response (Fig. S2.4A). *agb1* also exhibited a reduced callose deposition response that could not be rescued by constitutive expression of *AGB1* (Fig. S2.5), likely due to poor 35S promoter expression in seedling leaves (Kamo et al., 2000).

#### *Growth and defense are uncoupled in agg1 agg2 mutant*

BR signaling has been shown to antagonize FLS2-mediated immune responses downstream of receptor signaling (Albrecht et al., 2012; Belkhadir et al., 2012; Lozano-Durán et al., 2013; Fan et al., 2014). *agg1 agg2* exhibits enhanced growth under growth-inducing

conditions and defense-inducing conditions, consistent with the increased and decreased expression of respective BRI1 and FLS2 in this mutant (Figs. 2.1 and 2.2). To investigate whether the negative crosstalk between BR and flagellin signaling is preserved in *agg1 agg2*, we measured three FLS2-mediated immune responses (i.e., defense response gene transcription, callose deposition and seedling growth inhibition) in response to the BR hormone 24-epibrassinolide (BL). Consistent with a previous report (Albrecht et al., 2012), MAPK-activated transcription of defense response genes *CYP81F2* and *CYP82C2* (Boudsocq et al., 2010) was reduced in WT seedlings in response to co-treatment with 1  $\mu$ M BL and 100 nM flg22 compared to flg22 treatment alone (Fig. 2.3A). Similarly, callose deposition and growth inhibition were reduced in WT plants and unchanged in BRI1 signaling mutant *bak1* in response to co-treatment with BL and flg22 (Fig. 2.3B–C). By contrast, *agg1 agg2* exhibited no changes in defense gene transcription, smaller reductions in callose deposition relative to WT, and no changes in growth inhibition in response to BL and flg22 (Fig. 2.3A–C), whereas *agb1* resembled WT plants in all three FLS2-mediated immune response (Fig. 2.3A–C). These results indicate that growth and defense are uncoupled in the *agg1 agg2* mutant.

Interestingly, *agg1 agg2* and *agb1* exhibited reduced growth in response to 1  $\mu$ M BL alone (Fig. 2.3C). High BR concentrations and/or signaling can inhibit growth (Clouse et al., 1996; Müssig et al., 2003; González-García et al., 2011), indicating that an appropriate intensity of BR signaling is important for optimal plant growth. To investigate whether increased BRI1 signaling in *agg1 agg2* is responsible for its increased insensitivity to exogenous BL application, we measured hypocotyl lengths in response to 1 and 10  $\mu$ M BL. At 1  $\mu$ M BL, the concentration reported to result in nearly full BL responsiveness in this tissue (Clouse et al., 1996), *agg1 agg2* and *agb1* exhibited a normal hypocotyl elongation response, whereas at 10  $\mu$ M BL, they exhibited reduced BL responsiveness (Fig. S2.6A–B). By contrast, induced expression of *AGGI-RFP* and constitutive expression of *YFP-AGBI* restored WT level of BL sensitivity in respective

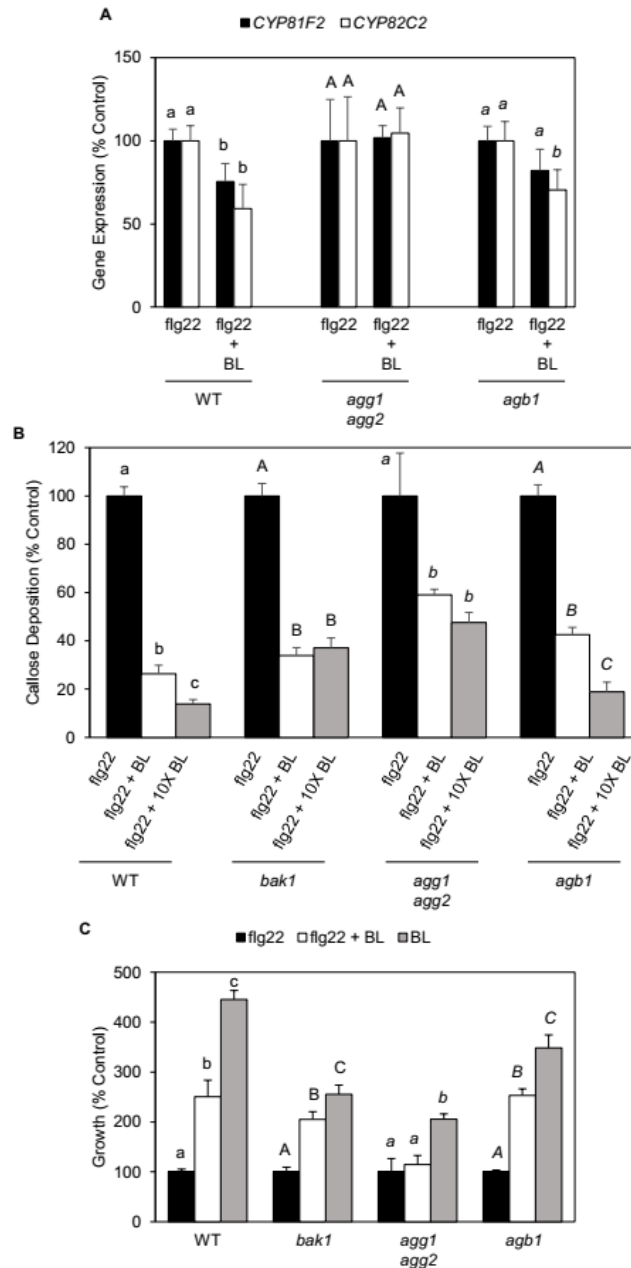


**Figure 2.3. Growth and defense are uncoupled in *agg1 agg2* mutant.** (A) qPCR analysis of MAPK-activated defense genes *CYP82C2* and *CYP81F2* in 9-day-old plants pretreated with water (mock), 1  $\mu$ M 24-epibrassinolide (BL), and/or 100 nM flg22 for 3 hr. Data represent mean  $\pm$  SD of four replicates of twelve seedlings. (B) Callose deposition analysis of 9-day-old plants pretreated with DMSO (control), 0.1  $\mu$ M or 1  $\mu$ M BL for 6 hr and then elicited with 1  $\mu$ M flg22 for 16-18 hr. Data represent mean  $\pm$  SE of fifteen replicates. (C) Growth analysis of 9-day-old plants pretreated with DMSO (mock), 100 nM flg22, and/or 100 nM BL for 6 days. Data represent mean  $\pm$  SD of five replicates of five seedlings. Different letters in (A–C) indicate significant differences ( $P$ -value  $< 0.05$ , two-tailed  $t$  test).

*agg1 agg2* and *agb1* plants treated with 10  $\mu$ M BL (Fig. S2.6B). These results lend further support to increased BRI signaling occurring in G-protein mutants.

*AGG1 and AGG2 are involved in UPR signaling in the absence of ER stress*

AGB1 is enriched in the ER, where it functions as an UPR sensor during ER stress (Wang et al., 2007; Chen and Brandizzi, 2012). To investigate whether UPR signaling is affected in the *agg1 agg2* mutant, we measured seedling growth inhibition in response to ER stress induced by tunicamycin (Tn). Consistent with previous reports on the *agb1* mutant (Chen and Brandizzi, 2012; Chakravorty et al 2015), *agg1 agg2* is hyper-responsive to long-term (14 days) Tn-induced ER stress (Fig. 2.4A). In fact, dose-response curves indicate that *agg1 agg2* is more sensitive to Tn-induced ER stress than UPR signaling mutants *agb1* and *ire1a ire1b* (Fig. 2.4A). We then looked for changes in expression of UPR-activated genes in response to short-term (5 hr) Tn-induced ER stress and observed increased expression of *IRE1A* and *IRE1B*, their spliced target *bZIP60s*, and G-protein genes *AGB1*, *AGG1* and *AGG2* (Fig. 2.4B). Furthermore, *IRE1A*, *IRE1B* and *bZIP60s* were expressed normally in *agg1 agg2* and *agb1* mutants in response to short-term Tn-induced ER stress, whereas *AGG1* and *AGB1* were downregulated in *ire1a ire1b* mutant (Fig. 2.4B), indicative of IRE1A/B-dependent transcription.

IRE1A/B and AGB1 have been shown to respectively upregulate and downregulate the gene expression of the chaperone and IRE1A/B ligand BIP3 in response to long-term (3 days) Tn-induced ER stress (Chen and Brandizzi, 2012). Consistent with this finding, combined BIP1–3 (BIP) protein expression was reduced in *ire1a ire1b* relative to WT and *agb1* independent of ER stress, whereas ER stress-induced expression of folding catalyst PDI was unchanged in *agg1 agg2*, *agb1* and *ire1a ire1b* (Fig. S2.7). Furthermore, *agg1 agg2* exhibited increased *BIP3* expression in response to short-term (5 hr) Tn-induced ER stress (Fig. 2.4B), whereas *BIP3* expression was unchanged in WT, *ire1a ire1b*, and *agb1* (Fig. 2.4B). More importantly, *ire1a ire1b* exhibited normal BRI1 and FLS2 protein expression (Figs. 2.1C and 2.2B), and *agg1 agg2*

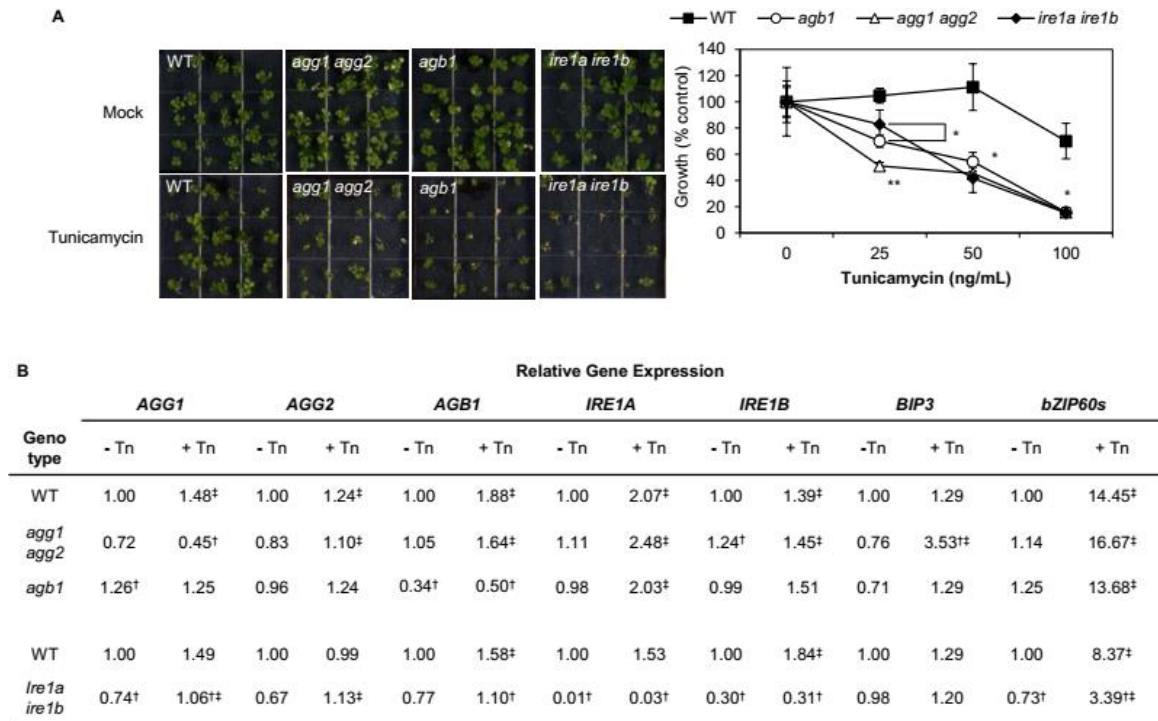


**Figure 2.4. AGG1 and AGG2 are involved in UPR signaling.** (A) Growth inhibition analysis of 14 day-old plants in response to 0 (control), 25, 50 and 100 ng mL<sup>-1</sup> tunicamycin. Data represent mean  $\pm$  SD of five replicates of five seedlings. Asterisks indicate significant differences from WT; double asterisks indicate significant differences from WT, *agb1* and *ire1a ire1b*. (B) qPCR analysis of UPR-activated genes in 9-day-old seedlings pretreated with 5  $\mu$ g mL<sup>-1</sup> tunicamycin (+Tn) or DMSO (-Tn) for 5 hr. Data represent mean  $\pm$  SD of four replicates of twelve seedlings. Single dagger indicates significant differences from WT; double daggers indicate significant differences from -Tn samples ( $P$ -value  $< 0.05$ , two-tailed  $t$  test; FDR  $< 0.5$ ).

and *agb1* exhibited no upregulation of *IRE1A/B*, *BIP3* and *bZIP60s* gene expression or PDI protein expression in the absence of ER stress (Fig. 2.4B; Fig. S2.7). Thus, IRE1A/B and G-proteins have distinct UPR functions independent of ER stress. Altogether, these findings suggest that AGB1 and AGG1/2 work together to promote FLS2 biogenesis and repress BRI1 biogenesis through UPR signaling in the absence of ER stress.

*AGB1-AGG1/2 interact with FLS2 and BRI1 at the ER membrane*

AGB1 forms obligate heterodimers with AGG1 and AGG2 (Mason and Botella, 2000; Adjobo-Hermans et al., 2006; Chakravorty and Botella, 2007), and interacts with FLS2 and BRI1 *in vivo* (Liang et al., 2016; Peng et al., 2018). To investigate whether AGB1 and/or AGG1 interact with nascent FLS2 and BRI1 proteins at the ER membrane, we first detected AGG1, AGB1, BRI1 and FLS2 proteins that were C-terminally tagged with GFP or RFP in *Nicotiana benthamiana* leaves. Consistent with a previous report (Adjobo-Hermans et al., 2006), AGG1 co-localized with AGB1 at the PM (Fig. S2.8A), and with FLS2 at plasmolysis-induced Hechtian strands, which are PM fragments still attached to the cell wall and separated from the cytosol (Fig. S2.8B). AGG1 also co-localized with AGB1 and FLS2 at the highly reticulated ER membrane and with the ER protein marker HDEL (Fig. 2.5A; Gomord et al., 1997). The ER localization of AGG1 was further validated in *agg1 agg2/XVE:AGG1-RFP* plants (Fig. S2.8C). AGG1 and AGB1 also co-localized with BRI1 at the ER membrane (Fig. S2.8D). These results confirmed that the C-terminal tag did not disrupt AGG1's lipid modification and subsequent localization of AGG1 and its partner AGB1 to membranes.

We then immunoprecipitated AGG1-GFP and AGB1-GFP proteins from PM and MM protein extracts of *N. benthamiana* leaves as well as YFP-AGB1 and AGG1-RFP proteins from PM and MM protein extracts of Arabidopsis seedlings. FLS2-RFP and native FLS2 protein co-immunoprecipitated with respective AGG1-GFP and AGG1-RFP at the PM and MM (Fig. 2.5B–C). Native FLS2 also co-immunoprecipitated with YFP-AGB1 at the PM and MM in Arabidopsis

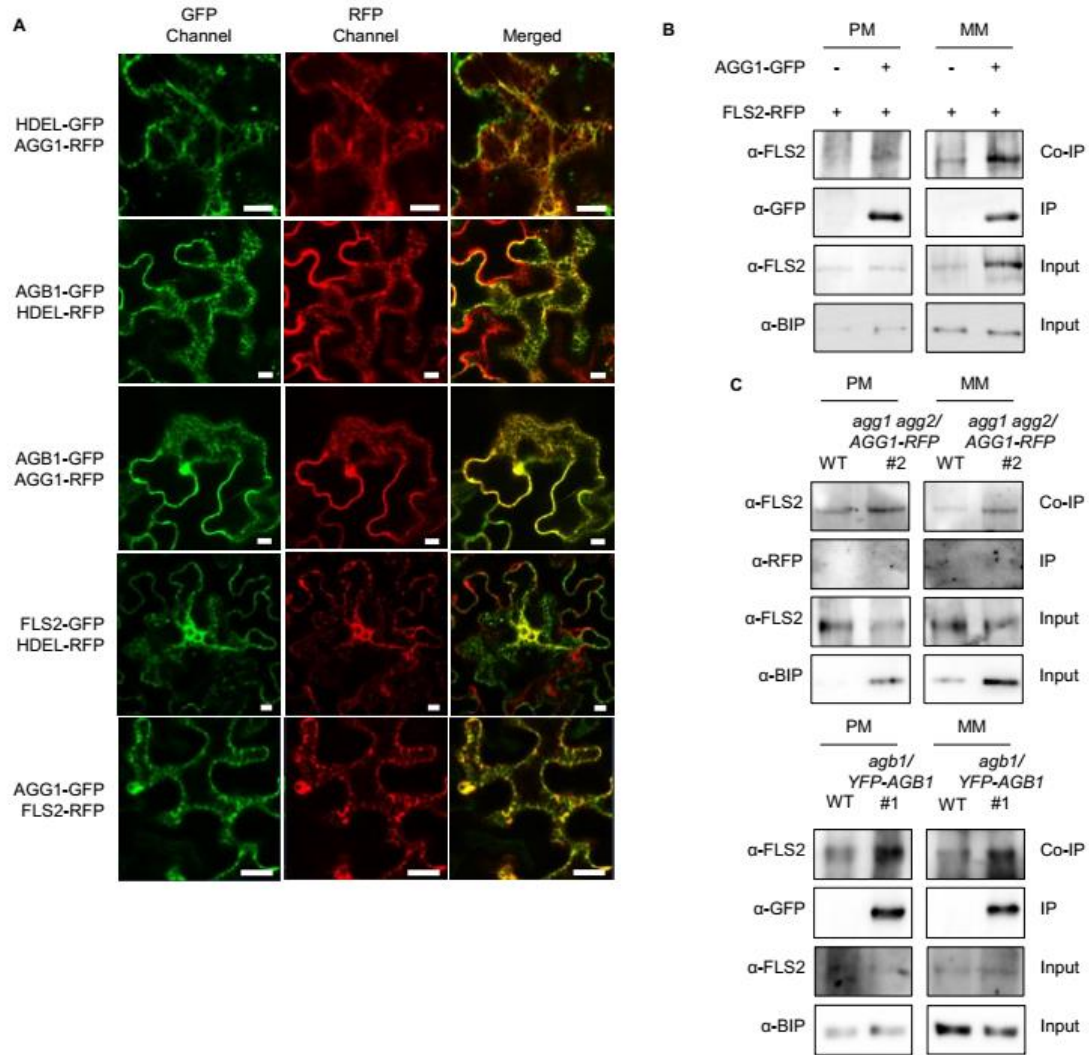


**Figure 2.5. AGB1-AGG1/2 interact with FLS2 at the ER membrane.** (A) Co-localization of AGG1 with AGB1 and FLS2 at the ER membrane in transfected *N. benthamiana* leaves pretreated with 20  $\mu$ M  $\beta$ -estradiol for 4-8 hr. HDEL is an ER marker. White bars represent 20  $\mu$ m. (B) Immunoprecipitation (IP) of AGG1-GFP and co-immunoprecipitation (Co-IP) of FLS2-RFP from plasma membrane (PM) and microsomal membrane (MM) protein extracts of transfected *N. benthamiana* leaves pretreated with 20  $\mu$ M  $\beta$ -estradiol for 10 hr. BIP is an ER membrane-associated protein in the absence of ER stress. (C) IP of AGG1-RFP and YFP-AGB1 and Co-IP of native FLS2 from PM and MM protein extracts of 9-day-old *agg1 agg2/XVE:AGG1-RFP* pretreated with 20  $\mu$ M  $\beta$ -estradiol for 48 hr and untreated *agb1/35S:YFP-AGB1* plants.

(Fig. 2.5C). Similarly, BRI1-RFP co-immunoprecipitated with AGG1-GFP and AGB1-GFP at the PM and MM in *N. benthamiana* (Fig. S2.9). We were unable to confirm the BRI1-AGB1/AGG1 interactions in Arabidopsis due to the relatively weak antibody for the native BRI1 protein. Our findings suggest that AGG1 and AGB1 work together in UPR signaling to mediate growth-defense tradeoffs that involve direct interactions with nascent FLS2 and BRI1 proteins at the ER membrane.

*Combination of *agg1 agg2* and *atg7/3* promotes robust growth and defense*

To investigate whether FLS2 protein is being targeted by UPR-associated protein degradation processes in *agg1 agg2*, we measured FLS2 protein expression in seedlings pretreated with chemical inhibitors of ERAD and autophagy. Co-treatment of proteasome inhibitor MG132 and autophagy inhibitor E-64D (Oh-ye et al., 2011) or concanamycin A (Con A) (Yoshimoto et al., 2004), or that of E-64d and Con A restored FLS2 protein expression in *agg1 agg2* to or above WT level, whereas single treatments did not (Fig. S2.10A). We then measured the flg22-induced seedling growth inhibition response in the presence of these inhibitors. Co-treatment of MG132 and E-64d restored growth inhibition in *agg1 agg2* to WT level, whereas single treatments did not (Fig. S2.10B). Furthermore, MG132 and E-64d co-treatments did not significantly affect growth in WT or *agg1 agg2* plants relative to mock treatment (Fig. S2.10C), whereas treatments with Con A at nano-molar concentrations proved toxic and were thus removed from analysis. These data suggest that UPR-associated degradation of nascent FLS2 proteins involves autophagy and/or ERAD.

To confirm these findings, we knocked out the two autophagy-requiring ubiquitin-like conjugation systems in the *agg1 agg2* mutant by introducing loss-of-function mutations in the E1-like *ATG7* and E2-like *ATG3* genes by intermutant crosses (Klionsky 2005; Ohsumi 2001; Kim et al., 2012). We then measured flg22-induced growth inhibition and FLS2 protein expression in the *agg1 agg2 atg7* and *agg1 agg2 atg3* triple mutants. Flg22-induced growth

inhibition and FLS2 protein expression were both restored in *agg1 agg2 atg7* and *agg1 agg2 atg3* to or greater than WT levels (Fig. 2.6A–B). To confirm that the recovered FLS2 proteins were not retained in the ER, we digested the proteins with endoglycosidase H (Endo H) enzyme to cleave off their ER-specific glycans. FLS2 proteins that exit the ER will acquire Golgi-specific glycans that are resistant to Endo H digestion. Wild-type FLS2 proteins were partially deglycosylated upon Endo H digestion, whereas FLS2 proteins produced in the *mns1 mns2 mns3* mutant lacked Golgi-specific glycans (Liebminger et al., 2009), and thus were fully deglycosylated (Fig. S2.11A). FLS2 proteins in the *agg1 agg2 atg7* and *agg1 agg2 atg3* plants were partially deglycosylated (Fig. S2.11A), indicating that they have exited the ER *en route* to the PM.

We then investigated whether inhibition of autophagy is sufficient to restore growth-defense tradeoffs in the *agg1 agg2* mutant. *agg1 agg2* exhibited reduced seedling flg22-induced MAPK activation response and adult leaf resistance to the virulent bacterial pathogen *Pseudomonas syringae* pv. *tomato* DC3000 (*Pto* DC3000), as well as enhanced seedling, vegetative and reproductive growth relative to WT (Fig. 2.6D; Figs. S2.1B and S2.11B). By contrast, *agg1 agg2 atg7* and *agg1 agg2 atg3* exhibited normal flg22-induced MAPK activation response and anti-bacterial defense, as well as normal growth and development relative to WT and *atg7/3* single mutants (Fig. 2.6C-D; Figs. S2.1 and S2.11B). Furthermore, *agb1* exhibited reduced anti-bacterial defense, whereas the double mutants *agb1 atg7* and *agb1 atg3* exhibited normal bacterial resistance and adult development relative to WT and *atg7/3* single mutants (Figs. S2.1 and S2.12). These findings indicate that AGB1 and AGG1/2 work together in UPR signaling to mediate growth-defense tradeoffs that involve repression of FLS2 protein degradation by autophagy.

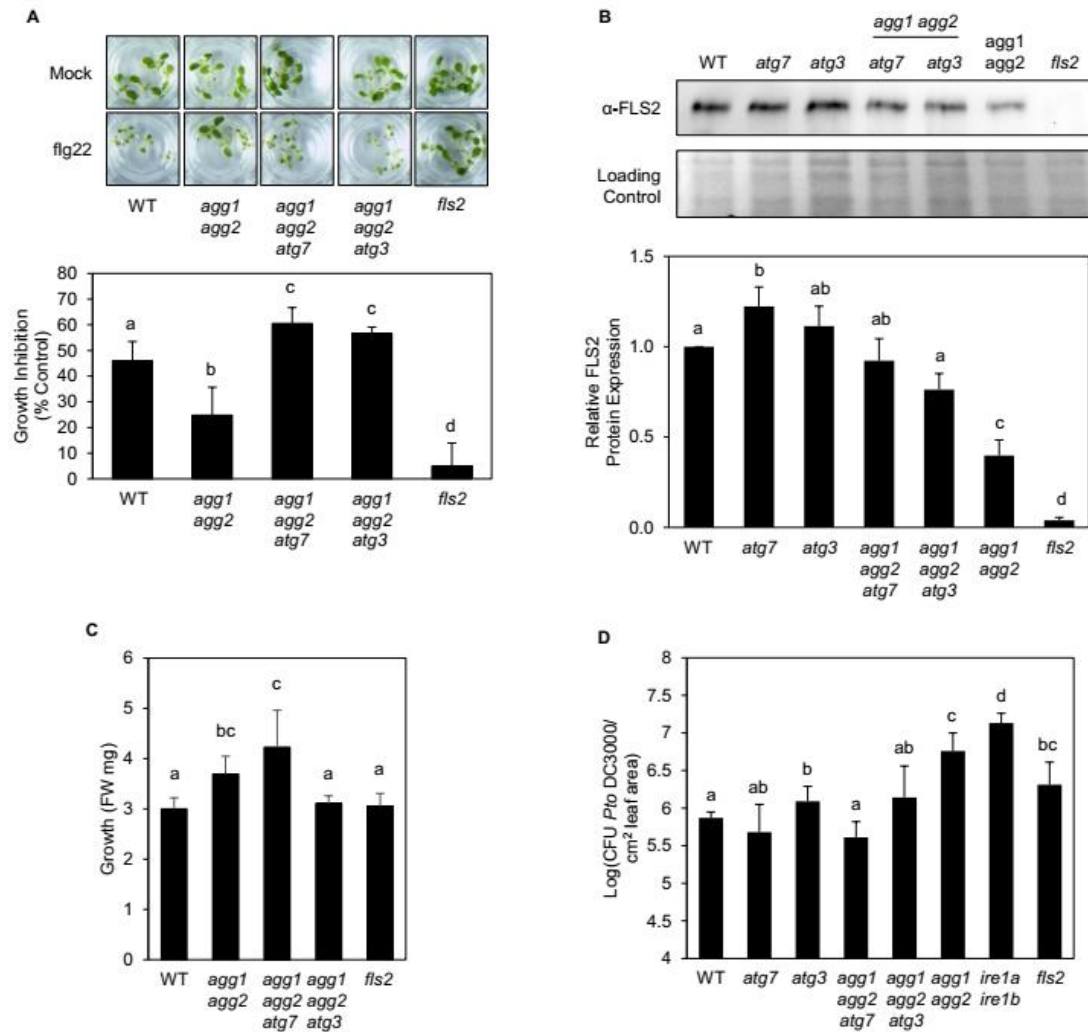


**Figure 2.6. Combination of *agg1 agg2* and *atg7/3* promotes robust growth and defense.** (A) Growth inhibition analysis of 9-day-old plants pretreated with water (control) or 100 nM flg22 for 6 days. Data represent mean  $\pm$  SD of four (*fls2*) or five (all others) replicates of five seedlings. (B) Immunoblot analysis of FLS2 protein in 9-day-old plants. Data represent mean  $\pm$  SD of six replicates of twelve seedlings. (C) Growth analysis of 9-day-old plants. Data represent mean  $\pm$  SD of four (*fls2*) or five (all others) replicates of five seedlings. (D) Growth analysis of bacterial pathogen *Pto* DC3000 in 5-week-old surface-inoculated leaves. Data represent mean  $\pm$  SD of six replicates. Different letters in (A–D) indicate significant differences ( $P$ -value  $< 0.05$ , two-tailed  $t$  test).

*UPR is hardwired to promote FLS2 protein degradation in the absence of ER stress*

To investigate whether UPR in growth-inducing conditions requires protein ‘triggers’ for selective protein degradation, we used the *XVE* system to drive expression of a *FLS2* transgene in *agg1 agg2 (agg1 agg2/XVE:FLS2)*. To our surprise, we obtained three independent lines (#2–4), whose *FLS2* protein expression was knocked-down to undetectable levels with or without *FLS2* induction, whereas their seedling growths were unchanged upon *FLS2* induction (Fig. 2.7A; Fig. S2.13). We also obtained one line (#1) whose *FLS2* protein expression and growth were increased to and greater than WT levels, respectively, in the absence of *FLS2* induction (Fig. 2.7A; Fig. S2.13). This finding lends further support to the uncoupling of growth and defense in the *agg1 agg2* mutant. Leaky expression of the *XVE* system has been reported in rice (Okuzaki et al., 2011) and appears to be sufficient to activate further increases in *FLS2* production and/or degradation. To confirm that *FLS2* production and subsequent degradation were activated in *agg1 agg2/XVE:FLS2* lines #2–4, we measured their *FLS2* protein expression after gene induction and co-treatment with E-64d and Con A and found *FLS2* protein expression to be restored to WT level for all three lines (Fig. 2.7B). Taken together, these data suggest that in the absence of *AGG1/2* and ER stress, UPR is hardwired to promote *BRI1* protein biogenesis and *FLS2* protein degradation via autophagy while at the same time responsive to transient and minute increases in *FLS2* protein expression (Fig. 2.7C).

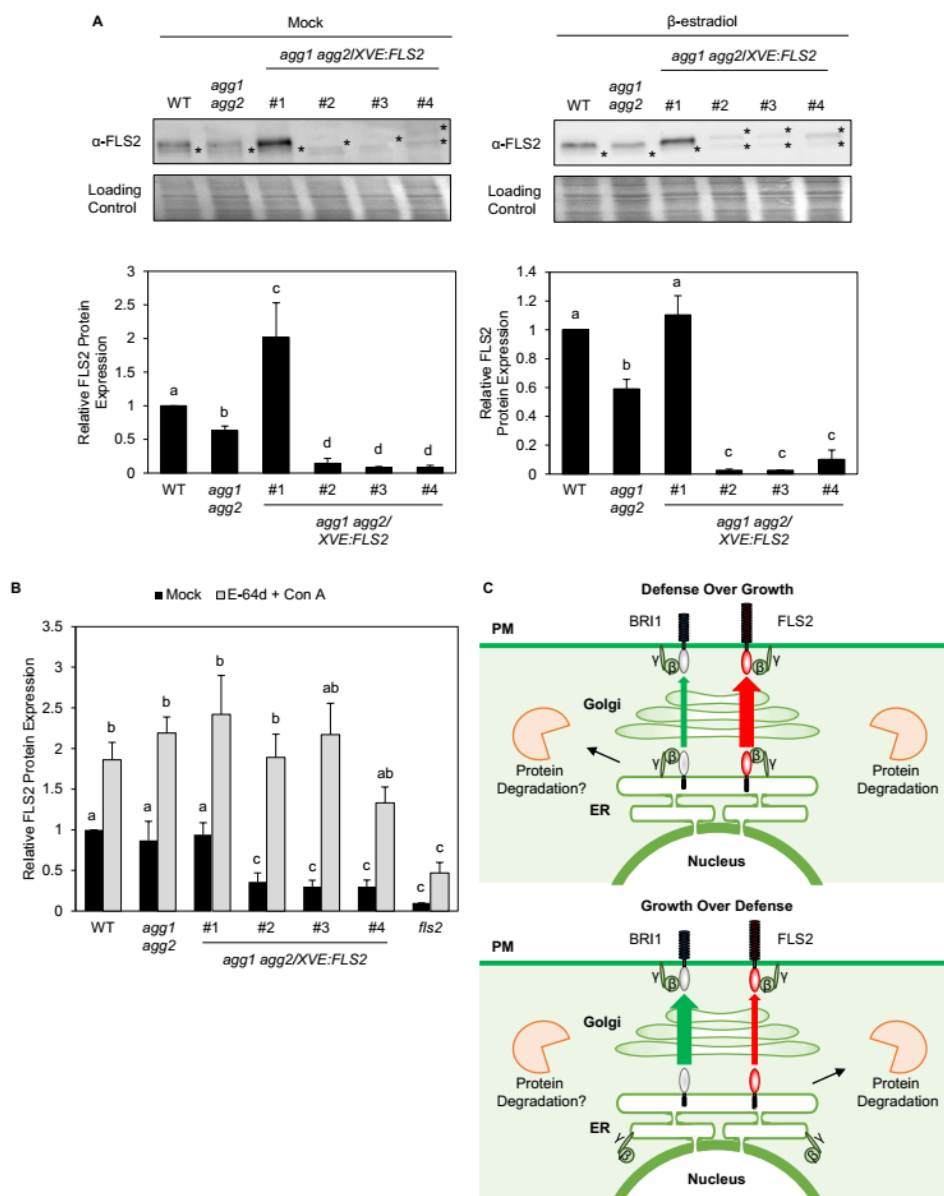


**Figure 2.7. UPR is hardwired to promote FLS2 protein degradation in the absence of ER stress.** (A) Immunoblot analysis of FLS2 protein in 9-day-old *agg1 agg2/XVE:FLS2* lines pretreated with DMSO (mock; left) or 20  $\mu$ M  $\beta$ -estradiol (right) for 48 hr. Asterisks indicate non-specific protein bands. Data represent mean  $\pm$  SD of three replicates of twelve seedlings. (B) FLS2 protein expression analysis of 6.5-day-old seedlings pretreated with 20  $\mu$ M  $\beta$ -estradiol for two days and then treated with DMSO (mock) or 20  $\mu$ M E-64d and 2  $\mu$ M Concanamycin A (Con A) for 1.5 days. Data represent mean  $\pm$  SE of four replicates of twelve seedlings. Different letters in (A–B) indicate significant differences ( $P$ -value  $< 0.05$ , two-tailed  $t$  test). (C) Proposed function of G-protein dimers in UPR under growth-inducing conditions. AGB1-AGG1/2 dimers mediate growth-defense tradeoffs between BL and flagellin signaling by interacting with nascent FLS2 proteins at the ER membrane and inhibiting their autophagic degradation either through signaling or sequestration. G-proteins also interact with nascent BRI1 proteins on the ER membrane to repress their biogenesis through an unknown mechanism.

## DISCUSSION

A key innovation of our study was the development of the *agg1 agg2 atg7/3* mutants and the *agg1 agg2/XVE:FLS2* transgenic lines. The removal of functionally redundant G $\gamma$  subunits caused hyperactivation of BRI1 protein biogenesis and FLS2 protein degradation and the uncoupling of growth and defense, while the removal of autophagy restored FLS2-mediated immune responses in *agg1 agg2* mutant. As a consequence, even though *agg1 agg2* plants exhibited enhanced growth and reduced defenses, *agg1 agg2 atg7/3* plants were able to grow and defend well at the same time. Transient FLS2 expression in *agg1 agg2* uncovered an anticipatory UPR-mediated response that appears hardwired to promote growth over defense and is actively repressed by G-proteins that directly interact with FLS2 at the ER. Although traditionally viewed as an adaptive response triggered by the accumulation of unfolded proteins in the ER, we show that UPR is also an anticipatory response that is activated well before the disruption of protein homeostasis. Our results provide the first evidence that G $\beta\gamma$  dimers mediate growth-defense tradeoffs through UPR signaling. Furthermore, their signaling function in the ER is independent of their canonical functions in the G $\alpha\beta\gamma$  heterotrimers at the PM. The ability to unlock or fine-tune growth-defense tradeoffs through UPR signaling provides a novel strategy to combine plant traits in ways that can have practical applications in biotechnology and agriculture.

A central premise underlying current views of growth-defense balance between BR and flagellin signaling is that the defense-defense antagonism is largely unidirectional (favoring growth over defense) and indirect (Lozano-Durán and Zipfel, 2015). This signaling architecture presumably serves to prevent autoimmunity and severe growth retardation from prolonged and/or de-regulated activation of immune receptors so that plants can excel in obtaining limited resources from their competitors. The ability of *agg1 agg2* plants to grow robustly at the expense of defense provides evidence that the growth-defense antagonism can be reversed to promote faster activation of immune receptors and overcome domestication-related tradeoffs against

defensive traits. Furthermore, AGB1-AGG1/2 heterodimers bind directly to BRI1 and FLS2 proteins at the ER membrane. In yeast and mammals, the binding of unfolded proteins to IRE1 directly activates UPR under ER stress-inducing conditions (Gardner and Walter, 2011; Karagöz et al., 2017). Similarly, the binding to BRI1 and FLS2 to AGB1-AGG1/2 may tune the homeostatic functions of UPR under conditions that favor growth and are independent of ER stress. Whether G-proteins in the ER also mediate growth-defense tradeoffs under defense-inducing conditions remains to be tested.

## METHODS

**Plant materials and growth conditions.** Surface-sterilized seeds of *Arabidopsis thaliana* accession Columbia-0 (Col-0) were stratified for at least 2 days and sown in 12- or 24-well microtiter plates sealed with parafilm. Each 12- or 24-well plate contained 12 and 5 seeds, respectively, with 1 and 0.5 mL of filter-sterilized 0.5X MS liquid (pH 5.7–5.8) [4.43 g/L Murashige and Skoog basal medium with vitamins (Murashige and Skoog, 1962) (Phytotechnology Laboratories, Shawnee Missions, KS), 0.05% (w/v) MES hydrate, 0.5% (w/v) sucrose], respectively. Alternatively, surface-sterilized and stratified seeds were sown on MS agar plates [0.5X MS, 0.75% (w/v) agar (PlantMedia, Chiang Mai, Thailand)] sealed with parafilm. Unless otherwise stated, sample-containing plates were placed on grid-like shelves over water trays on a Floralight cart (Toronto, Canada), and plants were grown at 21°C and 60% humidity under a 12-hr light cycle (70–80  $\mu\text{E m}^{-2} \text{s}^{-1}$  light intensity). Unless otherwise stated, media in microtiter plates were exchanged for fresh media on day 7. For bacterial infection experiments, *Arabidopsis* plants were grown on soil [3:1 mix of Fafard Growing Mix 2 (Sun Gro Horticulture, Vancouver, Canada) to D3 fine vermiculite (Scotts, Marysville, OH)] at 22°C daytime/18°C nighttime with 60% humidity under a 12-hr light cycle (100  $\mu\text{E m}^{-2} \text{s}^{-1}$  light intensity). *Nicotiana benthamiana* plants were grown on soil [3:1 mix] on a Floralight cart at 22°C under a 12-hr light cycle (100  $\mu\text{E m}^{-2} \text{s}^{-1}$  light intensity) for 4 weeks.

The following Col-0 T-DNA insertion lines and mutants were obtained from the Arabidopsis Biological Resource Center (ABRC, Columbus, Ohio): *agb1-1* (CS3976), *agb1-2* (CS6535), *agg1-1c* (CS16550), *agg2* (SALK\_039423), *agg1-1c/agg2-1* (CS16551), *atg7* (SAIL\_11\_H07), *fls2* (SAIL\_691\_C4).

**Vector construction and transformation.** To generate estradiol-inducible C-terminally tagged *GFP* and *RFP* (*XVE:X-G/RFP*) and *35S:YFP-AGBI* DNA constructs, *attB* sites were added via PCR-mediated ligation to the coding sequences of cDNAs, and the modified cDNAs were recombined into pDONR221 entry vector and then into pABindGFP, pABindRFP (Bleckmann et al., 2010) and pB7WGY2 (Karimi et al., 2002) destination vectors, according to manufacturer's instructions (Gateway manual; Invitrogen, Carlsbad, CA). *XVE:AGG1-RFP*, *XVE:FLS2-RFP*, and *35S:YFP-AGBI* constructs were introduced into *agg1-1c agg2-1* or *agb1-2* plants via *Agrobacterium*-mediated floral dip method (Clough and Bent, 1998), and transformants were selected on agar media containing 15 µg/mL hygromycin B (Invitrogen) or 15 µg/mL glufosinate (Cayman Chemical, Ann Arbor, MI). Transgene expression was induced 48 hr (or 5-6 days for growth assays) after elicitation with 20 µM β-estradiol (2 mM stock solution in DMSO; Sigma-Aldrich, St. Louis, MO). Transient expression of *XVE:X-G/RFP* constructs in *Nicotiana benthamiana* leaves was performed as previously described (Bleckman et al., 2010) with the following modification: transformed *Agrobacterium* strains were grown in LB medium supplemented with 50 µg/mL rifampicin, 30 µg/mL gentamycin, kanamycin 50 µg/mL and 100 µg/mL spectinomycin, in the absence of a silencing suppressor, to an OD<sub>600</sub> of 0.7. Transgene expression was induced 10 hr (for co-immunoprecipitation) and 4-8 hr (for microscopy) after spraying with 20 µM β-estradiol and 0.1% Tween-20.

**BL-induced hypocotyl elongation.** Seedlings were grown on MS agar supplemented with 1 or 10 µM 24-epibrassinolide (BL; Phytotechnology Laboratories). Sample-containing agar plates were placed vertically on a Floralight cart under a constant light cycle (140–180 µE m<sup>-2</sup> s<sup>-1</sup> light

intensity). Hypocotyl lengths were measured from images of 5-day-old seedlings using NIH ImageJ.

**Flg22-induced seedling growth inhibition.** Three-day-old seedlings in 24-well microtiter plates were elicited with water or 100 nM flg22 (QRLSTGSRINSAKDDAAGLQIA; Genscript, Nanjing, China) for 6 days. Fresh weights were measured from 9-day-old seedlings that were dried between paper towels for a few seconds.

**Flg22-induced Callose Deposition.** 9-day-old seedlings were elicited with 1  $\mu$ M flg22 for 16-18 hr. Alternatively, 9-day-old seedlings were treated with DMSO, 100 nM BL, or 1  $\mu$ M BL 6 hours prior to flg22 elicitation. Callose deposition staining was performed as previously described (Clay et al., 2009). Callose deposits were viewed on a Zeiss (Oberkochen, Germany) AxioObserver D1 fluorescence microscope under UV illumination with Filter Set 49 (excitation filter 365 nm; dichroic mirror 395 nm; emission filter 445/50 nm). Callose deposits were quantified using NIH ImageJ.

**Flg22-induced MAPK activation.** 9-day-old seedlings were elicited with 100 nM flg22 for 5, 15, and/or 30 min. MAPK activation assay was performed as previously described (Lawrence et al., 2017). 20  $\mu$ L of supernatant was loaded onto a 10% SDS-PAGE gel, and the separated proteins were transferred to PVDF membrane (Millipore) and probed with phosphor-p44/p42 MAPK (Cell Signaling Technology, Danvers, MA) and MPK3 antibodies (Sigma-Aldrich, St. Louis, MO) at 1:2000 dilution in 5% (w/v) nonfat milk in 1X PBS. The combined signal intensities of phosphorylated MPK3/4/6 were quantified using NIH ImageJ and normalized to that of total MPK3 (loading control).

**Total protein extraction, SDS-PAGE, and western blotting.** Total protein was extracted from snap-frozen seedlings into 80  $\mu$ L of extraction buffer [50 mM Tris-Cl (pH 7.5), 50 mM DTT, 4% (w/v) SDS, 10% (v/v) glycerol] using a 5-mm stainless steel bead and ball mill (20 Hz for 3 min).

Samples were centrifuged briefly, incubated at 95°C for 10 min, and centrifuged at 12,000 x g for 8 min to precipitate insoluble material. Endo H treatment was performed as previously described (Lawrence et al., 2017). 5 or 10 µL of extract were loaded onto a 8.5% SDS-PAGE gel, and the separated proteins were transferred to PVDF membrane (Millipore, Billerica, MA), stained with Ponceau S for labeling of total protein (loading control), and probed with either BRI1 (Agrisera), FLS2 (antigen: CTKQRPTSLNDEDSQ; Genscript), RFP (MBL International, Woburn, MA), GFP (Roche, Basel, Switzerland), BIP (Enzo Life Sciences, Farmingdale, NY), PDI antibodies at 1:500 (BRI1), 1:1000 (FLS2, RFP, GFP) and 1:5000 (BIP, PDI) dilutions in 5% (w/v) nonfat milk in 1X PBS. Signal intensities of immuno-detected proteins were quantified using NIH ImageJ and normalized to that of loading control.

**Aqueous 2-phase partitioning and immunoprecipitation.** Microsomal membrane (MM) and plasma membrane (PM) proteins were isolated from 250 mg of snap-frozen plant tissue using Minute Plasma Membrane Protein Isolation Kit for Plants (Invent Biotechnologies, Plymouth, MN). Membrane protein pellets were extracted into 250 µL of extraction buffer [50 mM Tris-Cl, pH 7.5, 150 mM NaCl, 1% NP-40, 10% glycerol, 2 mM EDTA, 5 mM DTT, complete-mini protease inhibitor cocktail (Roche), 5 µM AEBSF] for 1 hr at 4°C with rocking and clarified at 8,000 x g for 10 min. Twenty microliters of extract was set aside as input. Membrane proteins were immunoprecipitated with 2.5 µL of antibody for 4 hr at 4°C with rocking followed by 25 µL of 50% slurry of Protein A/G magnetic beads (EMD Millipore, Burlington MA) for 1 hr at 4°C with rocking, and washed 3x with 350 µL of wash buffer (50 mM Tris-Cl, pH 7.5, 150 mM NaCl). Enrichment of ER membrane proteins in the MM protein extracts was confirmed by western blotting using BIP antibody.

**RNA isolation and quantitative PCR (qPCR).** Total RNA was extracted into 1 mL of TRIzol reagent (Invitrogen) according to manufacturer's instructions. 2 µg of total RNA was reverse-transcribed with 3.75 µM random hexamers (Qiagen, Hilden, Germany) and 20 U of ProtoScript

II (New England Biolabs, Boston, MA). The resulting cDNA:RNA hybrids were treated with 10 U of DNase I (Roche) for 30 min at 37°C, and purified on PCR clean-up columns (Macherey-Nagel, Düren, Germany). qPCR was performed with Kapa SYBR Fast qPCR master mix (Kapa Biosystems, Wilmington, MA) and CFX96 or CFX384 real-time PCR machine (Bio-Rad, Hercules, CA). The thermal cycling program is as follows: 95°C for 3 min; 45 cycles of 95°C for 15 sec and 53°C or 55°C for 30 sec; a cycle of 95°C for 1 min, 53°C for 1 min, and 70°C for 10 sec; and 50 cycles of 0.5°C increments for 10 sec. Biological replicates of control and experimental samples, and three technical replicates per biological replicate were performed on the same 96- or 384-well PCR plate. Averages of the three Ct values per biological replicate were converted to differences in Ct values relative to that of control sample. Pfaffl method (Pfaffl 2001) and calculated primer efficiencies were used to determine the relative fold increase of the target gene transcript over the housekeeping *eIF4A1* gene transcript for each biological replicate. Primer sequences and efficiencies are listed in Supplementary Table 1.

**Confocal microscopy.** Live epidermal root cells of 5-day-old *Arabidopsis* seedlings and 4-week-old *N. benthamiana* leaves were imaged using a 40X 1.0 numerical aperture Zeiss water-immersion objective and a Zeiss LSM 510 Meta confocal microscopy system. GFP and RFP were excited with a 488-nm argon laser and 561-nm laser diode, respectively. GFP and RFP emissions were detected using a 500-550 nm and 575-630 nm filter sets, respectively. Plasmolysis was induced by 5-10 min treatment of *N. benthamiana* leaf strips with 0.8 mannitol, and co-localization of GFP/RFP-tagged proteins to Hechtian strands was made visible by over-exposing confocal images using ZEN software.

**ER stress induction.** For qPCR and western blots, 9-day-old seedlings were treated with 5 µg/mL tunicamycin (0.5 mg/mL stock solution in DMSO; Sigma-Aldrich) or solvent control (DMSO) for 5 hr. For growth inhibition, seedlings were grown on MS agar supplemented with 0, 25, 50, and 100 ng/mL tunicamycin for 14 days.

**Inhibition of protein translation and degradation.** For BRI1 westerns, 5-day-old seedlings were treated with DMSO (mock) or 50  $\mu$ M cycloheximide for 6 hr. For FLS2 westerns, 9-day-old seedlings were treated with 50  $\mu$ M cycloheximide for 0, 2 and 16 hr. 9-day-old seedlings were also treated with DMSO (mock), 50  $\mu$ M MG132 (50 mM stock solution in DMSO; Selleck Chemicals, Houston, TX), 20  $\mu$ M E-64d (20 mM stock solution in DMSO; Cayman Chemical), and/or 2  $\mu$ M concanamycin A (200  $\mu$ M stock solution in DMSO; Santa Cruz Biotechnology) for 24 hr. For growth inhibition, 3-day-old seedlings were elicited with 100 nM flg22 or water for 2 days, and then treated with DMSO, 50 nM MG132, and/or 20 nM E-64d for 4 days.

**Bacterial infection.** Pathogen assays on 4- to 5-week-old adult leaves were performed as previously described (Chezem et al., 2017).

SUPPLEMENTAL DATA



**Figure S2.1. The *agg1 agg2* mutant exhibits increased vegetative growth and faster transition to inflorescence development.** (A–B) Growth phenotypes of 5-week-old (A) and 8-week-old (B) *atg7* and *agg1 agg2 atg7* plants (left) and *atg3* and *agg1 agg2 atg3* plants (right) relative to *WT* and *agg1 agg2* plants. Growth phenotypes of 5-week-old (A) *agb1 atg7* and *agb1 atg3* plants are also included.

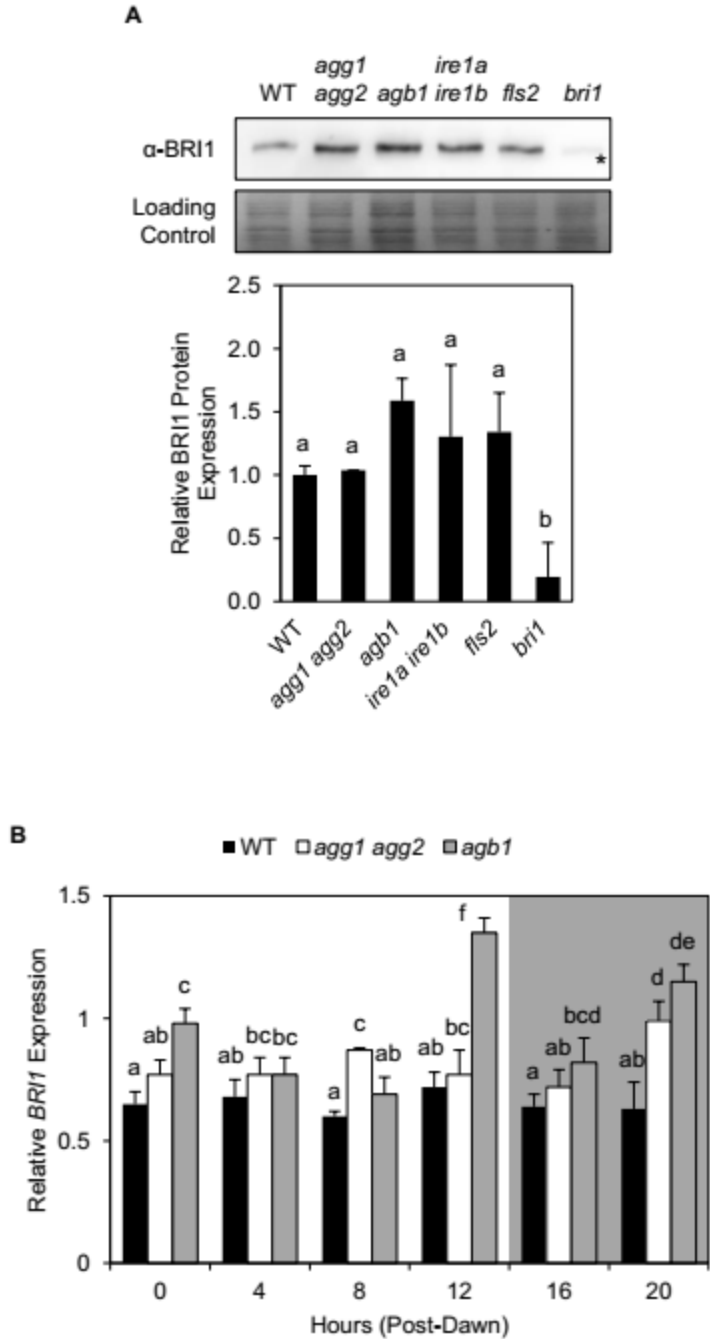


**Figure S2.2. *BRI1* transcript and protein expression are elevated due loss of *Gy* subunits.** (A) Immunoblot analysis of *BRI1* protein in 5-day-old WT, *agg1 agg2*, *agb1*, *ire1a ire1b*, *fls2*, and *bri1* plants. Asterisks indicate non-specific protein bands. FW, fresh weight. (B) Time course of *BRI1* gene expression in 9-day-old WT, *agg1 agg2* and *agb1* plants. Shading indicates night time. Data represent mean  $\pm$  SD of 4 replicates of 12 seedlings. Different letters in (A–B) indicate significant differences ( $P$ -value  $< 0.05$ , two-tailed  $t$  test).

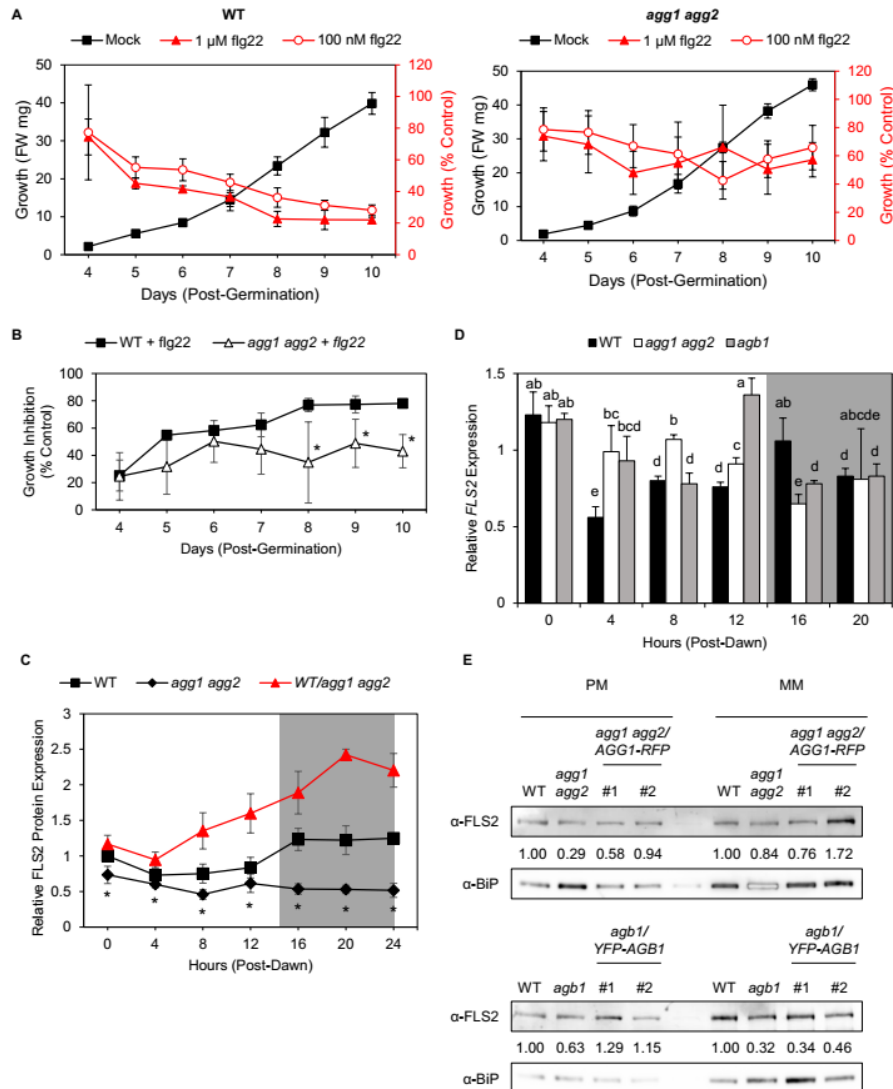


**Figure S2.3. Loss of AGG1/2 leads to reduced FLS2 protein on the plasma membrane.** (A) Growth curves of WT (left) and *agg1 agg2* (right) plants in response to water (mock/control), 100 nM flg22 or 1  $\mu$ M flg22 starting at three days post-germination. Data represent mean  $\pm$  SD of four replicates of five seedlings. (B) Growth inhibition curves of WT and *agg1 agg2* plants in response to water (control) or 1  $\mu$ M flg22 starting at three days post-germination. Data represent mean  $\pm$  SD of five replicates of five seedlings. Asterisks indicate significant differences from WT ( $P$ -value  $<0.05$ , two-tailed  $t$  test). (C) Time course of FLS2 protein expression in 9-day-old WT and *agg1 agg2*. Data represent mean  $\pm$  SD of three replicates of twelve seedlings. Asterisks indicate significant differences from WT ( $P$ -value  $<0.05$ , two-tailed  $t$  test). Shading indicates night time. (D) Time course of *FLS2* gene expression in 9-day-old WT, *agg1*, and *agb1* plants. Shading indicates night time. Data represent mean  $\pm$  SD of four replicates of twelve seedlings. Different letters indicate significant differences ( $P$ -value  $<0.05$ , two-tailed  $t$  test). (E) Immunoblot analysis of FLS2 protein from plasma membrane (PM) and microsomal membrane (MM) protein extracts of 9-day-old seedlings. Plants in the top panel were pretreated with 20  $\mu$ M  $\beta$ -estradiol for 48 hr. Numbers under immunoblots indicate FLS2 signal intensities normalized to those of ER membrane-associated BiP and relative to WT.

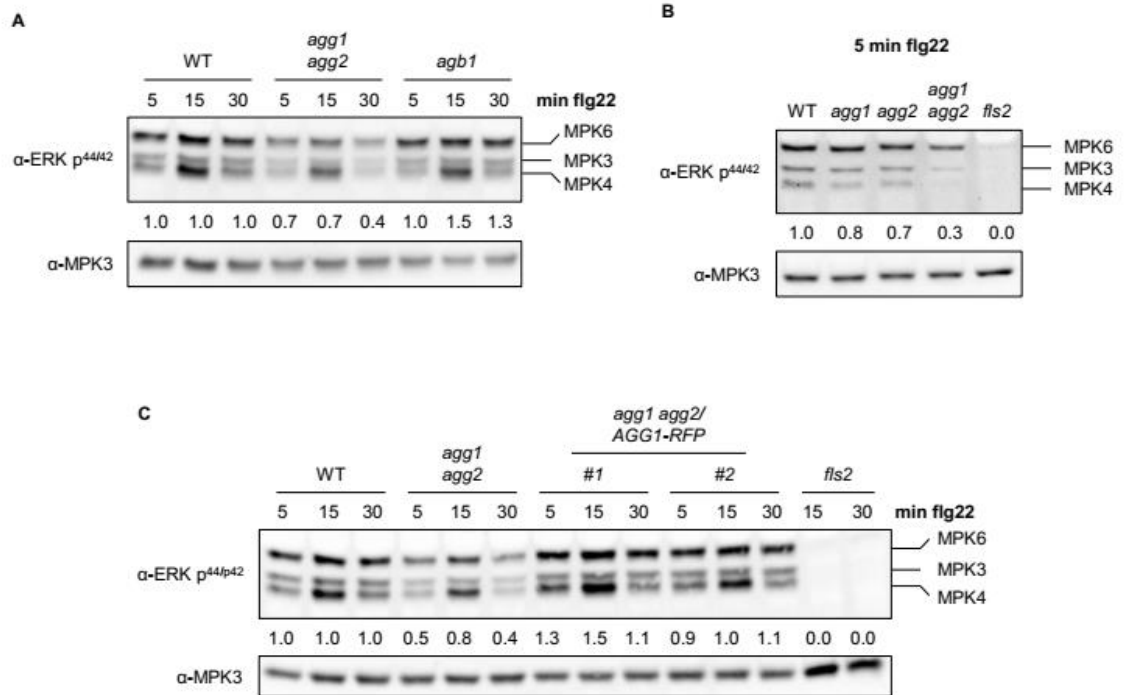


**Figure S2.4. MAPK activation is reduced in the absence of AGG1/2.** (A–C) Immunoblot analysis of activated MAPKs in 9-day-old WT, *agg1 agg2*, *agb1*, *agg1*, *agg2*, *fls2*, and *agg1 agg2/XVE:AGG1-RFP* lines in response to 100 nM flg22 for 5, 15, and/or 30 min. Numbers under immunoblots indicate combined phosphorylated MPK3/4/6 signal intensities normalized to those of total MPK3 (loading control) and relative to WT. Plants in (C) were pretreated with 20  $\mu$ M  $\beta$ -estradiol for 48 hr.

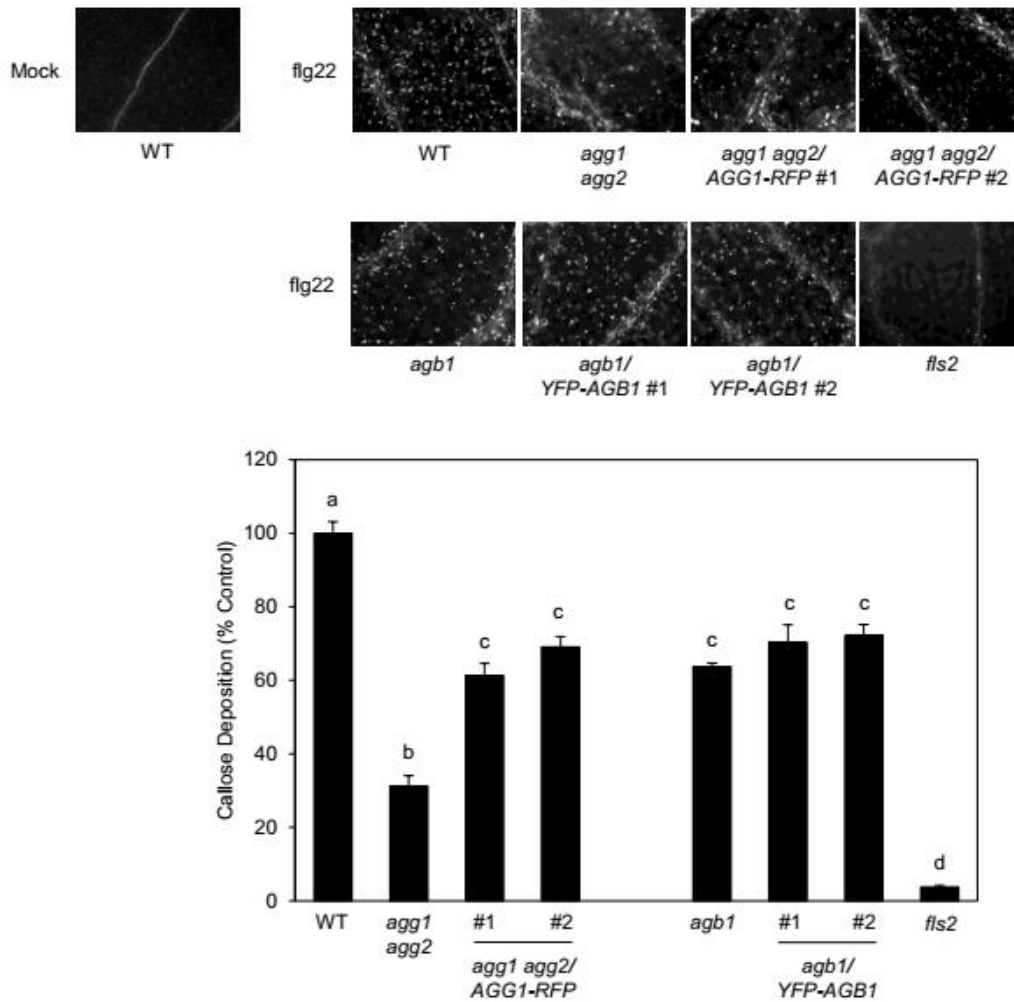


**Figure S2.5. Flg-induced callose deposition is reduced in the absence of AGG1/2.** Callose deposition analysis of 9-day-old WT, *aggl aggl2*, *aggl aggl2/XVE:AGG1-RFP*, *agb1*, *agb1/35S:YFP-AGB1*, and *fls2* plants in response to water (control) or 1  $\mu$ M flg22 for 16-18 hr. Plants on the left side of the graph were pretreated with 20  $\mu$ M  $\beta$ -estradiol for 48 hr. Data represent mean  $\pm$  SE of 14 (*agb1/35S:YFP-AGB1* #1) and 25 (all others) replicates. Different letters indicate significant differences ( $P$ -value < 0.05, two-tailed  $t$  test).

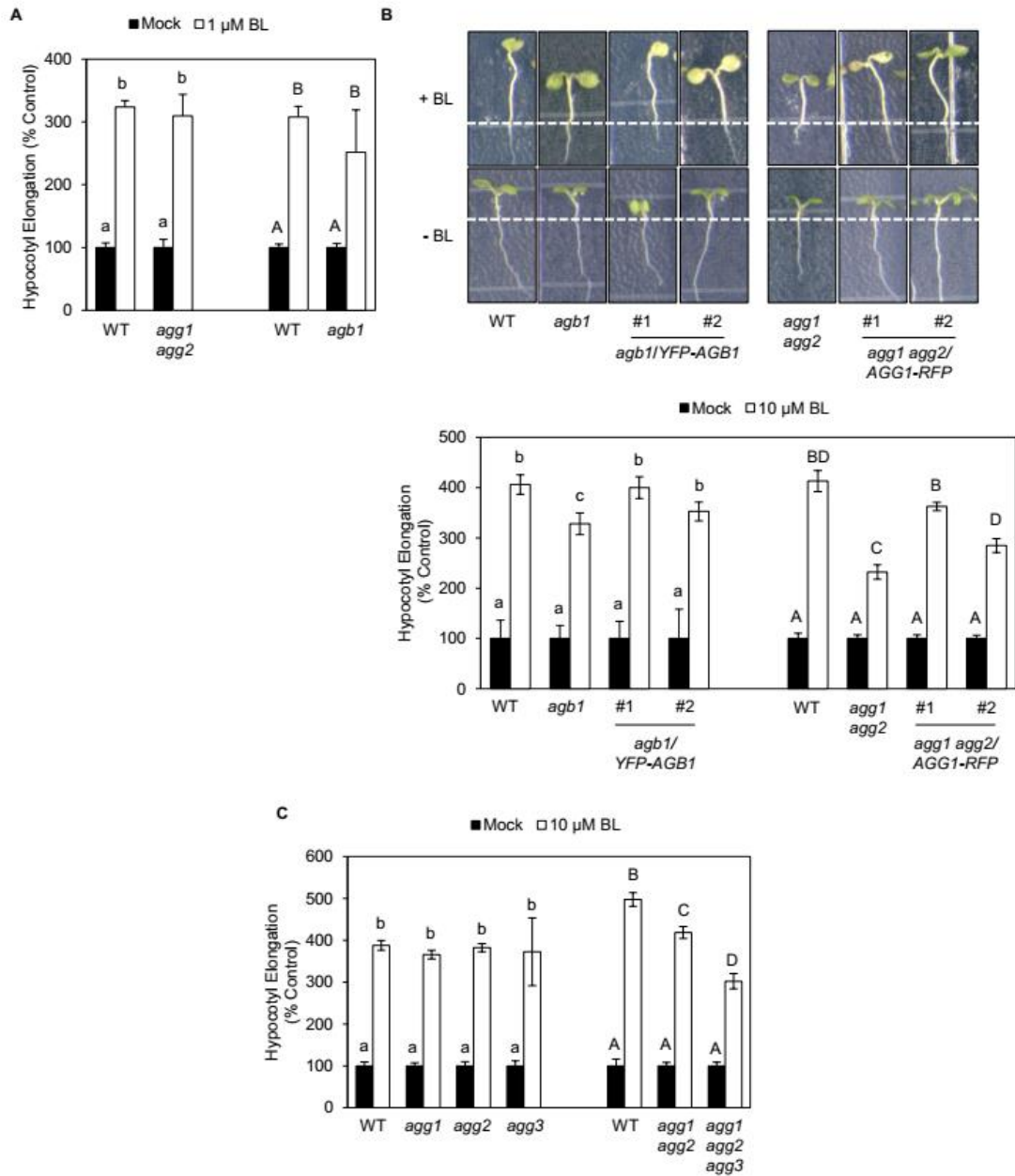


**Figure S2.6. High BL levels cause growth inhibition in *agg1 agg2*.** (A–C) Hypocotyl elongation analysis of 5-day-old WT, *agb1*, *agb1/35S:YFP-AGB1*, *agg1 agg2*, *agg1 agg2/XVE:AGG1-RFP*, *agg1*, *agg2*, *agg3*, and *agg1 agg2 agg3* plants in response to 0 (control), 1  $\mu$ M 24-epibrassinolide (BL) (A) or 10  $\mu$ M BL (B–C) for 5 days. Plants in (B, right) were additionally pretreated with 20  $\mu$ M  $\beta$ -estradiol for 48 hr. Dashed lines indicate locations of hypocotyl-root junction in each plant. Data in (A–C) represent mean  $\pm$  SD of six replicates. Different letters indicate significant differences ( $P$ -value  $< 0.05$ , two-tailed  $t$  test).

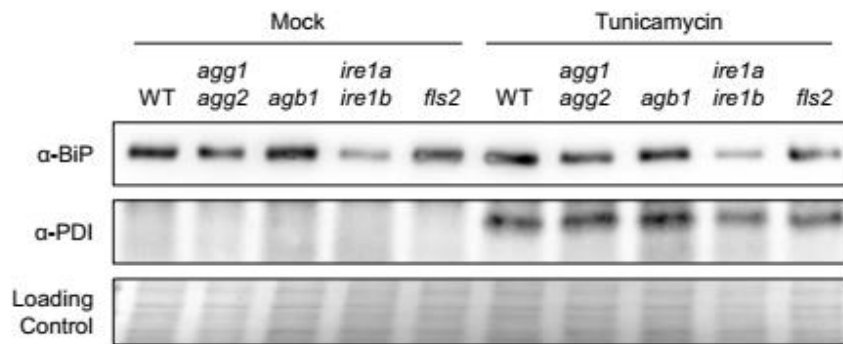


**Figure S2.7. UPR markers BIP and PDI are unaffected in *agg1 agg2*.** Immunoblot analysis of ER chaperone and folding proteins BIP and PDI in 9-day-old WT, *agg1 agg2*, *agb1*, *ire1a ire1b*, and *fls2* plants treated with DMSO (mock) or 5  $\mu\text{g mL}^{-1}$  tunicamycin for 5 hr.

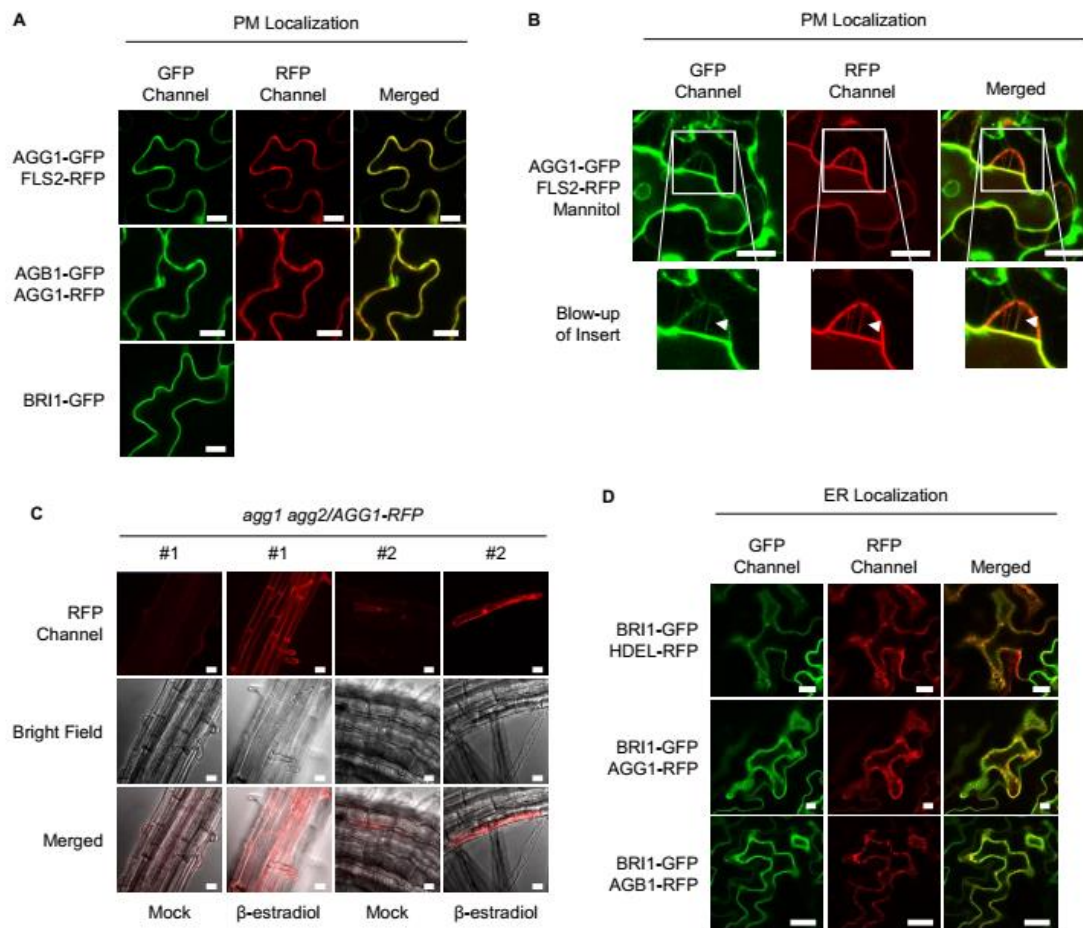


**Figure S2.8. C-terminal tag does not affect AGG1 subcellular localization.** (A) Co-localization of AGG1 with FLS2 and AGB1 at the PM. (B) Co-localization of AGG1 with FLS2 at plasmolysis-induced Hechtian strands (indicated by arrowheads). (C) Co-localization of AGG1-RFP to reticulate structures in 5-day-old *agg1 agg2/XVE:AGG1-RFP* plants pretreated with 20  $\mu$ M  $\beta$ -estradiol for 48 hr. (D) Co-localization of BRI1 with AGG1 and AGB1 at the ER membrane. HDEL is an ER marker. Experiments in (A, B, D) were performed on transfected *N. benthamiana* leaves pretreated with 20  $\mu$ M  $\beta$ -estradiol for 4 hr. White bars in (A–D) represent 20  $\mu$ m.

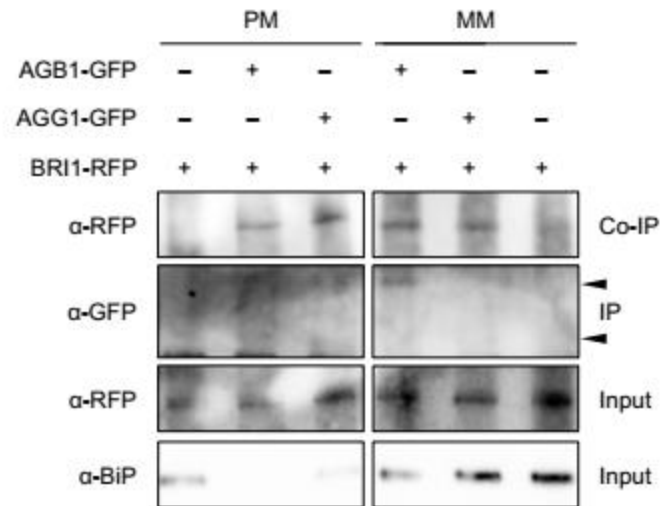


**Figure S2.9. G $\beta\gamma$  heterodimer interact with BRI1 at the ER membrane.** Immunoprecipitation (IP) of AGG1-GFP and AGB1-GFP (indicated by arrowheads) and co-immunoprecipitation (Co-IP) of BRI1-RFP from PM and MM protein extracts of transfected *N. benthamiana* leaves pretreated with 20  $\mu$ M  $\beta$ -estradiol for 10 hr. BiP is an ER membrane-associated protein in the absence of ER stress.

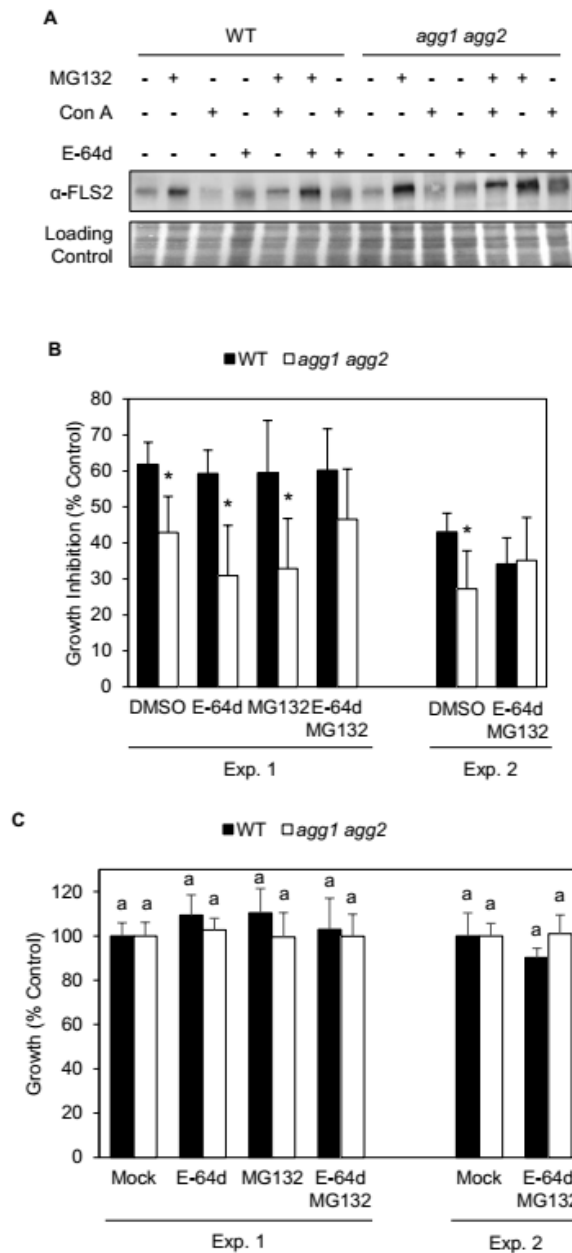


**Figure S2.10. Inhibiting autophagy and proteasome in *agg1 agg2* rescues flagellin response back to WT.** (A) Immunoblot analysis of FLS2 protein in 9-day-old WT and *agg1 agg2* plants pretreated with DMSO, 50  $\mu$ M MG132, 20  $\mu$ M E-64d, and/or 2  $\mu$ M Concanamycin A (Con A) for 24 hr. Data represent mean  $\pm$  SD of three replicates of twelve seedlings. (B) Two independent growth inhibition analyses of 9-day-old plants pretreated with water (control) or 100 nM flg22 for 2 days and then with DMSO (mock), 50 nM MG132, and/or 20 nM E-64d for 4 days. Data represent mean  $\pm$  SD of five replicates of five seedlings. Asterisks indicate significant differences from WT ( $P$ -value  $< 0.05$ , two-tailed  $t$  test). (C) Two independent growth analyses of 9-day-old WT and *agg1 agg2* plants pretreated with DMSO (mock), 50 nM MG132 and/or 20 nM E-64d. Data represent mean  $\pm$  SD of five replicates of five seedlings.

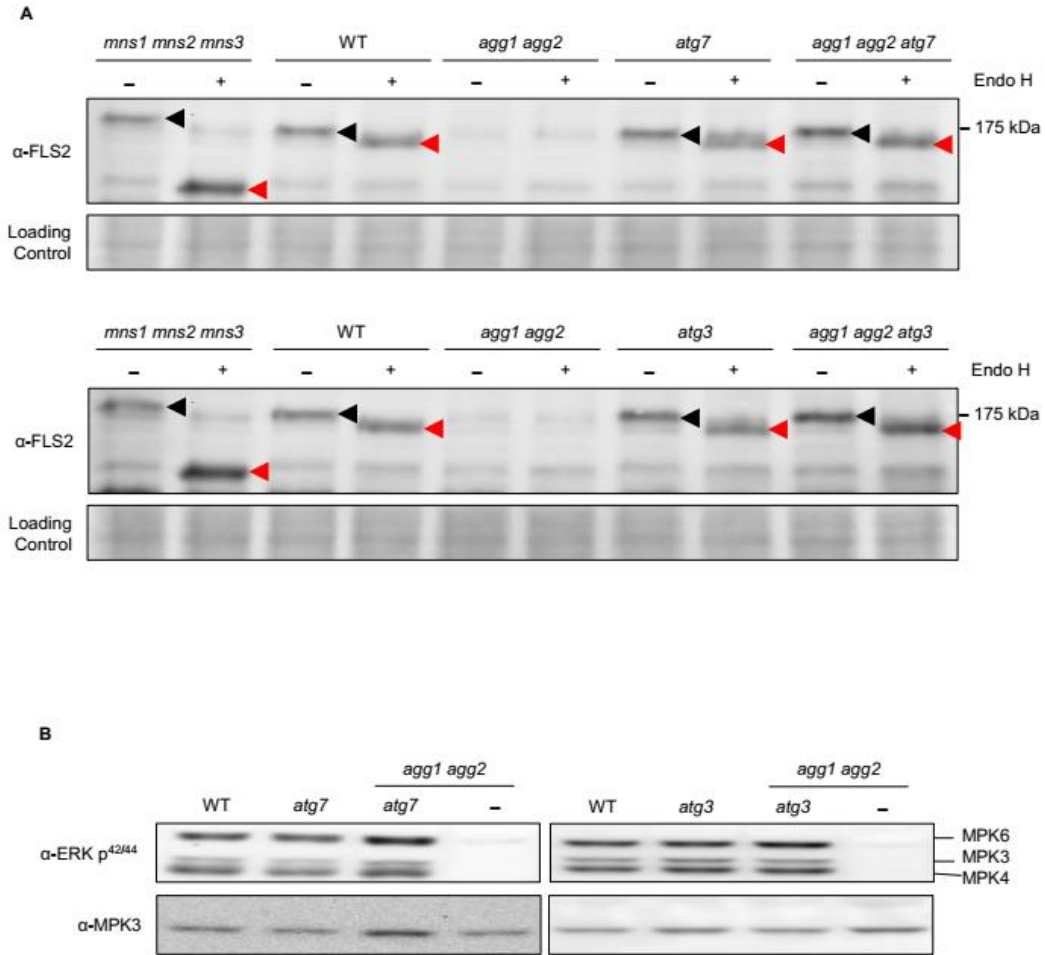


**Figure S2.11. *agg1 agg2 atg3/7* triple mutants have restored MAPK activation upon flagellin elicitation.** (A) Immunoblot analysis of FLS2 proteins in 9-day-old WT, *mns1 mns2 mns3*, *agg1 agg2*, *atg7*, *agg1 agg2 atg7* plants. Total protein extracts were treated with citrate buffer (mock) or 1,000 U of Endoglycosidase H (Endo H) for 1.5 hr prior to separation on SDS-PAGE gel. Black and red arrowheads indicate FLS2 protein bands that were treated with citrate buffer and Endo H, respectively. (B) Immunoblot analysis of activated MAPKs in 9-day-old WT, *atg7*, *agg1 agg2 atg7*, *atg3*, and *agg1 agg2 atg3* plants in response to 100 nM flg22 for 10 min.

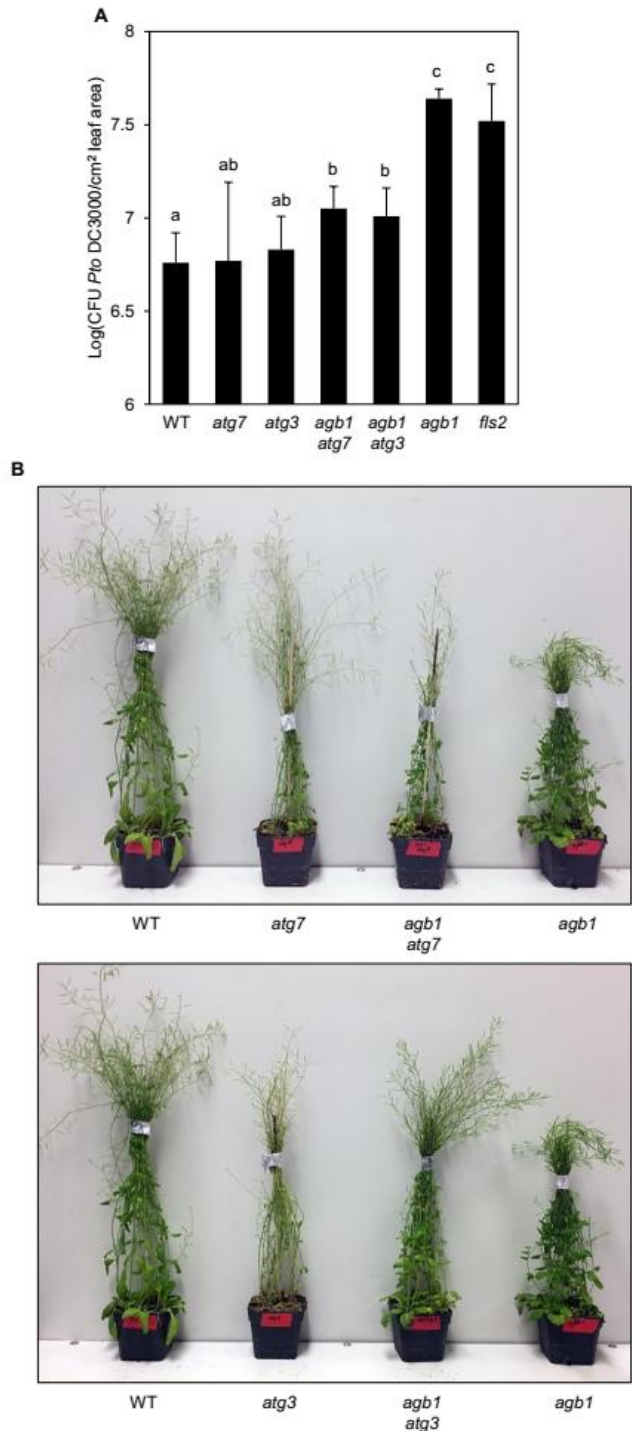


**Figure S2.12. *agg1 agg2 atg3/7* triple mutants exhibit WT bacterial resistance and adult growth.** (A) Growth analysis of bacterial pathogen *Pto* DC3000 in 5-week-old surface-inoculated leaves of WT, *atg7*, *atg3*, *agb1 atg7*, *agb1 atg3*, *agb1*, and *fls2* plants. Data represent mean  $\pm$  SD of 6 replicates. Different letters indicate significant differences ( $P$ -value  $< 0.05$ , two-tailed  $t$  test). (B) Growth phenotypes of 10-week-old *atg7* and *agb1 atg7* plants (top) and *atg3* and *agb1 atg3* plants (bottom) relative to WT and *agb1* plants.

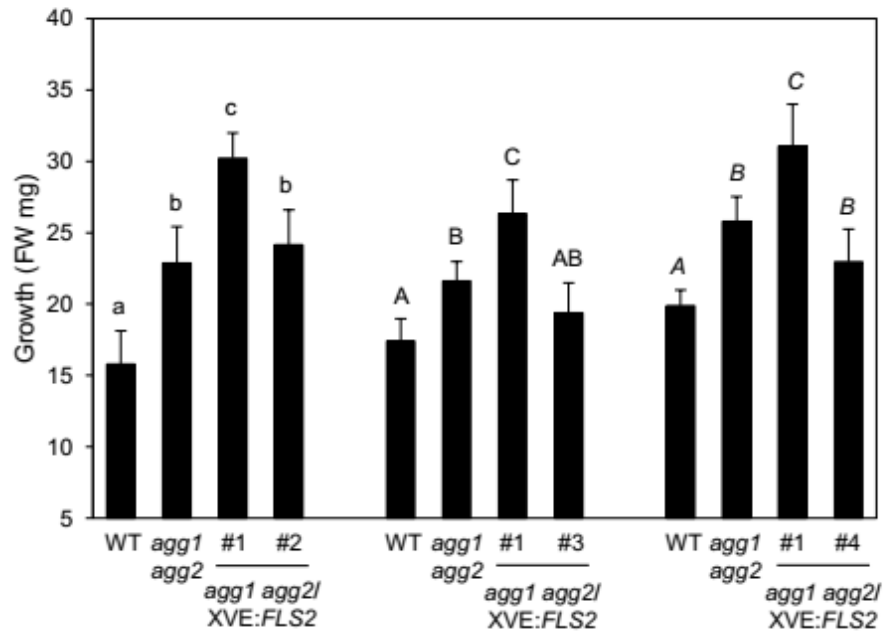


**Figure S2.13. The *agg1 agg2* mutant exhibits increased growth.** Growth analysis of *agg1 agg2/XVE:FLS2* lines. Data represent mean  $\pm$  SD of five replicates of five seedlings. Different letters indicate significant differences ( $P$ -value  $< 0.05$ , two-tailed  $t$  test). FW, fresh weight.

Gene		Primers Sequence	Primer Efficiency (%)	Efficiency Temp. (°C)
<i>AGB1</i>	Forward	5'-CTGATGTACTAAGCGTCTC-3'	97.6	55
	Reverse	5'-ATGAAAGGTACGCACTGCT-3'		
<i>AGG1</i>	Forward	5'-GTTGAACAGGAAGTCGCTT-3'	93.5	55
	Reverse	5'-TCTCGATGACAGATAGCAG-3'		
<i>AGG2</i>	Forward	5'-CAAGAAGCTCGATTCTTAGA-3'	91.9	55
	Reverse	5'-GTTTGCTGTCAACTGTC-3'		
<i>BRI1</i>	Forward	5'-AACAAAAGGAGACGTTTATAGT-3'	90	55
	Reverse	5'-CAGTTTTGCGTGCTGTTTCA-3'		
<i>CPD</i>	Forward	5'-TATTCTCATCGTTTAGAGC-3'	82.5	53
	Reverse	5'-GAGTTGCTCTGCCATCTC-3'		
<i>CYP81F2</i>	Forward	5'-CTCATGCTCAGTATGATGC-3'	86.2	53
	Reverse	5'-CTCCAATCTTCTCGTCTATC-3'		
<i>CYP82C2</i>	Forward	5'-CAAGCATGTCCGTGTTTCTG-3'	91.6	53
	Reverse	5'-GCATCTTCAGGGGATAACGA-3'		
<i>EIF4A</i>	Forward	5'-TCTGCACCAGAAGGCACA-3'	100	55
	Reverse	5'-TCATAGGATGTGAAGAACTC-3'		
<i>FLS2</i>	Forward	5'-ATACTCCTTGACAGTGACC-3'	100	55
	Reverse	5'-AACTCTGGAGCTAAGTATCC-3'		
<i>FRK1</i>	Forward	5'-GCAAGGACTAGAGTATCTTC-3'	96.5	53
	Reverse	5'-ATCTTCGCTTGGAGCTTCT-3'		
<i>IRE1A</i>	Forward	5'-ACGATAGCATCCGTGACTT-3'	84.6	55
	Reverse	5'-TGTTCCGACAAGTTCCTGA-3'		

**Table S2.1. Q-PCR primer sequences and efficiencies**

## **ACKNOWLEDGEMENTS**

We thank Nozomu Koizumi for the *ire1a-2/ire1b-2* (SALK\_018112, GABI\_638B07) mutant and Bonnie Bartel for the *atg3-1* mutant. We thank Rüdiger Simon for the pABindGFP and pABindmCherry vectors. The work was supported by T32 GM007499 (to S.A.L), T32 GM007223 (to J.C.M), and Yale University Elizabeth Brown Fellowship (to T.C.).

### **Chapter 3. Discovery of novel structurally similar $\beta$ -propeller WD40-repeat proteins SSB1/2 and their roles in plant immunity**

#### **Preface**

B.B. performed the phylogenetic analysis and edited the manuscript. J.C.M. performed the homology modeling, split-luciferase complementation, co-localization, MAPK assays, and Pto DC3000 infections. N.K.C. generated the *agb1 sgl1-1*, *agb1 sgl2-1*, and *sgl1 sgl2* mutants, performed the *A. brassicicola* fungal infections and Pto DC3000 infections. J.C.M. and N.K.C. interpreted and wrote the manuscript. J.M.G. helped write and edited the manuscript.

**Authors:** Jimi C. Miller<sup>\*</sup>, Brenden Barco<sup>†</sup>, Joshua M. Gendron<sup>†</sup>, & Nicole K. Clay<sup>\*†</sup>

#### **Affiliations:**

<sup>1</sup>Department of Molecular Biophysics and Biochemistry, Yale University, New Haven, CT 06510, USA.

<sup>2</sup>Department of Molecular, Cellular, and Developmental Biology, Yale University, New Haven, CT 06510, USA.

## ABSTRACT

Plant G proteins transduce cell-surface receptor signals to downstream pathways in growth and defense. *Arabidopsis* encodes multiple canonical and non-canonical G $\alpha$  and G $\gamma$  subunits that are involved in plant immune signaling. However, there has been no discovery of any non-canonical G $\beta$  proteins thus far. Here, we identify two structurally similar  $\beta$ -propeller WD40 proteins (SGL1 and SGL2) that negatively regulate plant immunity. SGL1 and SGL2 have high sequence homology and are predicted to form a  $\beta$ -propeller with an N-terminal domain similarly to AGB1. SGL2 localizes to the plasma membrane and interacts with the G $\gamma$  subunits AGG1 and AGG2, whereas SGL1 does not. Furthermore, SGL2 interacts with the G $\alpha$  subunits GPA1 and XLG1. Loss of SGL1 or SGL2 results in resistance to the biotrophic bacterial pathogen *Pseudomonas syringae*, while the *sgl1 ssgl2* double mutant confers broad-spectrum resistance to both *P. syringae* and the fungal pathogen *Alternaria brassicicola*. Taken together, our results suggest that SGL1/2 negatively regulates plant immune signaling.

## INTRODUCTION

Heterotrimeric G proteins in plants transduce signals from cell surface receptors to downstream effectors. In particular, plant G proteins are involved in both development and immunity (Temple and Jones 2007). The heterotrimeric G protein complex is comprised of a  $G\alpha$ ,  $G\beta$ , and  $G\gamma$  subunit. The  $G\alpha$  subunit binds GDP in its inactive state and becomes active when it binds GTP. The  $G\beta$  and  $G\gamma$  subunits form an obligate  $G\beta\gamma$  heterodimer that is inactive when it is bound to the  $G\alpha$  subunit and separates from the  $G\alpha$  subunit when the heterotrimeric G protein complex is activated (Temple and Jones, 2007). The  $G\beta$  subunit features a seven tandem WD40-repeat motif that adopts the formation of a seven-bladed  $\beta$ -propeller-like structure (Lambright et al., 1996; Smith et al., 1999; Ullah et al., 2008; Adams et al., 2011; Ruiz et al., 2012). Each blade of the propeller-like structure consists of four antiparallel  $\beta$  strands. The seven-bladed  $\beta$ -propeller structure is best demonstrated by the WD40 repeat protein receptor for activated C kinase 1 (RACK1) protein, which acts as a protein scaffold in signaling pathways (Ullah et al., 2008). Unlike RACK1 proteins, the  $G\beta$  subunit contains an N-terminal  $\alpha$ -helix that forms a coiled-coil structure with the  $G\gamma$  subunit localizing the  $G\beta$  subunit to the plasma membrane (Ullah et al., 2008).

Plants encode two different classes of heterotrimeric G proteins: canonical and non-canonical. The canonical G proteins include the  $G\alpha$  GPA1, the  $G\beta$  AGB1, and the  $G\gamma$  subunits AGG1 and AGG2, which were originally found through homology to animal G proteins (Ma et al., 1990; Weiss et al., 1994; Mason & Botella, 2000, 2001). The non-canonical G proteins include the  $G\alpha$  subunits XLG1, XLG2, and XLG3, and the  $G\gamma$  AGG3. These non-canonical G proteins were identified by looking for homologues to the canonical plant G proteins rather than the animal G proteins (Lee & Assmann, 1999; Assmann, 2002; Chakravorty et al., 2011).

The non-canonical G proteins XLG1-3 and AGG3 contain core elements found in the canonical G proteins such as GTP-binding and N-terminal coiled-coil domains, respectively, but they also

contain unique domains that are predicted to have novel functions (Lee & Assmann, 1999; Assmann, 2002; Chakravorty et al., 2011). For example, the XLG proteins are approximately twice the size of the canonical G $\alpha$  subunit GPA1 and include an N-terminal domain whose function remains unknown, but encodes a nuclear localization sequence (Chakravorty et al., 2015). On the other hand, AGG3 is more than twice the size of AGG1 and AGG2, and it contains a C-terminal trans-membrane domain that is sufficient but not required for plasma membrane localization along with an extracellular cysteine-rich C-terminal domain (Wolfensetter et al., 2015).

Recent reports show that the canonical and non-canonical plant G proteins are involved in immunity and development. Loss of either XLG2 or XLG3 results in increased susceptibility to the bacterial pathogen *Pseudomonas syringae* and the fungal pathogen *Fusarium oxysporum* (Maruta et al., 2015). Interestingly, only XLG2 seems to be involved in resistance toward the fungal pathogen *Alternaria brassicicola* (Maruta et al., 2015). However, loss of both XLG2 and XLG3 causes severe susceptibility to all three pathogens (Maruta et al., 2015). Recently, reports have shown that XLG2 and XLG3 interact with the G $\beta\gamma$  heterodimer as well as the flagellin-binding cell-surface receptor FLAGELLIN SENSING 2 (FLS2) (Maruta et al., 2015; Liang et al., 2016). Specifically, XLG2 forms a heterotrimer with AGB1-AGG1/2 which in turn binds to FLS2 in its inactive state. Upon flagellin binding, FLS2 induces dissociation of the heterotrimeric complex leading to the phosphorylation of XLG2, which in turn enhances the production of reactive oxygen species (Liang et al., 2016).

Loss of AGG3 exhibits results in flat, wide siliques, rounder and cabbage-like leaves, and flowers with distinctly shorter petals relative to wild-type (Chakravorty et al., 2011). These developmental phenotypes resemble the *agb1* mutant (Chakravorty et al., 2011; Li et al., 2012).

The discovery of non-canonical G $\alpha$  and G $\gamma$  proteins raises the question of whether non-canonical G $\beta$  proteins exist. Plant genomes typically encode more than 200 putative WD40-containing

proteins (Ouyang et al., 2012; van Nocker and Ludwig, 2003), presenting a challenge in the identification of non-canonical G $\beta$  proteins using homology-based screens. To identify if non-canonical G $\beta$  subunits exist that modulate immunity, we screened for WD40 proteins whose expression is altered upon flagellin elicitation. We identified two  $\beta$ -propeller WD40 proteins (*SGL1/2*) that are structurally similar to the canonical G $\beta$  protein AGB1, negatively regulate plant immunity, and interact with other G proteins, indicating they may be non-canonical G $\beta$  subunits. Moreover, loss of both SGL1 and SGL2 results in broad spectrum resistance toward biotrophic bacterial and fungal pathogens. These results suggest that SGL1 and SGL2 negatively regulate plant immunity.

## RESULTS

### *WD40 G $\beta$ -like proteins SGL1 and SGL2 are part of a novel protein family and shares similar protein structures to AGB1*

In order to search for putative novel G $\beta$  subunits, we searched published microarray data for WD40 proteins that exhibited modulated expression upon flg22 elicitation (Denoux et al. 2008). We found two genes (*AT1G55680* and *AT3G13340*) whose expression were down-regulated upon elicitation, suggesting that they may be involved in immunity (Figure S3.1). The protein sequence identity between these two genes and AGB1 is 20.2% and 22.3%, respectively (Figure 3.1), thus to determine if these two genes had a similar protein structure to the canonical G $\beta$  subunit AGB1, we used the PHYRE2 Protein Fold Recognition Server to predict their protein structures. Both genes were predicted to form a seven-bladed  $\beta$ -propeller-like structure with an N-terminal domain, similar to the human G $\beta$  subunit GNB1 and the *Arabidopsis* G $\beta$  subunit AGB1, but had an additional 50 amino acids at the N-terminus differentiating them from RACK1A (Figure 3.1). Thus, we termed *AT1G55680* and *AT3G13340* as Structurally similar G $\beta$ -Like 1 and 2 (SGL1/2), respectively. AGB1 N-terminally interacts with the G $\gamma$  protein by forming coiled-coils; we used the COILS prediction software to test if SGL1/2 are similarly predicted to form N-terminal

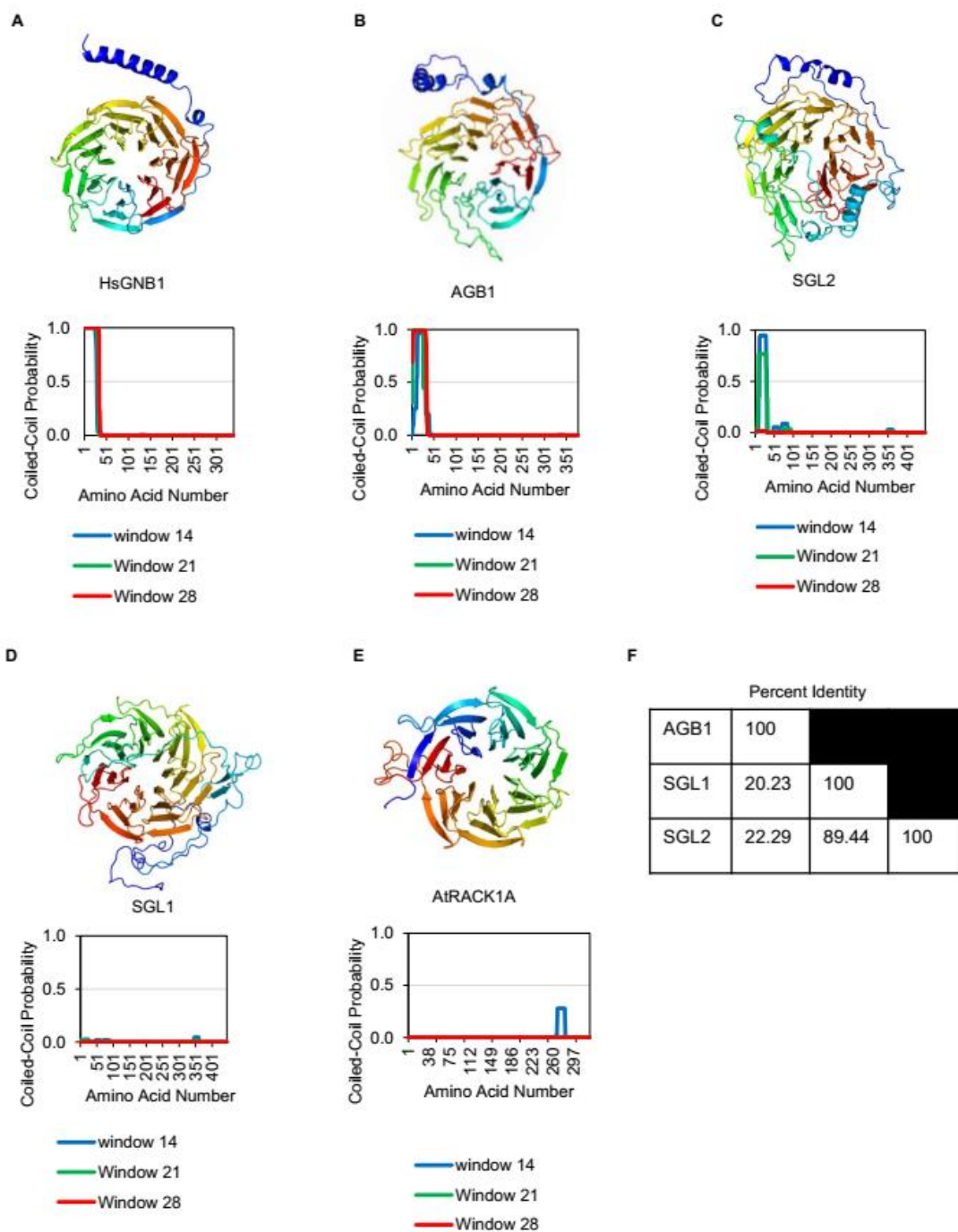


**Figure 3.1. SGL1 and SGL2 proteins share similar protein structures as canonical AGB1.** (A–E) (Top) Protein structures were predicted using homology models based on the known structure of HsGNB1 as well as from multiple sequence templates using the Phyre 2.0 server (<http://www.sbg.bio.ic.ac.uk/phyre2/html/page.cgi?id=index>). (Bottom) Coiled-coil domains were predicted using the COILS prediction program. Windows depict three independent predictions. (F) Percent identity matrix. Protein sequences were aligned and using Clustal Omega.

coiled-coils. SGL2 was predicted to form coiled-coils while SGL1 was not (Figure 3.1). To identify other G $\beta$ -like proteins, we searched for homologues to SGL1/2 and we identified three other close homologues. Additionally, we performed a phylogenetic analysis to determine if this protein family was distinct from other WD40 repeat proteins and AGB1. We found 168 seven WD40 repeat-containing proteins that formed six different clades. SGL1/2 and their homologues were phylogenetically distinct from AGB1 (Figure 3.2). Taken together, these data suggest that SGL1 and SGL2 may be non-canonical G $\beta$  proteins.

*SGL1 and SGL2 interact with Arabidopsis G proteins and localize to the plasma membrane*

To confirm SGL1/2 as potential non-canonical G $\beta$  proteins, we tested if they interact with other G proteins via an *in-planta* split-luciferase complementation. SGL2 interacted with the G $\gamma$  proteins AGG1 and AGG2 (Figure 3.3). Moreover, SGL2 interacted with the canonical G $\alpha$  protein GPA1 and the non-canonical G $\alpha$  XLG1 (Figure 3.4). However, SGL1 did not interact with any of the G proteins (Figures 3.3 and 3.4). Together, these results indicate that SGL2 may be a non-canonical G $\beta$  protein.

As G proteins typically function at the plasma membrane, we tested the sub-cellular localization of SGL1 and SGL2. Using tobacco leaves, we transiently expressed fluorescently tagged SGL1 and SGL2 proteins with the G $\gamma$  subunit AGG1 and plasma membrane receptor FLS2. SGL2 localized to the plasma membrane with AGG1 and FLS2 (Figure 4.5A). However, SGL1 did not localize to the plasma membrane with FLS2 and localized to the cytoplasm (Figure 3.5A). To verify membrane localization, we performed plasmolysis experiments with mannitol to recede most of the plasma membrane from the cell wall, a process which leaves several membrane remnants known as Hechtian strands. Using the plasma membrane marker FM4-64, we observed the presence of SGL2-GFP signal in several Hechtian strands, verifying that SGL2 localizes to the plasma membrane (Figure 3.5B).

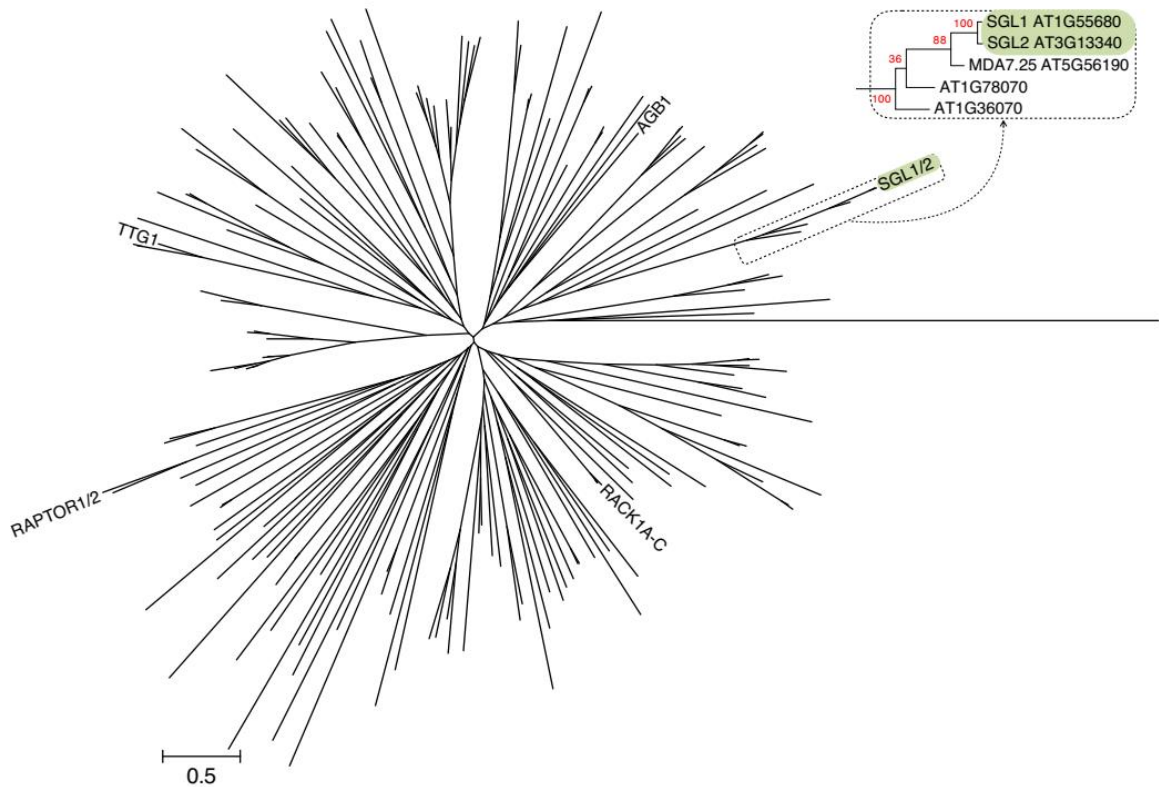


**Figure 3.2. SGL1/2 are phylogenetically distinct from that of AGB1 and RACK1 proteins.** Maximum Likelihood-based tree of 168 seven WD repeat-containing proteins based on the JTT matrix-based model in MEGA7. All amino acid positions with less than 90% site coverage were eliminated. Scale bar denotes the number of substitutions per site.

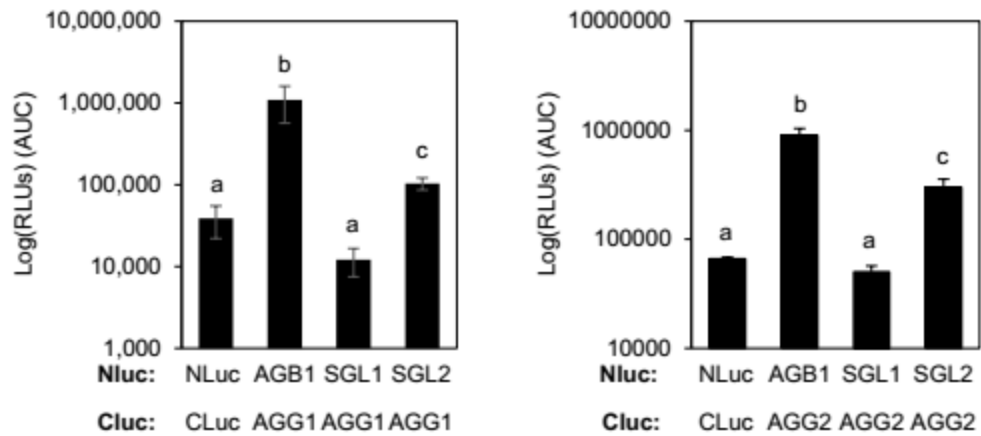


**Figure 3.3. SGL2 interacts with G $\gamma$  subunits AGG1/2.** Quantitative assessment of protein-protein interactions between AGG1/2 and AGB1-3 using a reconstituted luciferase activity readout. NLuc-CLuc interaction is negative control; AGB1-AGG1/2 and AGB1-AGG1/2 interactions are positive controls. Data represent median  $\pm$  SD of four replicates. Different letters denote statistically significant differences ( $P < 0.05$ , two-tailed  $t$  test).

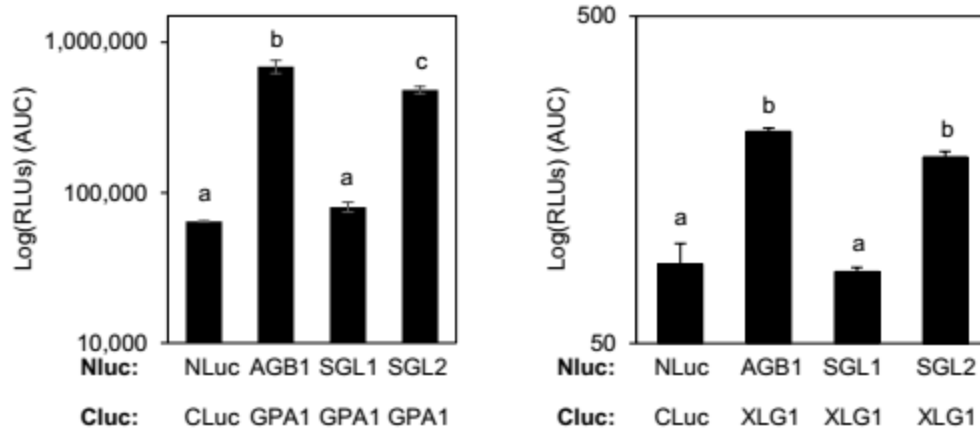


**Figure 3.4. SGL2 interacts with Gα subunits GPA1 and XLG1.** Quantitative assessment of protein-protein interactions between GPA1/XLG1 and AGB1-3 using a reconstituted luciferase activity readout. NLuc-CLuc interaction is negative control; AGB1-GPA1/XLG1 and AGB1-AGG1/2 interactions are positive controls. Data represent median  $\pm$  SD of four replicates. Different letters denote statistically significant differences ( $P < 0.05$ , two-tailed  $t$  test).

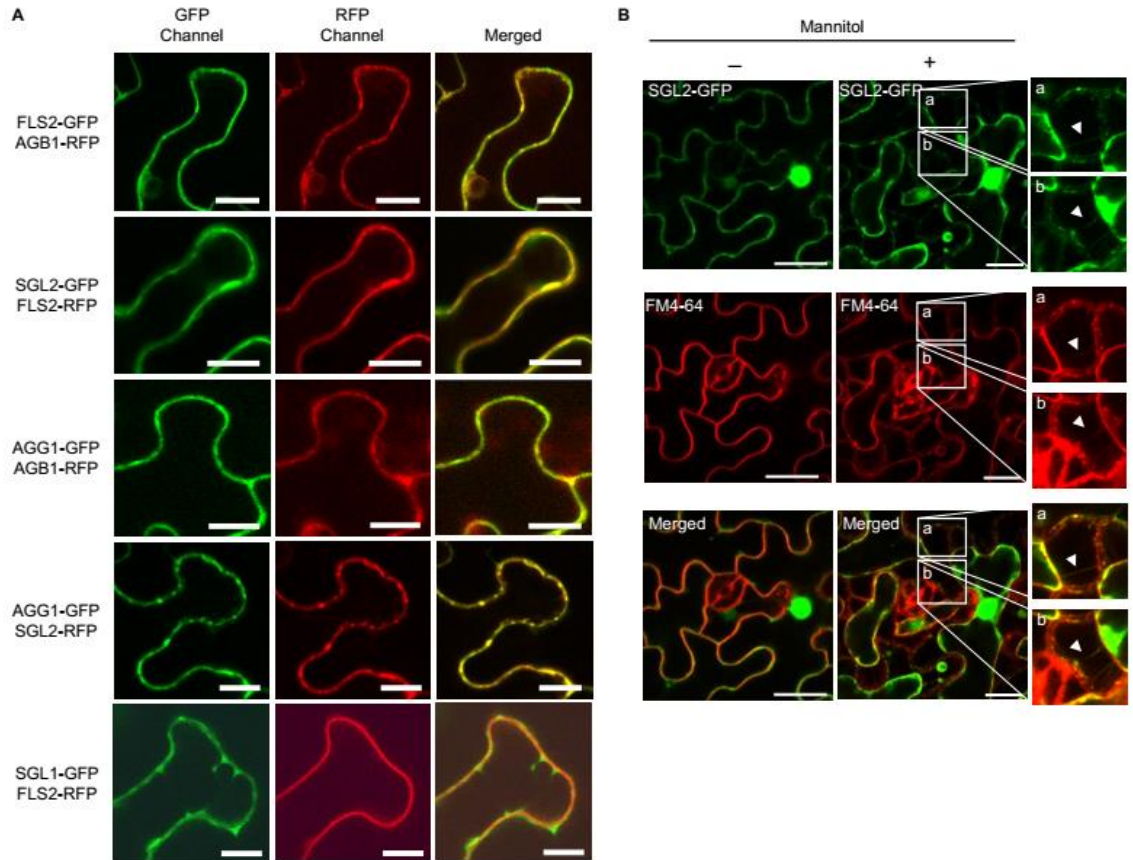


**Figure 3.5. SGL2 localizes to the plasma membrane.** (A–B) Co-localization of SSB2 with AGG1 and FLS2 at the plasma membrane in transfected *N. benthamiana* leaves pretreated with 20  $\mu$ M  $\beta$ -estradiol for 4–8 hr. White bars represent 20  $\mu$ m. (B) Co-localization of SSB2 with FM4-64 stained plasma membrane at plasmolysis-induced Hechtian strands (indicated by arrowheads).

### SGL1/2 negatively regulate plant immune defenses

As many of the plant G proteins are involved in immunity, we sought to determine if SGL1/2 are involved in defense, and we obtained T-DNA insertion mutants, *sgl1-1*, *sgl1-2*, and *sgl2*, from ABRC. These mutants lack the round, cabbage-like leaf phenotype of the *agb1* and *agg3* mutants and instead resembled wild-type (Chakravorty et al., 2011; Li et al., 2012) (Figure S3.2). We then tested MAPK activation in the *sgl1-1*, *sgl1-2*, and *sgl2-1* single mutants upon flg22 elicitation. All mutants tested had MAPK activation similar to wild-type (Figure 3.6A). Since defects in MAPK signaling have not been observed in the *agb1* mutant (Liu et al., 2013), we questioned whether SGL1 or SGL2 were in the same MAPK signaling pathway as AGB1. Therefore, we generated *agb1 sgl1-1* and *agb1 sgl2-1* double mutants and tested their MAPK activation upon flg22 elicitation. MAPK activation in the *agb1 sgl1-1* and *agb1 sgl2-1* double mutants were comparable to wild-type (Figure 3.6A). Both *agb1 sgl1-1* and *agb1 sgl2-1* displayed round, cabbage-like leaf phenotypes typical of the *agb1* and *agg3* mutants, implying that SGL1 and SGL2 are not involved in AGB1-mediated growth signaling.

SGL1 and SGL2 share a sequence identity of 89.4%, suggesting that these two proteins could have redundant functions. Thus, we generated a *sgl1 sgl2* double mutant and tested its MAPK activation upon flg22 elicitation. MAPK activation in *sgl1 sgl2* was similar to that of wild-type (Figure 3.6B). Furthermore, the morphology of the *sgl1 sgl2* double mutant resembled that of wild-type (Figure S3.2).

Next, we screened the *sgl1* and *sgl2* mutants against the fungal pathogen *Alternaria brassicicola* and bacterial pathogen *Pseudomonas syringae* pv. *tomato* DC3000 (Pto DC3000). We found that the *sgl1-1*, *sgl1-2*, and *sgl2-1* single mutants exhibited defense phenotypes indistinguishable from both wild-type and *agb1* against *A. brassicicola* (Figure 3.7A). However, when these mutants were infected with Pto DC3000, they were all significantly more resistant compared to wild-type (Figure 3.7B). Both *agb1 sgl1-1* and *agb1 sgl2-1* double mutants were as susceptible as wild-type

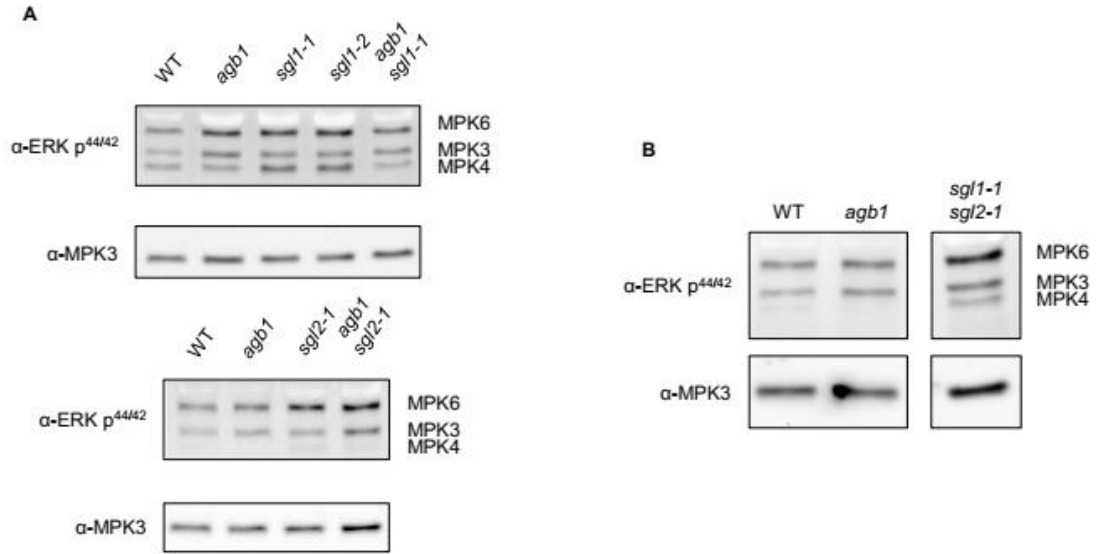


**Figure 3.6. Loss of SGL1 and SGL2 does not affect MAPK activation.** (A–B) Immunoblot analysis of activated MAPKs in 9-day-old seedlings in response to 100 nM flg22 for 5 min. Numbers under immunoblots indicate combined phosphorylated MPK3/4/6 signal intensities normalized to those of total MPK3 (loading control) and relative to WT.

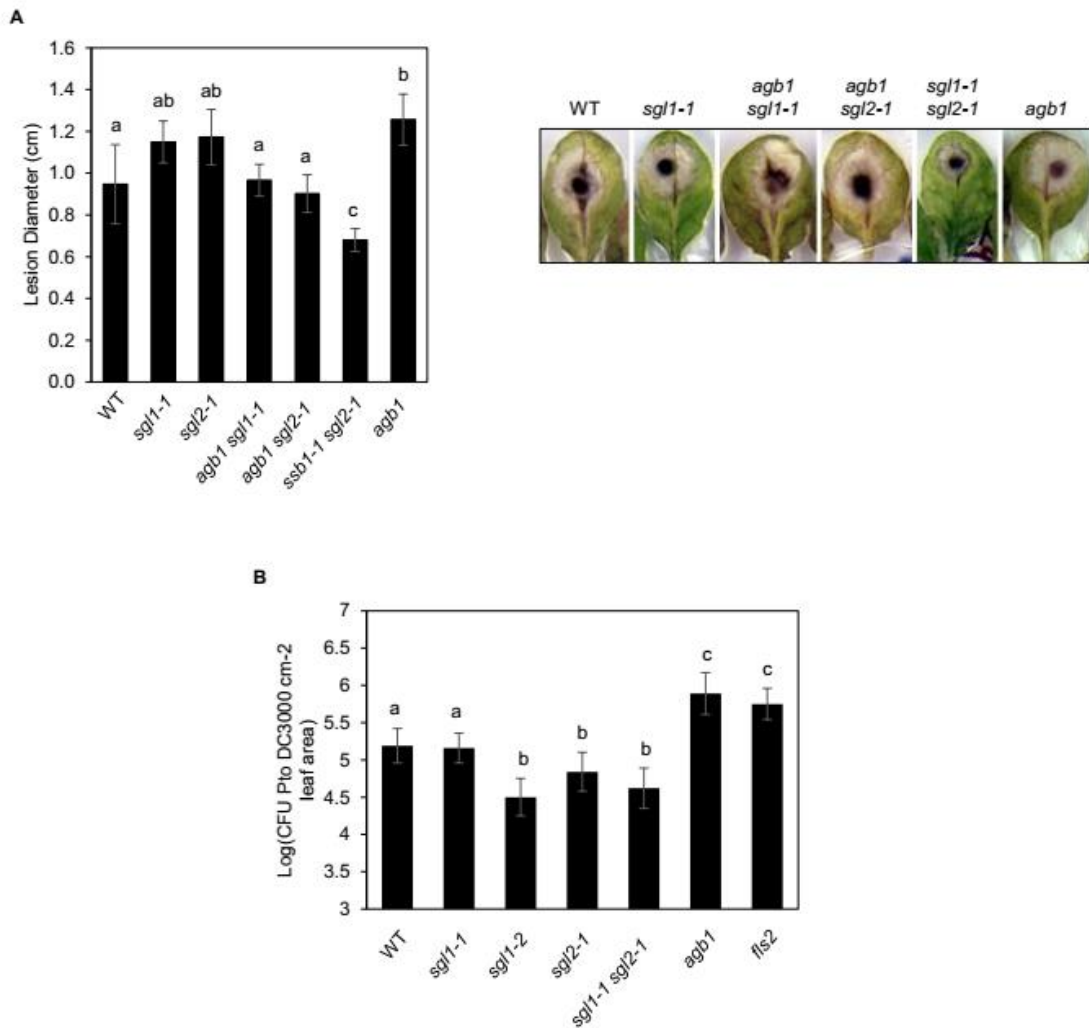


**Figure 7. SGL1 and SGL2 negatively regulate plant immunity.**

**Figure 3.7. SGL1 and SGL2 negatively regulate plant immunity.** (A) Lesion development of 4-5-week-old leaves 3 days after inoculation with *A. brassicicola*. Different letters in (A) indicate significant differences ( $P$ -value  $< 0.05$ , two-tailed  $t$  test). (B) Growth analysis of bacterial pathogen *Pto* DC3000 in 5-week-old surface-inoculated leaves. Data represent mean  $\pm$  SD of six replicates. Different letters in (B) indicate significant differences ( $P$ -value  $< 0.05$ , two-tailed  $t$  test).

against *A. brassicicola* and as susceptible as the *agb1* mutant against *Pto* DC3000 with the *agb1/YFP:AGB1* complementation line as a control (Figure 3.7A and S3.3). Interestingly, the *sgl1 sgl2* double mutant exhibited significant increased resistance to both *A. brassicicola* and *Pto* DC3000 compared to wild-type, suggesting that SGL1 and SGL2 may be redundant in negatively regulating plant immunity (Figure 3.7A and B).

## DISCUSSION

Although plants encode canonical and non-canonical  $G\alpha$  and  $G\gamma$  proteins, no non-canonical  $G\beta$  proteins have previously been reported. In this study, we have discovered two WD40 repeat proteins, structurally similar  $G\beta$ -like 1 and 2 (SGL1/2), that are transcriptionally modulated upon flg22 elicitation (Figure S3.1). Moreover, SGL1/2 are predicted form a seven-bladed  $\beta$ -propeller with an N-terminal domain similar to that of the canonical  $G\beta$  subunit AGB1 (Figure 3.1). SGL1/2 have 50 more amino acids at their N-terminus than AGB1, which could mean that the N-terminal domain may have novel functions in addition to forming coiled-coils with the  $G\gamma$  subunit and tethering to the plasma membrane. SGL1/2 are phylogenetically related to three other WD40 repeat proteins, and this clade is phylogenetically distinct from that of AGB1 (Figure 3.2). This group of WD40 repeat proteins may be a novel family of non-canonical  $G\beta$  subunits, but further experiments are necessary for this conclusion.

SGL2 interacts with the  $G\alpha$  subunits GPA1/XLG1 and the  $G\gamma$  subunits AGG1/2 (Figures 3.3 and 3.4). Additionally, SGL2 localizes to the plasma membrane, including to Hechtian strands (Figure 3.5). Despite high homology with SGL2, SGL1 did not interact with any of the G proteins nor did it localize to the plasma membrane (Figures 3.3 and 3.4). SGL1 may possibly function as a protein scaffold away from the membrane and in the cytoplasm.

WD40 repeat protein  $\beta$ -propellers function as protein scaffolds that are involved in signaling pathways. AGB1 is shown to only be involved in FLS2-dependent defense reactive oxygen

species production (Xu et al., 2017; Tunc-Ozdemir & Jones 2017; Liang et al., 2016; Lorek et al., 2013) as well as BRI1-dependent brassinolide sugar signaling (Peng et al, 2018). Similarly, SGL1/2 are involved in plant immune signaling. Specifically, SGL1/2 work to negatively regulate plant defense against fungal pathogen *A. brassicicola* and bacterial pathogen *P. syringae* (Figure 3.7). However, further experiments are needed to better understand the molecular mechanism of SGL1/2 in plant immunity.

## CONCLUSION

This study provides evidence of novel WD40 repeat proteins that are predicted to form a seven-fold symmetrical  $\beta$ -propeller with an N-terminal domain that is structurally similar to the G $\beta$  subunit AGB1. Furthermore, one of these WD40 repeat proteins, SGL2, interacts with the *Arabidopsis* Ga and G $\gamma$  subunits. Loss of either SGL1 or SGL2 results in significant resistance against the bacterial pathogen *P. syringae*. Moreover, loss of both SGL1/2 results in broad spectrum resistance to the fungal pathogen *A. brassicicola* and *P. syringae*. Overall, this work identifies WD40 repeat proteins that have a role in plant immunity by negatively regulating it.

## MATERIALS AND METHODS

**Identification of seven WD repeat orthologs.** *Arabidopsis thaliana* WD40 protein annotations (N=358) were downloaded from the WD40-repeat protein Structure Predictor database (<http://wu.scbb.pkusz.edu.cn/wdsp/index.jsp>; Wang et al., 2015). From these annotations, 262 proteins were identified as having exactly seven WD repeats and a subset of 168 proteins with TAIR IDs were used for further analysis. Protein sequences were aligned in MUSCLE and maximum likelihood trees were generated based on the JTT matrix-based model in MEGA7 (Kumar et al., 2016). Initial tree(s) for the heuristic search were obtained automatically by applying Neighbor-Join and BioNJ algorithms to a matrix of pairwise distances estimated using a JTT model, and then selecting the topology with superior log likelihood value. All amino acid

positions with less than 90% site coverage were eliminated, leaving a total of 266 positions in the final dataset.

**Plant Materials and Growth Conditions.** Surface-sterilized seeds of *Arabidopsis thaliana* accession Columbia-0 (Col-0) were stratified for at least 2 days and sown in 12-well microtiter plates sealed with parafilm. Each 12-well plate contained 12 seedlings with 1 of filter-sterilized 0.5X MS liquid (pH 5.7–5.8) [4.43 g/L Murashige and Skoog basal medium with vitamins (Murashige and Skoog, 1962) (Phytotechnology Laboratories, Shawnee Missions, KS), 0.05% (w/v) MES hydrate, 0.5% (w/v) sucrose], respectively. Alternatively, surface-sterilized and stratified seeds were sown on MS agar plates [0.5X MS, 0.75% (w/v) agar (PlantMedia, Chiang Mai, Thailand)] sealed with parafilm. Unless otherwise stated, plates were placed on grid-like shelves over water trays on a Floralight cart (Toronto, Canada), and plants were grown at 21°C and 60% humidity under a 12 hr light cycle (70–80  $\mu\text{E m}^{-2} \text{s}^{-1}$  light intensity). Unless otherwise stated, media in microtiter plates were exchanged for fresh media on day 7. For bacterial infection experiments, *Arabidopsis* plants were grown on soil [3:1 mix of Fafard Growing Mix 2 (Sun Gro Horticulture, Vancouver, Canada) to D3 fine vermiculite (Scotts, Marysville, OH)] at 22°C daytime/18°C nighttime with 60% humidity under a 12 hr light cycle (100  $\mu\text{E m}^{-2} \text{s}^{-1}$  light intensity). *Nicotiana benthamiana* plants were grown on soil (3:1 mix) on a Floralight cart at 22°C under a 12 hr light cycle (100  $\mu\text{E m}^{-2} \text{s}^{-1}$  light intensity) for 4 weeks.

The following homozygous Col-0 T-DNA insertion lines and mutants were obtained from the Arabidopsis Biological Resource Center (ABRC, Columbus, Ohio): *agb1* (CS3976), *sgl1-1* (SALK\_142665C), *sgl1-2* (SALK\_098040C), *sgl2-1* (WiscDsLox3E04/CS849082), *fls2* (SAIL\_691\_C4).

**Plant Binary Vector Construction and Transformation.** To generate estradiol-inducible C-terminally tagged *GFP* and *RFP* (*XVE:X-GFP/RFP*) DNA constructs, *attB* sites were added via PCR-mediated ligation to the coding sequences of cDNAs, and the modified cDNAs were

recombined into pDONR221 entry vector and then into pABindGFP and pABindRFP destination vectors (Bleckmann et al., 2010), according to manufacturer's instructions (Gateway manual; Invitrogen, Carlsbad, CA). Transient expression of *XVE:X-GFP/RFP* constructs in *N. benthamiana* leaves was performed as previously described (Bleckman et al., 2010) with the following modification: transformed *Agrobacterium* strains were grown in LB medium supplemented with 50 µg/mL rifampicin, 30 µg/mL gentamycin, 50 µg/mL kanamycin and 100 µg/mL spectinomycin, in the absence of a silencing suppressor, to an OD<sub>600</sub> of 0.7. Transgene expression was induced 10 hr (for co-immunoprecipitation) and 4-8 hr (for microscopy) after spraying with 20 µM  $\alpha$ -estradiol and 0.1% Tween-20.

**Confocal Microscopy.** 4-week-old *N. benthamiana* leaves were imaged using a 40X 1.0 numerical aperture Zeiss water-immersion objective and a Zeiss LSM 510 Meta confocal microscopy system. GFP and RFP were excited with a 488-nm argon laser and 561-nm laser diode, respectively. GFP and RFP emissions were detected using a 500-550 nm and 575-630 nm filter sets, respectively. Plasmolysis was induced by 5-10 min treatment of *N. benthamiana* leaf strips with 0.8 mannitol, and co-localization of GFP/RFP-tagged proteins to Hechtian strands was made visible by over-exposing confocal images using ZEN software.

**MAPK Activation Assay.** 9-day-old seedlings were elicited with 100 nM flg22 for 5, 15, and/or 30 min. MAPK activation assay was performed as previously described (Lawerence et al., 2017). 20 µl of supernatant was loaded onto a 10% SDS-PAGE gel, and the separated proteins were transferred to PVDF membrane (Millipore) and probed with phosphor-p44/p42 MAPK (Cell Signaling Technology, Danvers, MA) and MPK3 antibodies (Sigma-Aldrich, St. Louis, MO) at 1:2000 dilution in 5% (w/v) nonfat milk in 1X PBS. The combined signal intensities of phosphorylated MPK3/4/6 were quantified using NIH ImageJ and normalized to that of total MPK3 (loading control).

**Split-Luciferase Complementation Assay.** *Arabidopsis* protoplasts were isolated and transfected as previously described (Sheen (<http://genetics.mgh.harvard.edu/sheenweb/>)). In brief, 3-4 week-old *Arabidopsis* plants were cut into 0.5-1.0 mm leaf strips and incubated in enzyme solution (400 mM mannitol, 20 mM KCl, 20 mM MES pH 5.7, 100 mg Cellulase R10, 20 mg Macerozyme, 10 mM CaCl<sub>2</sub>, 0.1% BSA [Sigma A7906] sterile filtered) at room temperature for 4-8 hr. 1X volume of cold W5 solution (30.8 mM NaCl, 125 mM CaCl<sub>2</sub>, 5 mM KCl, 2 mM MES pH 5.7, 50 mM glucose) was added to the enzyme solution and filtered through a 20 µm nylon mesh into a polystyrene test tube. Samples were centrifuged at 100 x g for 2 minutes, removed supernatant, washed cells twice with cold W5 solution, and suspended protoplasts in 3 mL cold W5 solution. Protoplasts were quantified using a hemocytometer and resuspended in cold MMg solution (400 mM mannitol, 15 mM MgCl<sub>2</sub>, 4 mM MES pH 5.7) to yield a concentration of 5x10<sup>5</sup> cells mL<sup>-1</sup>. 10 µg of each vector was mixed to 200 µL of 5 x 10<sup>5</sup> cells and gently mixed. 1X volume of PEG solution was added (200 mM mannitol, 100 mM CaCl<sub>2</sub>, 40% (w/v) PEG 4000) to samples, tubes were gently inverted 10 times, and then incubated at room temperature for 15 minutes. 1 mL of W5 solution was added to each sample and gently mixed. Samples were then centrifuged at 100 x g for 2 minutes, the supernatant removed and the cells washed with 1 mL W5 solution. Samples were centrifuged again at 100 x g for 1 minute and 900 µL of supernatant was removed. Protoplasts were transferred to 6-well plates, coated with 10% calf-bovine serum, with 1 mL W5 solution. Protoplasts were incubated under constant light for 18-24 hr.

**Bacterial Pathogen Infection Assay.** Pathogen assays on 4- to 5-week-old adult leaves were performed as previously described (Chezem et al., 2017). In brief, *Pseudomonas syringae* pv. *tomato* DC3000 (*Pto* DC3000) was grown overnight in LB and 25 µg/mL rifampicin (Sigma-Aldrich) and then washed in sterile water twice. *P. syringae* was resuspended in water to the desired OD<sub>600</sub> and adult leaves of 4- to 5-week-old plants were surface-inoculated with the bacterial inoculum (OD<sub>600</sub> = 0.002 or 10<sup>6</sup> colony-forming units (CFU)/cm<sup>2</sup> leaf area) in the

presence of 0.0075% Silwet L-77 (Phytotechnology Laboratories) and incubated on 0.8% (w/v) tissue-culture water agar plates for 4 days. Leaves were surface-sterilized in 70% ethanol, washed in sterile water, and dried on paper towels. Bacteria were extracted into water, using an 8-mm stainless steel bead and a ball mill (25 Hz for 3 min). Serial dilutions of the extracted bacteria were plated on LB agar plates for CFU counting.

**Fungal Pathogen Infection Assay.** *Alternaria brassicicola* strain FSU218 (Fungal Reference Center, Jena, Germany) was used for fungal infections. *A. brassicicola* was grown on PDA (1% Potato Dextrose Agar) plates at 21°C, 16 hr photoperiod, <100  $\mu\text{E m}^{-2} \text{s}^{-1}$ , wrapped in parafilm to maintain high humidity for 3 weeks before collecting spores. *A. brassicicola* conidia spores were harvested and resuspended in sterile water, and incubated at RT for 24 hr. Conidia were quantified using a hemocytometer and the spore inoculum was adjusted to a concentration of  $5 \times 10^5$  spores  $\text{mL}^{-1}$ . 5  $\mu\text{L}$  droplets were placed on the surface of detached leaves and leaves were incubated at 21°C, 16-hr photoperiod, >100  $\mu\text{E m}^{-2} \text{s}^{-1}$ , in high humidity for 3 days before imaging leaves.

## SUPPLEMENTAL DATA

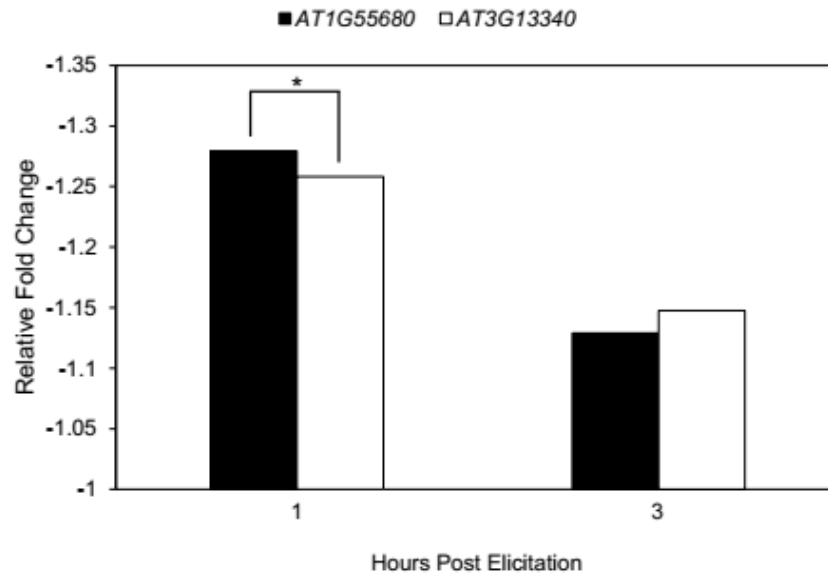


**Figure S3.1. WD40 repeat proteins SGL1 and SGL2 are down-regulated upon flg22 elicitation.** Microarray data of SGL1/2 upon flg22 elicitation at 1 and 3 hours post elicitation (Denoux et al., 2007).

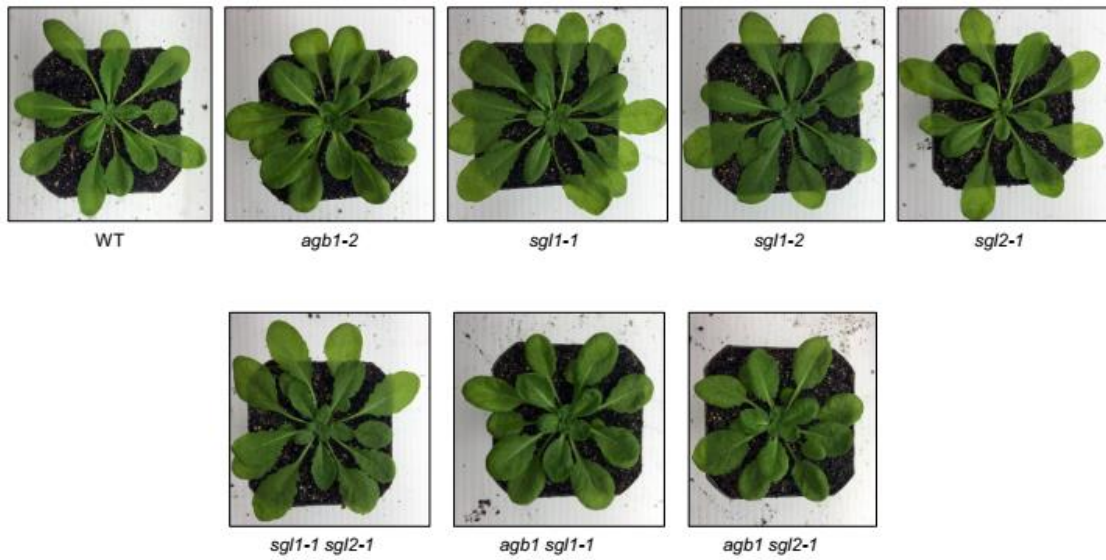


**Figure S3.2. *sgl1/2* single and double mutants resemble WT growth development.** Pictures of 4-week-old plants grown in 12/12 day/night light cycle.

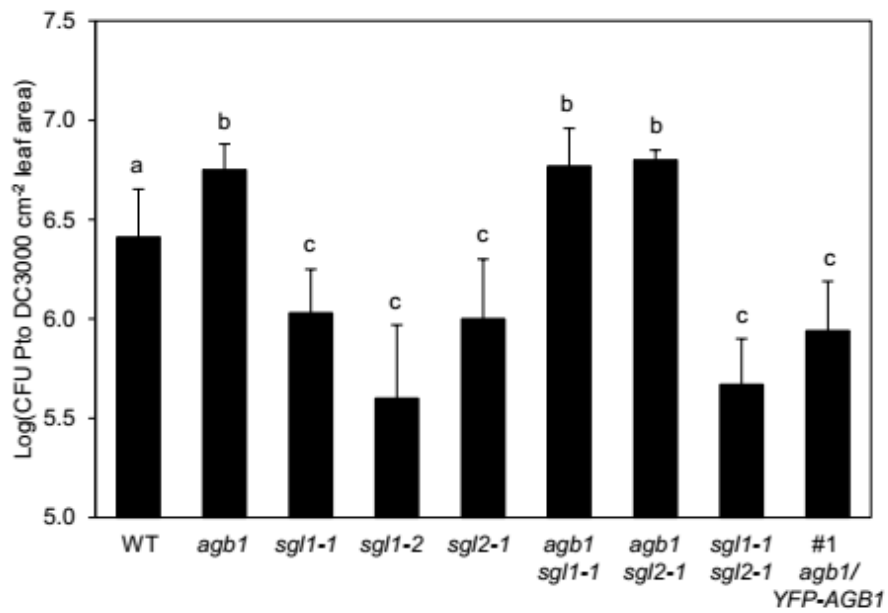


**Figure S3.3. *agb1 sgl1/2* double mutants are as susceptible as *agb1* against *P. syringae*.** Growth analysis of bacterial pathogen *Pto* DC3000 in 5-week-old surface-inoculated leaves. Data represent mean  $\pm$  SD of six replicates. Different letters indicate significant differences ( $P$ -value  $<0.05$ , two-tailed  $t$  test).

## **ACKNOWLEDGEMENTS**

This work was supported by T32 GM007223 (to J.C.M).

## REFERENCES

- Adams, D. R., Ron, D., Kiely, P. A. (2011). RACK1, A multifaceted scaffolding protein: Structure and function. *Cell Commun. Signal.* 9, 22.
- Albrecht, C., Freddy Boutrot, Cécile Segonzac, Benjamin Schwessinger, Selena Gimenez-Ibanez, Delphine Chinchilla, John P. Rathjen, Sacco C. de Vries, Cyril Zipfel (2012). Brassinosteroids inhibit pathogen-associated molecular pattern-triggered immune signaling independent of the receptor kinase BAK1. *Proc. Natl. Acad. Sci.* 109, 1, 303-308
- Aranda-Sicilia, M. N., Trusov, Y., Maruta, N., Chakravorty, D., Zhang, Y., Botella, J. R. (2015). Heterotrimeric G proteins interact with defense-related receptor-like kinases in *Arabidopsis*. *J. Plant Physiol.* 188, 44-48.
- Assmann, S. (2002). Heterotrimeric and unconventional GTP binding proteins in plant cell signaling. *The Plant Cell*. S355-S373
- Bakker, P. A., Pieterse, C. M., van Loon, L. C. (2007). Induced systemic resistance by fluorescent *Pseudomonas* spp. *Phytopathol.* 97, 239-243.
- Beck, M. Ji Zhou, Christine Faulkner, Daniel MacLean, Silke Robatzek (2012). Spatio-Temporal Cellular Dynamics of the *Arabidopsis* Flagellin Receptor Reveal Activation Status-Dependent Endosomal Sorting. *The Plant Cell*. 24, 4205-4219.
- Belkhadir Y, Yang L, Hetzel J, Dangl JL, Chory J. (2014). The growth-defense pivot: Crisis management in plants mediated by LRR-RK surface receptors. *Trends in biochemical sciences.* 39, 10, 447-456.
- Bhardwaj, D., Sheikh, A. H., Sinha, A. K., Tuteja, N. (2011). Stress induced  $\beta$  subunit of heterotrimeric G-proteins from *Pisum sativum* interacts with mitogen activated protein kinase. *Plant Signal Behav.* 6, 287-292.
- Blanc, G., Barakat, A., Guyot, R., Cooke, R., & Delseny, M. (2000). Extensive duplication and reshuffling in the *Arabidopsis* genome. *The Plant Cell*, 12(7), 1093-1101.
- Bommert, P., Je, B. Il, Goldshmidt, A., Jackson, D. (2013). The maize *Ga* gene *COMPACT PLANT2* functions in *CLAVATA* signalling to control shoot meristem size. *Nature* 502, 555-8.
- Bradford, W., Buckholz, A., Morton, J., Price, C., Jones, A. M., Urano, D. (2013). Eukaryotic G protein signaling evolved to require G protein-coupled receptors for activation. *Sci. Signal.* 6, ra37.
- Burki, F. (2014). The eukaryotic tree of life from a global phylogenomic perspective. *Cold Spring Harb. Perspect. Biol.* 6, a016147.
- Chakravorty, D., Trusov, Y., Zhang, W., Acharya, B. R., Sheahan, M. B., McCurdy, D. W., et al. (2011). An atypical heterotrimeric G-protein  $\gamma$ -subunit is involved in guard cell  $K^{+}$ -channel regulation and morphological development in *Arabidopsis thaliana*. *Plant J.* 67, 840-851.
- Chakravorty, D., Gookin, T. E., Milner, M. J., Yu, Y., Assmann, S. (2015). Extra-large G proteins (XLGs) expand repertoire of subunits in *Arabidopsis* heterotrimeric G protein signaling. *Plant Physiol.* 169, 512-529.
- Chen, Y. & Brandizzi, F. (2011). AtIRE1A/AtIRE1B and AGB1 independently control two essential unfolded protein response pathways in *Arabidopsis*. *The Plant Journal.* 69, 2, 266-277.

- Cheng, Z., Li, J.-F., Niu, Y., Zhang, X.-C., Woody, O. Z., Xiong, Y., et al. (2015). Pathogen-secreted proteases activate a novel immune pathway. *Nature* 521, 213-216.
- Chinchilla, D., Zipfel, C., Robatzek, S., Kemmerling, B., Nürnberger, T., Jones, D.G., Felix, G., Boller, T. (2007). A flagellin-induced complex of the receptor FLS2 and BAK1 initiates plant defence. *Nature*. 448, 497–500.
- Consonni, C., Humphry, M. E., Hartmann, H. A., Livaja, M., Durner, J., Westphal, L. (2006). Conserved requirement for a plant host cell protein in powdery mildew pathogenesis. *Nature Genet.* 38, 716–720.
- De Mendoza, A., Sebé-Pedrós, A., Ruiz-Trillo, I. (2014). The evolution of the GPCR signaling system in eukaryotes: Modularity, conservation, and the transition to metazoan multicellularity. *Genome Biol. Evol.* 6, 606–619.
- Dereeper, A., Guignon, V., Blanc, G., Audic, S., Buffet, S., Chevenet, F., et al. (2008). Phylogeny.fr: robust phylogenetic analysis for the non-specialist. *Nucleic Acids Res.* 1, W465-W469.
- Delgado-Cerezo, M., Sánchez-Rodríguez, C., Escudero, V., Miedes, E., Fernández, P. V., Jordá, L., et al. (2012). Arabidopsis heterotrimeric G-protein regulates cell wall defense and resistance to necrotrophic fungi. *Mol. Plant* 5, 98–114.
- Devoto, A., Hartmann, H. A., Piffanelli, P., Elliott, C., Simmons, C., Taramino, G., et al., (2003). Molecular phylogeny and evolution of the plant-specific seven-transmembrane MLO family. *J. Mol. Evol.* 56, 77–88.
- Ding, L., Pandey, S., Assmann, S. M. (2008). Arabidopsis extra-large G proteins (XLGs) regulate root morphogenesis. *Plant J.* 53, 248-263.
- Dixon, R. A. (2001). Natural products and plant disease resistance. *Nature* 411, 843-847.
- Friedman, E. J., Temple, B. R. S., Hicks, S. N., Sondek, J., Jones, C. D., Jones, A. M. (2009). Prediction of protein-protein interfaces on G-protein  $\beta$  subunits reveals a novel phospholipase C  $\beta 2$  binding domain. *J. Mol. Biol.* 392, 1044-1054.
- Fritz-Laylin, L. K., Krishnamurthy, N., Tör, M., Sjölander, K. V., Jones, J. D. G. (2005). Phylogenomic analysis of the receptor-like proteins of rice and Arabidopsis. *Plant Physiol.* 138, 611-623.
- Geldner, N., Hyman, D. L., Wang, X., Schumacher, K., Chory, J. (2007). Endosomal signaling of plant steroid receptor kinase BRI1. *Genes & Dev.* 21, 1598-1602.
- González-García, M.P., J. Vilarrasa-Blasi, M. Zhiponova, F. Divol, S. Mora García, E. Russinova, A.I. Caño-Delgado (2011). Brassinosteroids control meristem size by promoting cell cycle progression in *Arabidopsis* roots. *Development*, 138, 849-859.
- Guerriero, G., Silvestrini, L., Obersriebnig, M., Hausman, J. F., Strauss, J., Ezcurra, I. (2016) A WDR gene is a conserved member of a chitin synthase gene cluster and influences the cell wall in *Aspergillus nidulans*. *Int. J. Mol. Sci.* 17, 1031.
- Hacham, Y., N. Holland, C. Butterfield, S. Ubeda-Tomas, M.J. Bennett, J. Chory, S. Savaldi-Goldstein (2011). Brassinosteroid perception in the epidermis controls root meristem size. *Development*, 138, 839-848.
- Hackenberg, D., Sakayama, H., Nishiyama, T., Pandey, S. (2013). Characterization of the heterotrimeric G-protein complex and its regulator from the green alga *Chara braunii* expands the evolutionary breadth of plant G-protein signaling. *Plant Physiol.* 163, 1510–7.

- Heese, A., Dagmar R. Hann, Selena Gimenez-Ibanez, Alexandra M. E. Jones, Kai He, Jia Li, Julian I. Schroeder, Scott C. Peck, John P. Rathjen. (2007). The receptor-like kinase SERK3/BAK1 is a central regulator of innate immunity in plants. *Proc. Natl. Acad. Sci. USA* 104, 29, 12217-12222.
- Heo, J. B., Sung, S., Assmann, S. M. (2012). Ca<sup>2+</sup>-dependent GTPase, Extra-large G protein 2 (XLG2), promotes activation of DNA-binding protein Related to Vernalization 1 (RTV1), leading to activation of floral integrator genes and early flowering in *Arabidopsis*. *J. Biol. Chem.* 287, 8242-8253.
- Hillenbrand, M., Schori, C., Schöppe, J., Plückthun, A. (2015). Comprehensive analysis of heterotrimeric G-protein complex diversity and their interactions with GPCRs in solution. *Proc. Natl. Acad. Sci. USA* 112, E1181-E1190.
- Humphry, M., Consonni, C., Panstruga, R. (2006). Mlo-based powdery mildew immunity: silver bullet or simply non-host resistance? *Mol. Plant Pathol.* 7, 605-610.
- Im, M. J., Holzhofer, A., Bottinger, H., Pfeuffer, T., Helmreich, E. J. (1988). Interactions of pure beta gamma-subunits of G-proteins with purified beta 1-adrenoceptor. *FEBS Lett.* 227, 225-229.
- Ishida, T., Tabata, R., Yamada, M., Aida, M., Mitsumasa, K., Fujiwara, M., et al. (2014). Heterotrimeric G proteins control stem cell proliferation through CLAVATA signaling in *Arabidopsis*. *EMBO Rep.* 15, 1202-1209.
- Ishikawa, A. (2009). The *Arabidopsis* G-protein  $\beta$ -subunit is required for defense response against *Agrobacterium tumefaciens*. *Biosci. Biotechnol. Biochem.* 73, 47-52.
- Janda, L., Tichy, P., Spízek, J., Petříček, M. (1996). A deduced *Thermomonospora curata* protein containing serine/threonine protein kinase and WD-repeat domains. *J. Bacteriol.* 178, 1487-1489.
- Jones, J. C., Duffy, J. W., Machius, M., Temples, B. R. S., Dohlman, H. G., Jones, A. M. (2011a). The crystal structure of a self-activating G protein  $\alpha$  subunit reveals its distinct mechanism of signal initiation. *Sci. Signal.* 4, ra8.
- Jones, J. C., Temple, B. R., Jones, A. M., Dohlman, H. G. (2011b). Functional reconstitution of an atypical G protein heterotrimer and regulator of G protein signaling protein (RGS1) from *Arabidopsis thaliana*. *J. Biol. Chem.* 286, 13143-13150.
- Jones, J. D. G., Dangl, J. L. (2006). The plant immune system. *Nature* 444, 323-329.
- Keeling, P. J., Burger, G., Durnford, D. G., Lang, B. F., Lee, R. W., Pearlman, R. E., Roger, A. J., Gray, M. W. (2005). The tree of eukaryotes. *Trends Ecol. Evol.* 20, 670-676.
- Kelley, L. A., Sternberg, M. J. E. (2009). Protein structure prediction on the Web: a case study using the Phyre server. *Nat. Protoc.* 4, 363-371.
- Kisselev, O., Gautam, N. (1993). Specific interaction with rhodopsin is dependent on the gamma subunit type in a G protein. *J. Biol. Chem.* 268, 24519-2422.
- Koizumi N, Martinez IM, Kimata Y, Kohno K, Sano H, Chrispeels MJ. (2001). Molecular Characterization of Two *Arabidopsis* Ire1 Homologs, Endoplasmic Reticulum-Located Transmembrane Protein Kinases. *Plant Physiology.* 127, 3,949-962.
- Krattiger, A.F. (1997). Insect resistance in crops: a case study of *Bacillus thuringiensis* (Bt) and its transfer to developing countries. *ISAAA Briefs* 2.

- Krishnan, A., Mustafa, A., Almén, M. S., Fredriksson, R., Williams, M. J., Schiöth, H. B. (2015). Evolutionary hierarchy of vertebrate-like heterotrimeric G protein families. *Mol. Phylogenet. Evol.* 91, 27–40
- Kumar S, Stecher G, Tamura K. 2016. MEGA7: Molecular Evolutionary Genetics Analysis version 7.0 for bigger datasets. *Molecular Biology and Evolution.* 22;33:1870-1874.
- Lambright, D. G., Sondek, J., Bohm, A, Skiba, N. P., Hamm, H. E., Sigler, P. B. (1996). The 2.0 Å crystal structure of a heterotrimeric G protein. *Nature* 379, 311-319.
- Lee, Y. R., Assmann, S. M. (1999). *Arabidopsis thaliana* ‘extra-large GTP-binding protein’ (AtXLG1): a new class of G-protein. *Plant Mol. Biol.* 40, 55-64.
- Lee, S., Rojas, C. M., Ishiga, Y., Pandey, S., Mysore, K. S. (2013). Arabidopsis heterotrimeric G-proteins play a critical role in host and nonhost resistance against *Pseudomonas syringae* pathogens. *PLoS One* 8, e82445.
- Letunic, I., Doerks, T., Bork, P. (2014). SMART: recent updates, new developments and status in 2015. *Nucleic Acids Res.* 43, D257-D260.
- Li, J., Wen, J., Lease, K.A., Doke, J.T., Tax, F.E., Walker, J.C. (2002). BAK1, an Arabidopsis LRR receptor-like protein kinase, interacts with BRI1 and modulates brassinosteroid signaling. *Cell.* 110, 2, 213-22.
- Li, L., Wright, S. J., Krystofova, S., Park, G., Borkovich, K. A. (2007). Heterotrimeric G protein signaling in filamentous fungi. *Annu. Rev. Microbiol.* 61, 423-452.
- Liang X, Ding P, Lian K, et al. (2016) Arabidopsis heterotrimeric G proteins regulate immunity by directly coupling to the FLS2 receptor. Nürnberg T, ed. *eLife.* 5:e13568.
- Lin W, Lu D, Gao X, et al. (2013) Inverse modulation of plant immune and brassinosteroid signaling pathways by the receptor-like cytoplasmic kinase BIK1. *Proc. Natl. Acad. Sci. USA.* 110, 29, 12114-12119.
- Liu, J., Ding, P., Sun, T., Nitta, Y., Dong, O., Huang, X., et al. (2013). Heterotrimeric G Proteins Serve as a Converging Point in Plant Defense Signaling Activated by Multiple Receptor-Like Kinases. *Plant Physiol.* 161, 2146–2158.
- Llorente, F., Alonso-Blanco, C., Sánchez-Rodríguez, C., Jorda, L., Molina, A. (2005). ERECTA receptor-like kinase and heterotrimeric G protein from Arabidopsis are required for resistance to the necrotrophic fungus *Plectosphaerella cucumerina*. *Plant Journal* 43, 165–180.
- Lobell, D. B., Schlenker, W., Costa-Roberts, J. (2011). Climate trends and global crop production since 1980. *Science* 333, 616-620.
- Lobell, D. B., Gourdji, S. M. (2012). The influence of climate change on global crop productivity. *Plant Physiol.* 160, 1686-1697.
- López-Bergami, P., Habelhah, H., Bhoumik, A., Zhang, W., Wang, L. H., Ronai, Z. (2005). Receptor for RACK1 mediates activation of JNK by protein kinase C. *Mol. Cell* 19, 309–320.
- Lorek, J., Griebel, T., Jones, A. M., Kuhn, H., Panstruga, R. (2013). The role of Arabidopsis heterotrimeric G-protein subunits in MLO2 function and MAMP-triggered immunity. *Mol. Plant-Microbe Interact.* 26, 991–1003.

- Lozano-Durán R, Zipfel C (2015). Trade-off between growth and immunity: role of brassinosteroids. *Trends Plant Sci.* 20, 12–19.
- Lozano-Durán R., Belkhadir Y. (2017) A Technical Framework for Studying the Signaling Nexus of Brassinosteroids and Immunity. In: Russinova E., Caño-Delgado A. (eds) Brassinosteroids. Methods in Molecular Biology, vol 1564. Humana Press, New York, NY
- Lyons, E., & Freeling, M. (2008). How to usefully compare homologous plant genes and chromosomes as DNA sequences. *The Plant Journal*, 53(4), 661-673. Waterhouse AM, Procter JB, Martin DMA, Clamp M, Barton GJ. 2009. Jalview Version 2 - a multiple sequence alignment editor and analysis workbench. *Bioinformatics* 25: 1189-1191.
- Ma, H., Yanofsky, M. F., Meyerowitz, E. M. (1990). Molecular cloning and characterization of GPA1, a G protein  $\alpha$  subunit gene from *Arabidopsis thaliana*. *Proc. Natl. Acad. Sci. USA* 87, 3821-3825.
- Macho, A., Zipfel, C. (2014). Plant PRRs and the Activation of Innate Immune Signaling. *Molecular Cell*. 54, 263-272.
- Maeda, K., Houjyou, Y., Komatsu, T., Hori, H., Kodaira, T., Ishikawa, A. (2009). AGB1 and PMR5 Contribute to PEN2-Mediated Preinvasion Resistance to *Magnaporthe oryzae* in *Arabidopsis thaliana*. *Mol. Plant-Microbe Interact.* 22, 1331-1340.
- Maruta, N., Trusov, Y., Brenya, E., Parekh, U., Botella, J. R. (2015). Membrane-Localized Extra-Large G Proteins and G $\beta\gamma$  of the Heterotrimeric G Proteins Form Functional Complexes Engaged in Plant Immunity in *Arabidopsis*. *Plant Physiol.* 167, 1004–1016.
- Mason, M. G., Botella, J. R. (2001). Isolation of a novel G-protein  $\gamma$ -subunit from *Arabidopsis thaliana* and its interaction with G $\beta$ . *Biophys. Acta* 1520, 147-153.
- Mason, M. G., Botella, J. R. (2000). Completing the heterotrimer: isolation and characterization of an *Arabidopsis thaliana* G protein  $\gamma$ -subunit cDNA. *Proc. Natl. Acad. Sci. USA* 97, 1478-1488.
- Meziane, H., Van der Sluis, I., van Loon, L. C., Hofte, M., Bakker, P. A. H. M. (2005). Determinants of *Pseudomonas putida* WCS358 involved in inducing systemic resistance in plants. *Mol. Plant Pathol.* 6, 177-185.
- Mockler TC, Michael TP, Priest HD, Shen R, Sullivan CM, Givan SA, McEntee C, Kay S, Chory J (2007) THE DIURNAL PROJECT: Diurnal and circadian expression profiling, model-based pattern matching and promoter analysis. *Cold Spring Harb Symp Quant Biol.* 72, 353-63.
- Nam, K.H. & Li, J. (2002). BRI1/BAK1, a receptor kinase pair mediating brassinosteroid signaling. *Cell*. 110, 2, 203-212.
- Oldham, W. M., Hamm, H. E. (2008). Heterotrimeric G protein activation by G-protein-coupled receptors. *Nat. Rev. Mol. Cell Biol.* 9, 60-71.
- Ouyang, Y., Huang, X., Lu, Z., Yao, J. (2012). Genomic survey, expression profile and co-expression network analysis of OsWD40 family in rice. *BMC Genomics* 13, 100.
- Pandey S, Assmann, S. M. (2004). The Arabidopsis putative G protein-coupled receptor GCR1 interacts with the G protein  $\alpha$  subunit GPA1 and regulates abscisic acid signalling. *Plant Cell* 16: 1616-1632.

- Pandey, S., Nelson, D. C., Assmann, S. M. (2009). Two novel GPCR-type G proteins are abscisic acid receptors in *Arabidopsis*. *Cell* 136, 136-148.
- Peng., Y., Chen, L., Li, S., Zhang, Y., Xu, R., Liu, Z., Liu, W., Kong, J., Huang, X., Wang, Y., Cheng, B., Zheng., L., Li, Y. (2018). BRI1 and BAK1 interact with G proteins and regulate sugar-responsive growth and development in *Arabidopsis*. *Nature Communications*. 9, 1522
- Perfus-Barbeoch, L., Jones, A. M., Assmann, S. M. (2004). Plant heterotrimeric G protein function: insights from *Arabidopsis* and rice mutants. *Curr. Opin. Plant Biol.* 7, 719-731.
- Ron, D., Chen, C. H., Caldwell, J., Jamieson, L., Orr, E. Mochly-Rosen, D. (1994). Cloning of an intracellular receptor for protein kinase C: a homolog of the  $\beta$  subunit of G proteins. *Proc. Natl. Acad. Sci. USA* 91, 839–843.
- Ruberti C, Brandizzi F. (2014). Conserved and plant-unique strategies for overcoming endoplasmic reticulum stress. *Frontiers in Plant Science*. 5,69.
- Ruiz Carrillo, D., Chandrasekaran, R., Nilsson, M., Cornvik, T., Liew, C. W., Tan, S. M., Lescar, J. (2012). Structure of human Rack1 protein at a resolution of 2.45Å. *Acta Crystallogr. Sect. F: Struct. Biol. Cryst. Commun.* 68, 867–872.
- Russinova, E. Jan-Willem Borst, Mark Kwaaitaal, Ana Caño-Delgado, Yanhai Yin, Joanne Chory, Sacco C. de Vries. (2004). Heterodimerization and Endocytosis of *Arabidopsis* Brassinosteroid Receptors BRI1 and AtSERK3 (BAK1). *The Plant Cell*. 16, 3216-3229.
- Sato, M., Mitra, R. M., Coller, J., Wang, D., Spivey, N. W., Dewdney, J., Denoux, C., Glazebrook, J. Katagiri, F. (2007). A high-performance, small-scale microarray for expression profiling of many samples in *Arabidopsis*-pathogen studies. *Plant Journal*. 3, 565-577.
- Schwessinger B, Roux M, Kadota Y, Ntoukakis V, Sklenar J, et al. (2011) Phosphorylation-Dependent Differential Regulation of Plant Growth, Cell Death, and Innate Immunity by the Regulatory Receptor-Like Kinase BAK1. *PLOS Genetics* 7(4): e1002046.
- Shi, H., Shen, Q., Qi, Y., Yan, H., Nie, H., Chen, Y., Ting, Z., Katagiri, F., Tang, D. (2013) BR-SIGNALING KINASE1 Physically Associates with FLAGELLIN SENSING2 and Regulates Plant Innate Immunity in *Arabidopsis*. *The Plant Cell*. DOI: <https://doi.org/10.1105/tpc.112.107904>
- Shiu, S.H., Bleecker, A.B. (2001). Plant receptor-like kinase gene family: diversity, function, and signaling. *Sci. STKE* 2001, 22.
- Shiu, S.H., Bleecker, A.B. (2003). Expansion of the receptor-like kinase/Pelle gene family and receptor-like proteins in *Arabidopsis*. *Plant Physiol.* 132, 530-543.
- Smith, T. F., Gaitatzes, C., Saxena, K., Neer, E. J. (1999). The WD repeat: A common architecture for diverse functions. *Trends in Biochem. Sci.* 24, 181–185.
- Sondek, J., Bohm, A, Lambright, D. G., Hamm, H. E., Sigler, P. B. (1996). Crystal structure of a G-protein beta gamma dimer at 2.1Å resolution. *Nature*. 379, 369-374.
- Stirnemann, C. U., Petsalaki, E., Russell, R. B., Muller, C. W. (2010). WD40 proteins propel cellular networks. *Trends Biochem. Sci.* 35, 565–574.
- Stone, J. M., Walker, J. C. (1995). Plant protein kinase families and signal transduction. *Plant Physiol.* 108, 451-457.

- Taddese, B., Upton, G. J. G., Bailey, G. R., Jordan, S. R. D., Abdulla, N. Y., Reeves, P. J., Reynolds, C. A. (2014). Do plants contain G protein-coupled receptors? *Plant Physiol.* 164, 287-307.
- Taylor, J. M., Jacob-Mosier, G. G., Lawton, R. G., Remmers, A. E., Neubig, R. R. (1994). Binding of an alpha 2 adrenergic receptor third intracellular loop peptide to G beta and the amino acid terminus of G alpha. *J. Biol. Chem.* 269, 27618-27624.
- Taylor, J. M., Jacob-Mosier, G. G., Lawton, R. G., VanDort, M., Neubig, R. R. (1996). Receptor and membrane interaction sites on Gbeta. A receptor-derived peptide binds to the carboxyl terminus. *J. Biol. Chem.* 271, 3336-3339.
- Temple, B. R. S. & Jones, A. M. (2007). The plant heterotrimeric G-protein complex. *Ann. Rev. Plant Biol.* 58, 249-266.
- Thung, L., Trusov, Y., Chakravorty, D., Botella, J. R. (2012).  $G\gamma 1+G\gamma 2+G\gamma 3=G\beta$ : The search for heterotrimeric G-protein  $\gamma$  subunits in *Arabidopsis* is over. *J. Plant Physiol.* 169, 542-545.
- Thung, L., Chakravorty, D., Trusov, Y., Jones, A. M., Botella, J. R. (2013). Signaling specificity provided by the *Arabidopsis thaliana* heterotrimeric G-protein  $\gamma$  subunits AGG1 and AGG2 is partially but not exclusively provided through transcriptional regulation. *PLoS One* 8, e58503.
- Torres, M. A., Morales, J., Sánchez-Rodríguez, C., Molina, A., Dangl, J. L. (2013). Functional interplay between *Arabidopsis* NADPH oxidases and heterotrimeric  $\gamma$  protein. *Mol. Plant-Microbe Interact.* 26, 686-94.
- Trusov, Y., Rookes, J. E., Chakravorty, D., Armour, D., Schenk, P. M., Botella, J. R. (2006). Heterotrimeric G proteins facilitate *Arabidopsis* resistance to necrotrophic pathogens and are involved in jasmonate signaling. *Plant Physiol.* 140, 210-220.
- Trusov, Y., Rookes, J. E., Tilbrook, K., Chakravorty, D., Mason, M. G., Anderson, D., et al. (2007). Heterotrimeric G protein  $\gamma$  subunits provide functional selectivity in  $G\beta\gamma$  dimer signaling in *Arabidopsis*. *Plant Cell* 19, 1235-1250.
- Trusov, Y., Sewelam, N., Rookes, J. E., Kunkel, M., Nowak, E., Schenk, P. M., Botella, J. R. (2009). Heterotrimeric G proteins-mediated resistance to necrotrophic pathogens includes mechanisms independent of salicylic acid-, jasmonic acid/ethylene- and abscisic acid-mediated defense signaling. *Plant J.* 58, 69-81.
- Trusov, Y., Chakravorty, D., Botella, J. R. (2012). Diversity of heterotrimeric G-protein  $\gamma$  subunits in plants. *BMC Res. Notes* 5, 608.
- Ullah, H., Scappini, E. L., Moon, A. F., Williams, L. V., Armstrong, D. L., Pedersen, L. C. (2008). Structure of a signal transduction regulator, RACK1, from *Arabidopsis thaliana*. *Protein Sci.* 17, 1771-1780.
- United Nations, Department of Economic and Social Affairs, Population Division (2013). World population prospects: the 2012 revision, Press Release (13 June 2013).
- Urano, D., Chen, J. G., Botella, J. R., Jones, A. M. (2013). Heterotrimeric G protein signalling in the plant kingdom. *Open Biol.* 3, 120186.
- Urano, D., Jones, A. M. (2014). Heterotrimeric G protein-coupled signaling in plants. *Annu. Rev. Plant Biol.* 65, 365-84.

- van Nocker, S., Ludwig, P. (2003). The WD-repeat protein superfamily in Arabidopsis: conservation and divergence in structure and function. *BMC Genomics* 4, 50.
- Van Wees, S. C., Pieterse, C. M., Trijssenaar, A., Van 't Westende, Y. A., Hartog, F., van Loon, L. C. (1997). Differential induction of systemic resistance in *Arabidopsis* by biocontrol bacteria. *Mol. Plant-Microbe Interact.* 10, 716-724.
- Wall, M. A., Coleman, D. E., Lee, E., Iñiguez-Lluhi, J. A., Posner, B. A., Gilman, A. G., Sprang, S. R. (1995). The structure of the G protein heterotrimer  $G_{i\alpha 1}\beta_1\gamma_2$ . *Cell.* 83, 1047-1058.
- Wang, Z.Y., Wang, Q., Chong, K., Wang, F., Wang, L., Bai, M., Jia, C. (2006). The brassinosteroid signal transduction pathway. *Cell Research.* 16, 427-434.
- Wang, S., Narendra, S., Fedoroff, N. (2007). Heterotrimeric G protein signaling in the Arabidopsis unfolded protein response. *Proc.Natl. Acad. Sci. USA.* 104, 3817–3822.
- Weiss, C. A., Gamaat, C. W., Mukai, K., Hu, Y., Ma, H. (1994). Isolation of cDNAs encoding guanine nucleotide-binding protein  $\beta$ -subunit homologues from maize (ZGB1) and Arabidopsis (AGB1). *Proc. Natl. Acad. Sci. USA* 91, 9554-9558.
- Wettschureck, N., Offermanns, S. (2005). Mammalian G proteins and their cell type specific functions. *Physiol. Rev.* 85, 1159-1204.
- Witzel, F., Maddison, L., Blüthgen, N. (2012). How scaffolds shape MAPK signaling: what we know and opportunities for systems approaches. *Front. Physiol.* 3, 475.
- Wolfensetter, S., Chakravorty, D., Kula, R., Urano, D., Trusov, Y., Sheahan, M. B., McCurdy, D., Assmann, S. M., Jones, A. M., Botella, J. R. (2015). Evidence for an unusual transmembrane configuration of AGG3, a class C  $G\gamma$  subunit of Arabidopsis *The Plant Journal.* 81, 388-398.
- Xu, D., Chen, M., Ma, Y., Xu, Z., Li, L., Chen, Y., Ma, Y. (2015). A G-Protein  $\beta$  Subunit, AGB1, Negatively Regulates the ABA Response and Drought Tolerance by Down-Regulating AtMPK6-Related Pathway in *Arabidopsis*. *Plos One* 10, e0116385.
- Zhang T, Xu P, Wang W, et al. (2017) *Arabidopsis* G-Protein  $\beta$  Subunit AGB1 Interacts with BES1 to Regulate Brassinosteroid Signaling and Cell Elongation. *Frontiers in Plant Science.*8, 2225.
- Zeng, W., He, S. Y. (2010). A prominent role of the flagellin receptor FLAGELLIN-SENSING2 in mediating stomatal response to *Pseudomonas syringae* pv *tomato* DC3000 in Arabidopsis. *Plant Physiol.* 153, 1188-1198.
- Zhang, W., He, S. Y., Assmann, S. M. (2008). The plant innate immunity response in stomatal guard cells invokes G-protein-dependent ion channel regulation. *Plant J.* 56, 984-996.
- Zhu, H., Li, G. J., Ding, L., Cui, X., Berg, H., Assmann, S. M., Xia, Y. (2009). Arabidopsis extra large G-protein 2 (XLG2) interacts with the  $G\beta$  subunit of heterotrimeric G protein and functions in disease resistance. *Mol. Plant* 2, 513–525.
- Zipfel, C. (2014). Plant pattern-recognition receptors. *Trends Immunol.* 35, 345-351.